The role of peroxisomes in osteoblast differentiation and functions

Inaugural Dissertation

submitted to the

Faculty of Medicine

in partial fulfillment of the requirements

for the PhD-Degree

of the Faculties of Veterinary Medicine and Medicine

of the Justus Liebig University Giessen

By

Fan, Wei

Of

Zhengzhou China

Giessen 2014

From the Institute for Anatomy and Cell Biology, Division of Medical Cell Biology

Director/Chairperson: Prof. Dr. Eveline Baumgart-Vogt

of the Faculty of Medicine of Justus Liebig University Giessen

First Supervisor and Committee Member: Prof. Dr. Eveline Baumgart-Vogt

Second Supervisor and Committee Member: Prof. Dr. Martin Diener

Examination chair and Committee Member: Prof. Dr. Klaus-Dieter Schlüter

Date of Doctoral Defense: 22nd September 2015

Declaration

"I declare that I have completed this dissertation single-handedly without the unauthorized help of a second party and only with the assistance acknowledged therein. I have appropriately acknowledged and referenced all text passages that are derived literally from or are based on the content of published or unpublished work of others, and all information that relates to verbal communications. I have abided by the principles of good scientific conduct laid down in the charter of the Justus Liebig University of Giessen in carrying out the investigations described in the dissertation."

Giessen, November 25th 2014   Fan, Wei

Table of Contents

1. Literature Review and Introduction

1.1. The peroxisome structure, functions and biogenesis

1.1.1. Basic morphology and metabolic function of peroxisomes

Peroxisomes are a diverse group of organelles which accommodate many activities related to lipid metabolism. The morphology of peroxisomes differs significantly among various tissues and species. The size, abundance and enzyme content of peroxisomes can be affected by various environmental, metabolic, and developmental factors. In typical human cells peroxisomes are mostly spherical and their diameter ranges from 0.2 µm to1 µm. In oleate grown yeast their size is approximately 0.5 µm, whereas they tend to be significantly smaller in yeast grown on glucose containing medium (0.1-0.2 µm). The basic structure of peroxisomes consists of a lipid bilayer surrounding a fine granular protein matrix core with a crystalline (urate oxidase) in some species (see figure 1). The occurrence of tubular structures has been reported in several organisms, some seeming to interconnect the spherical compartments (Baumgart, 1997; Yamamoto and Fahimi, 1987).
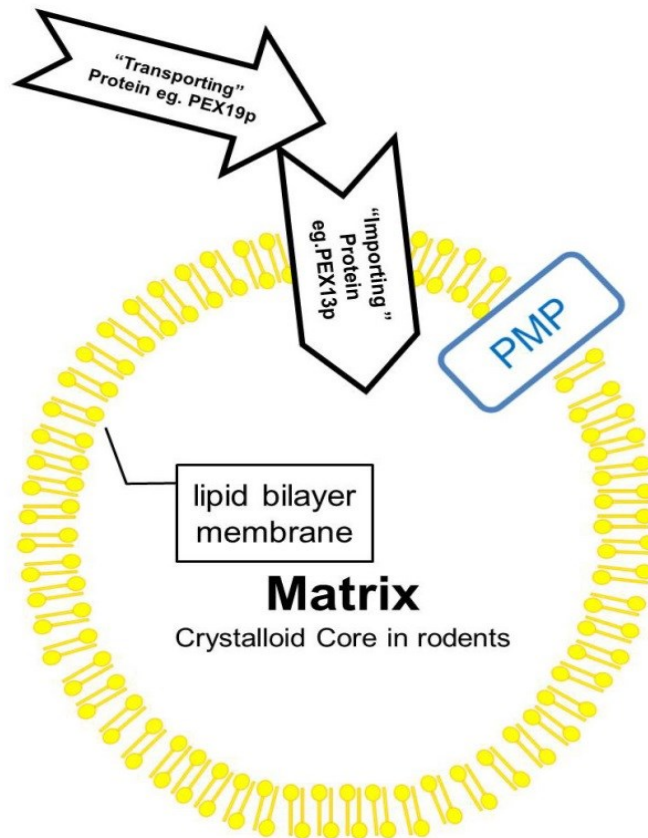
Figure.1. Schematic representation of the basic structure the peroxisome: mainly consist of a surrounding lipid bilayer and a fine granular matrix with a crystalline core of urate oxidase in rodeuts. PMP = peroxisome membrane protein (e.g. substrate transporters)

Peroxisomes have been reported to have a very electron dense matrix with a paracrystalline structures core of urate oxidase or margiual plates made of α-hydroxyacid oxidase B (Angermüller et al., 1986; Baumgart, 1997; Zaar et al., 1986). The Woronin body of the filamentous fungi *Neurospora crassa* is a new type of specialized peroxisome which contains a hexagonal crystalloid core and appears to obstruct septal pores of the syncytium upon cellular damage (Jedd and Chua, 2000).

Peroxisomes were thought to arise *de novo,* nowadays thought to be built directly(Hettema et al., 2014) or multiply by fission of preexisting peroxisomes (Anthonio et al., 2009). The relative contribution of both pathways to the total

number of peroxisomes in wild type cells is not yet clear. Furthermore, the molecular mechanisms governing these processes are only beginning to be unraveled (Anthonio et al., 2009).

As an important functional ubiquitous cell organelle, the peroxisomes play important roles in a variety of metabolic processes, which are as widespread as their morphologies throughout the eukaryotic kingdom. These can be listed as:

a) The metabolism of hydrogen peroxide: Hydrogen peroxide (H_2O_2) respiration is a well-conserved function throughout all peroxisomal metabolic tasks. In particular a variety of peroxisomal oxidases produce H_2O_2 as byproduct during the oxidation of their substrates and Catalase degrades the toxic H_2O_2 within the peroxisomal matrix.

b) Degradation of toxic or bioactive lipid derivatives, such as bile acid intermediates phytanic acid and eicosanoids: Peroxisomes exert complementary functions to mitochondria by degradation of fatty acids. Further peroxisomes can comprise the β-oxidative degradation of a specific set of lipids which cannot be processed by mitochondria, such as the very long chain fatty acids (VLCFA), long chain dicarboxylic acids, various unsaturated fatty acids, di- and trihydroxycholestanoic acids and pristanoic acid and eicosanoids (prostaglandins and leukotrienes).

c) Synthesis of membrane lipids like cholesterol, the biogenesis of etherlipids (e.g.plasmalogens) and ester-phospholipids (glycerolphospholipids): peroxisome associate with the smooth Endoplasmic Reticulum (ER), since plasmalogens are synthesized cooperatively in the ER and the peroxisome, with the peroxisome being the site of introduction of the ether linkage into the plasmalogens. While the precise role of the plasmalogens is not clear, probably ROS trapping or regulation of physical membrane properties (Karnati and Baumgart-Vogt, 2008), severe pathological consequences of a deficiency in the plasmalogen synthesis hint at a central role in the human organism (Eckert and Erdmann, 2003).

Since peroxisomes have various biological and metabolic functions their abundance and their enzyme composition in distinct cell types, tissues or organs is very heterogenous, depending on the specific metabolic pathway (Baumgart, 1997). Up to now, a lot of effort has been invested into determining the functional properties of peroxisomes in humans. Human peroxisome do not contain urate oxidase core since the appropriate gene carries a mutation deleting this enzyme (Alvares et al., 1992). Human peroxisomes harbour most often pathway mentioned above and take part in the *de novo* synthesis of cholesterol from different precursor molecules and play a major role in isoprenoid metabolism (Biardi et al., 1994; Krisans, 1992; Krisans et al., 1994) Furthermore, the glyoxylate aminotransferase, which transforms toxic glyoxylate into alanine, is localized in the peroxisome (Noguchi and Fujiwara, 1988).

1.1.2. Peroxisome biogenesis

1.1.2.1. Basic routine of peroxisome formation

Peroxisome biogenesis describes the combination of processes which are involved in the formation of the peroxisomal membrane, the import of proteins into the peroxisomal matrix and the proliferation of the peroxisomes. Combined genetic and biochemical approaches lead to the identification of more than 30 *Pex genes* which encode proteins required for the biogenesis of peroxisomes, named peroxins "PEX proteins = PEX …." (Distel et al., 1996; Smith and Aitchison, 2009). The proxins have got their number according to their date of discovery, independent of their function in peroxisome biogenesis and cellular location.

Two of the most important components of the peroxisome are the matrix and the membrane proteins which are synthesized by ribosomes in the cytosol and are then imported into the peroxisome. Whereby the machineries to perform the protein import, targeting and insertion of peroxisomal membrane proteins are completely different (Eckert and Erdmann, 2003).

The roles of several groups of peroxins are distinctly different. In particular PEX3, PEX16 and PEX19 of the peroxisomal membrane have been found to play particular roles. Human cells lacking one of these peroxins neither have peroxisomes nor peroxisomal remnants (Ghaedi et al., 2000; Honsho et al., 1998; Matsuzono et al., 1999; Sacksteder et al., 2000; Shimozawa et al., 2000; South and Gould, 1999). In contrast deletions of any of the other peroxins result in the presence of "ghost" peroxisomal structures with a spherical membranous structure containing several peroxisomal membrane proteins. (Eckert and Erdmann, 2003). To sum up, all peroxins and their roles in the biogenesis of peroxisomes can be classified according to different processes of peroxisome formation. Peroxins involved in the formation of peroxisomal membrane, the import of matrix proteins, peroxins controlling peroxisome size and abundance and peroxisome inheritance (see Table.1.) (Smith and Aitchison, 2009).

Table.1. The summary of proteins and corresponding functions involved in peroxisome in the model of Yeast. Table adjusted according to (Fransen et al., 2002; Smith and Aitchison, 2009).

Proteins involved in formation of peroxisomes and pre-peroxisomal vesicles from the ER		Proteins involved in import of matrix proteins	
Pex3p	Membrane receptor for PMP recruitment lipid binding protein	Pex1p[#]	AAA ATPase; PMP
Pex16p	PMP that traffics through the ER; membrane receptor for PMP recruitment in mammalian cells	Pex2p[#]	PMP; RING finger protein
Pex19p[#]	PMP chaperone and transporter; farnesylated and mostly cytosolic	Pex4p	PMP anchored by Pex22p; ubiquitin-conjugating enzyme involved in receptor recycling
Proteins involved in controlling peroxisome size and number		Pex5p[#]	PTS1 receptor; predominantly cytoplasmic
Pex11p[#]	Integral PMP involved peroxisomal fission and proliferation (Li et al., 2002a)	Pex6p[#]	AAA ATPase; PMP
Pex25p	Peripheral PMP; interacts with paralog Pex27p; recruits Rho1p to peroxisomes	Pex7p[#]	PTS2 receptor; predominantly cytoplasmic
Pex27p	interacts with paralog Pex25p	Pex8p	Intraperoxisomal PMP; links docking and RING finger complex
Pex28p /Pex24p	PMP known as Pex28p in S. cerevisiae and Pex24p in *Y. lipolytica*.	Pex10p[#]	PMP; RING finger protein; E3 ligase for Ubc4p dependent ubiquitination of Pex5p
Pex29p	PMP with yet unkown functions	Pex12p[#]	PMP; RING finger protein
Pex30p/ Pex23p	PMP; known as Pex30p in S. cerevisiaeand Pex23p in Y. lipolytica; contains a dysferlin domain; partially functionally redundant with Pex31p and Pex32p	Pex13p[#]	PMP; docking complex component
Pex31p	PMP; contains dysferlin domain	Pex14p[#]	PMP; docking complex component
Pex32p	PMP; contains dysferlin domain	Pex15p/ Pex26p	functional homologs in yeast and mammals, respectively; PMP involved in membrane anchor of Pex6p
DRPs[#]	Dynamin-related proteins includeVps1p and Dnm1p in yeast and Dlp1p in mammalian cells	Pex17p	PMP; docking complex component
Fis1p/Mdv1 p/Caf4p	DRP recruitment to peroxisomes	Pex20p	Co-receptor required for Pex7p binding cargo; *Saccharomyces cerevisiae* has functional homologs Pex21p/Pex18p instead
Rho1p	Guanosine triphosphatase involved in actin assembly on peroxisomes; interacts with Pex25p and Pex30p	Pex22p	PMP that anchors Pex4p to the membrane
		Cytosolic chaperones	Chaperones including members of Hsp70 family and DnaJ-like proteins may be involved in import
Proteins involved in peroxisome inheritance			
Inp1	PMP involved in retention of peroxisomes in mother and daughter cells by attaching peroxisomes to cell cortex		
Inp2	PMP involved in peroxisome movement through interaction with Myo2	Myo2p	Motor that propels peroxisomes along actin cables

PMP, peroxisomal membrane protein; peroxins are known to have similar roles in yeast and in higher eukaryotes.

A model to demonstrate how peroxisomes might be generated was established based on the latest literature. The principle was hypothesized which comprises two ways as following: Peroxisomes arise *de novo* or multiply by fission of preexisting peroxisomes(Hettema et al., 2014).

The hypothesized route of peroxisome biogenesis begins with a preperoxisomal membrane vesicle originating from an endomembrane which can be understood as the ER or a "peroxisomal pre-structure" that could act as a template for the growing and maturing organelle and could already contain the pioneer peroxins such as Pex3p or Pex15p (Eckert and Erdmann, 2003). Further, peroxisome membrane proteins (PMP) could be incorporated for later process and the last step to complete the peroxisome maturation process could be import of peroxisomal matrix proteins into the matured peroxisomal membrane (Eckert and Erdmann, 2003; Hettema et al., 2014). The way of peroxisome formation could be also based on the growth and division model which suggested that the posttranslational import of matrix and membrane proteins into presenting peroxisomes could be followed by the proliferation of peroxisomes(Lazarow and Fujiki, 1985). This hypothesis described the generation of new peroxisomes by presenting mature peroxisomes or could be also by the "peroxisomal pre-structure" growing through a continuous import of PMPs and matrix proteins and a final division. This process is possibly controlled directly or indirectly by Pex11p. (Eckert and Erdmann, 2003; Li et al., 2002a; Schrader et al., 2012)

It was assumed that these two routes could occur simultaneously in peroxisome biogenesis (Figure.2.). The fractions of each route's contribution to the overall peroxisome biogenesis are still unknown.
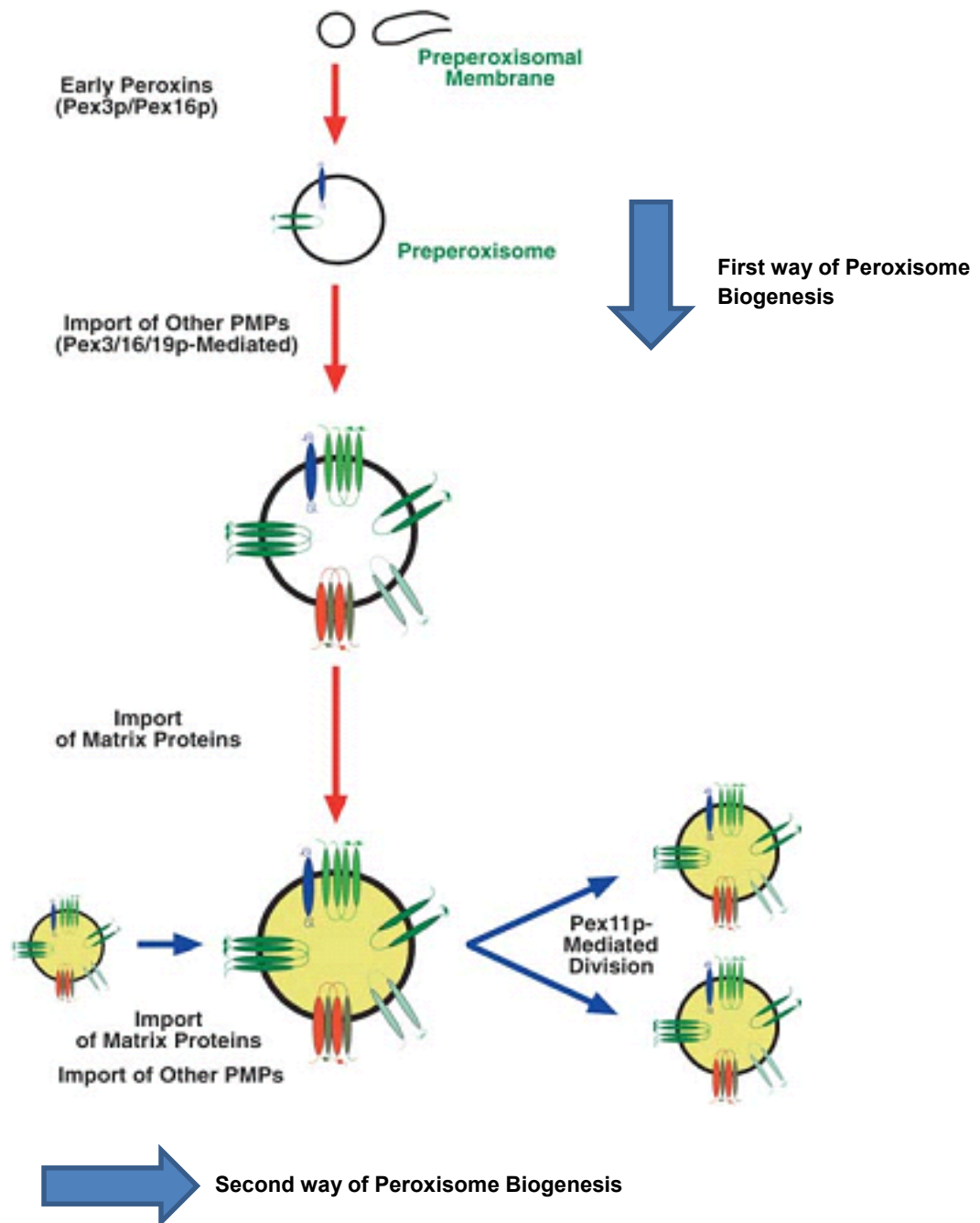
Figure.2. Schematic representation of the two-way model of peroxisome biogenesis in Yeast model. The graph was modified from (Eckert and Erdmann, 2003).

1.1.2.2. Topogenesis of peroxisomal membrane proteins

Within different processes of peroxisome biogenesis, the PMPs import pathway has very unique features. It has been believed that the most PMPs can post-translationally target the peroxisome directly from the cytosol. In this respect peroxin Pex19p plays an essential role as a master transporter in the translocation process (Diestelkotter and Just, 1993; Imanaka et al., 1996; Pause et al., 2000; van der Zand et al., 2006).

Since the participation of the Pex19p is critical in the topogenesis of peroxisomal membrane proteins, Eckert and Erdmann summarized that all PMPs can be classified into three types (I-III) according to their translocation process (Figure.3.)
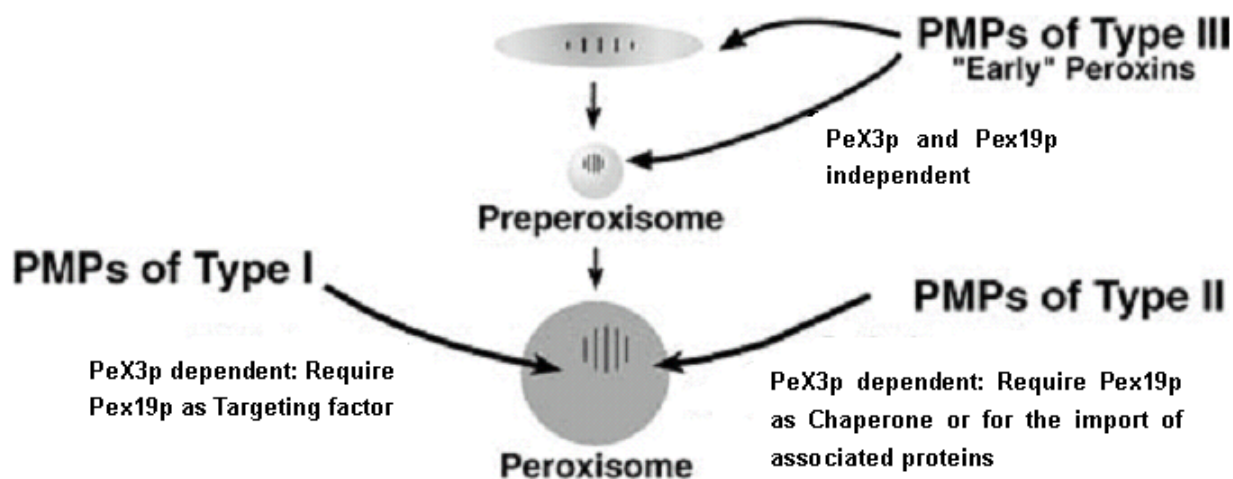
Figure.3. Model of branched pathways for the topogenesis of peroxisomal membrane proteins in Yeast model (Eckert and Erdmann, 2003).

The type I PMPs, such as newly formed PMP34, PMP47 and Pex11p, can be recognized directly and guided to the peroxisomal membrane docking site via signaling effect of Pex19p. It has been presumed that the Pex3p may contribute to the insertion of type I PMP after the PMP translocation has been achieved (Eckert and Erdmann, 2003).

Type II PMPs can be bound by cytosolic Pex19p to form a complex and this complex can be directed and transported to the peroxisomal membrane with the

contribution of Pex19p. Pex19p actually acts as a "chaperone" in this type of PMP translocation process (van der Zand et al., 2006). In the further process, the membrane-integrated Pex3p may contribute to PMPs membrane targeting by recruiting this complex to the peroxisomal membrane. The translocation process is completed through the release of PMPs from the complex and the released PMPs are inserted into the membrane(Eckert and Erdmann, 2003).

Therefore, the transport system for type II PMPs comprises of cytosolic Pex19p and membrane-spanning protein Pex3p. The translocation of type II PMPs into peroxisomal membranes is depicted in Figure.4.
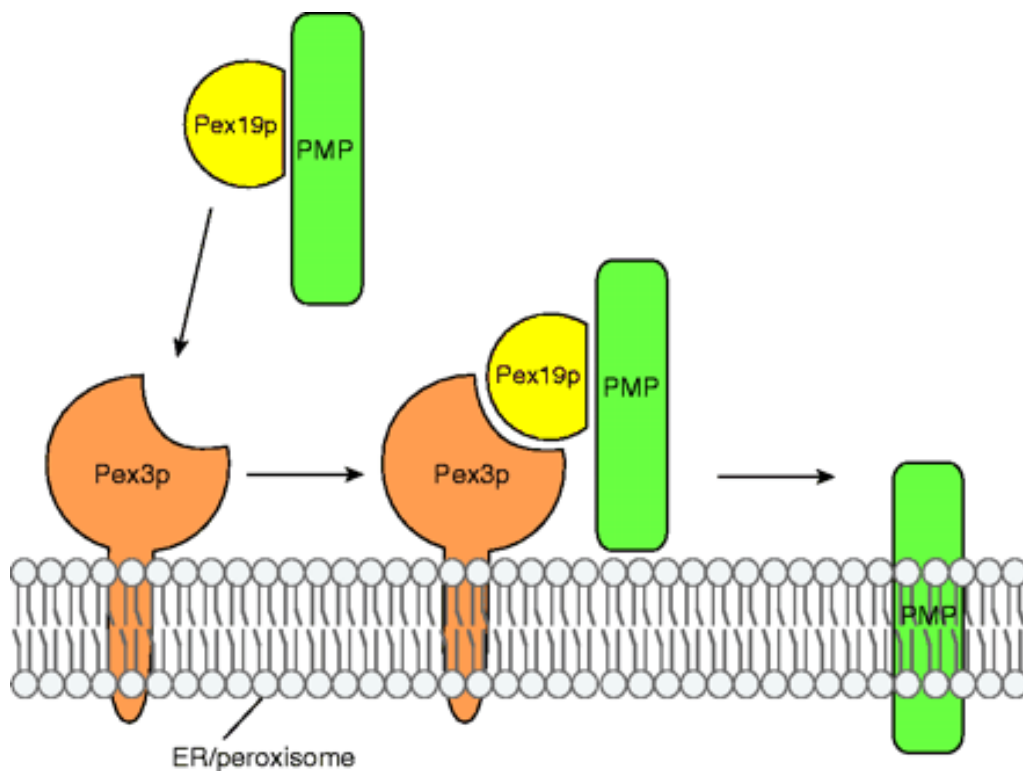
Figure.4. Model for the roles of Pex3p and Pex19p play in the insertion of PMPs into the peroxisomal membrane (van der Zand et al., 2006).

It has been assumed that the formation of the peroxisome initiates insertion of Pex3p into to membrane of the ER. The following step is that Pex19p is recruited to the membrane, resulting in the formation of the "peroxisomal pre-structure". In the cytosol, the Pex19p is continuously involved in the PMPs import by binding PMPs and targeting them to this "pre-peroxisomal" membrane to accomplish peroxisome membrane formation (Eckert and Erdmann, 2003; Hettema et al., 2014). The functional maturation of the "peroxisomal pre-structure" to a peroxisome is achieved with the import of peroxisomal matrix proteins which starts after the completion of the insertion of the PMPs (Eckert and Erdmann, 2003).

The type III PMPs are comprised of early peroxins which are proposed to efficiently target peroxisomes or the "peroxisomal pre-structure" completely independent of Pex19p and Pex3p (Eckert and Erdmann, 2003).

1.1.2.3. Import of peroxisomal matrix proteins

The peroxisomal import machinery accepts folded proteins, oligomerized proteins, and items of large diameter such as gold particles fused to import signals as substrates (McNew and Goodman, 1994; Walton et al., 1995). Most of the peroxisomal proteins are equipped with distinct peroxisomal targeting signals (PTS) which consists of both of PTS1 located in protein carboxyl-terminal with consensus sequence (S/C/A) (K/R/H) (L/M) and PTS2 located in protein amino-terminus with the consensus sequence $(R/K)(L/V/I)(X)_5(H/Q)(L/A)$(Gould et al., 1989; Rachubinski and Subramani, 1995; Rehling et al., 1996; Swinkels et al., 1991). The PTS sufficiently enables peroxisomal matrix proteins to be recognized and guided from the cytosol into the peroxisomal matrix (Subramani, 1993; Wanders, 2004a).

The "shuttling receptor" model of the mechanism for peroxisomal matrix protein translocation has mostly been supported by the latest literature. The predominantly in the cytosol localized proteins Pex5p and Pex7p can individually or simultaneously be recognized, either one or two PTS (Pex5p can recognize

PTS1 and PEX7 can recognize PTS2), which have been harbored in the cytosol formed peroxisomal matrix protein (Dammai and Subramani, 2001; Ghys et al., 2002; Girzalsky et al., 2009; Mukai et al., 2002).Therefore in this model, the Pex5p and Pex7p can be recognized as "PTS receptors" and the peroxisomal matrix protein can recognize it as "cargo" protein. The whole process of this mechanism can be divided into 3 steps. Figure.5. displays the complete translocation machinery for peroxisomal matrix proteins from the cytosol to the peroxisomal matrix.
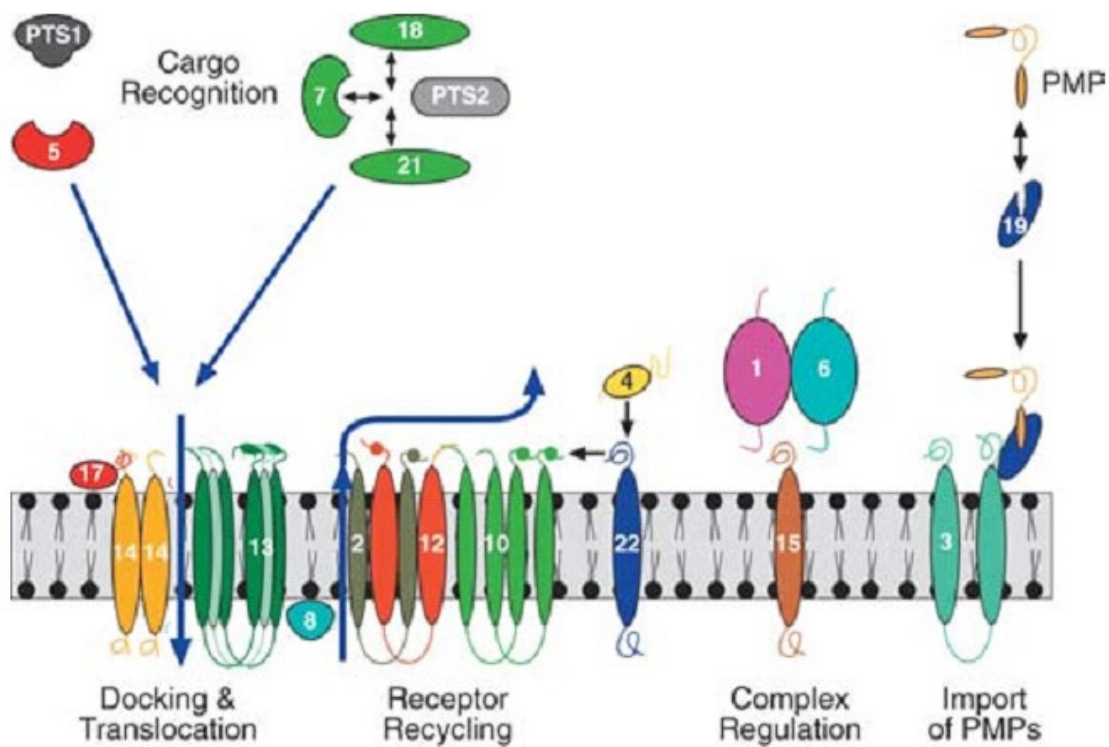
Figure.5. Model of the peroxisomal protein import cascade (Eckert and Erdmann, 2003).

Step 1 - recognition and translocation: This step is the starting event to initiate the peroxisome matrix protein import cascade. The cargo protein can be recognized and bound by PTS receptors, in particular Pex5p and Pex7p, to form an import competent complex the cytosol, followed by the transportation of this

complex to the peroxisomal membrane where common docking and translocation complexes are available for the next step.

Step 2 - peroxisomal membrane docking: The peroxisomal membrane docking system mainly comprises 3 types of peroxisome transmembrane proteins, Pex13p, Pex14p and Pex17p which are featured with Pex5p and Pex7p binding sites (Albertini et al., 1997). Pex13p is a peroxisomal integral membrane protein which plays a direct role in both PTS1 and PTS2 protein import, or indirectly prevents matrix protein import by disrupting peroxisomal membrane formation, in particular, Pex13p is a transmembrane protein which exposes both termini to the cytosol. The N-terminal domain has been shown to provide the binding site for Pex7p (Albertini et al., 1997; Stein et al., 2002). Pex5p and Pex14p bind to the C-terminal Src homologe (SH3) domain of Pex13p (Gould et al., 1996). A typical proline-rich SH3-ligand motif in Pex14p is responsible for the binding to the SH3 domain of Pex13p (Girzalsky et al., 1999; Pires et al., 2003).

Step 3 - dissociation, translocation and lumen releasing: The "receptor-cargo" complex can dissociate from the peroxisomal membrane docking system, followed by the "cargo" protein being released from the "receptor-cargo" complex into the peroxisomal lumen to complete the whole peroxisomal matrix translocation process.

After the dissociation from the complex, the "PTS receptor" proteins Pex5p and Pex7p are destined to be recycled and brought back to the cytosol thus they can be re-used in further translocation cycles.

1.1.2.4. Peroxisome proliferation

Up to now, the mechanism of peroxisome growth and division processes is still not understood. Several genes have been suggested to be involved in peroxisome proliferation. In particular, the dynamin-like protein DLP1 and dynamin-related protein Vps1p, both of which belong to the dynamin family of large GTPases, whose function have been understood as involving in tubulation and fission events of cellular membranes (Danino and Hinshaw, 2001; McNiven,

1998). The dynamin-like protein (DLP1) has been found required for peroxisome fission process in mammalian cells (Koch et al., 2003; Li and Gould, 2003) and further the functional domain of DLP1 has been identified to be responsible for this requirement because the expression of a dominant-negative DLP1 mutant deficient in GTP hydrolysis (K38A) inhibited peroxisomal division (Koch et al., 2003). The dynamin-related protein Vps1p mediates peroxisome division in Saccharomyces cerevisiae (Hoepfner et al., 2001). The general understanding of peroxisome proliferation, which has been mostly accepted, is that the replication of peroxisomes starts from pre-existing peroxisomes fission to form new ones, coordinated by Pex11p (Li and Gould, 2002).

Among the genes or proteins which were suggested to have critical functions for peroxisome proliferation, only Pex11p has been generally and dominantly accepted to have conserved functions for peroxisome proliferation and implicated in the regulation of peroxisome growth in size and abundance (Erdmann and Blobel, 1995; Li et al., 2002a; Li and Gould, 2002; Marshall et al., 1995; Passreiter et al., 1998; Schrader et al., 1998).This mechanism has been supported by the experiments in which peroxisome elongation and vice-versa that subsequent division has been induced by *Pex11* gene overexpression and the peroxisome abundance decrease by the reduction of *Pex11* gene expression (Li et al., 2002b; Marshall et al., 1995; Schrader et al., 1998). The PEX11 proteins exist universally in peroxisomal membranes from yeast, protozoan, parasites to mammal cells. Within them the *Pex11* genes in mammals have been very well investigated and characterized, including three different isoforms, PEX11α, β and γ (Li et al., 2002a; Li et al., 2002b).

The constructive isoform PEX11β can promote peroxisome proliferation in the absence of extracellular stimuli in human and rat cells (Schrader et al., 1998),and *Pex11β* has currently been connected to mechanisms regulating peroxisome proliferation, by which the PEX11β protein plays the role of a coordinator to recruit DLP1 to the peroxisome membrane position where the DLP1 functions as

a 'pinchase' to release the newly formed daughter organelles(Kozlov, 1999). Thereafter the PEX11β protein is separated from DPL1 (Li and Gould, 2003).

However, the roles of these 3 *PEX11 Protein* isoforms in the peroxisome proliferation process are very different and most of the details of the mechanisms on how these genes regulate peroxisome proliferation are still not understood. Even some phenomenons which have been observed are still not understood. There are two typical examples. One phenomenon that has been observed is that PEX11α can regulate peroxisome abundance in response to extracellular stimulation of peroxisome proliferator clofibrate and di-(2-ethylhexyl)-phthalate (Passreiter et al., 1998). In contrast, peroxisome proliferation also occurs in the liver of PEX11α knockout (KO) mice after treatment with both of these drugs (Li et al., 2002a). The second example is that it has been suggested that PEX11β may be involved in the elongation/tubulation of peroxisomes, while DLP1 should mediate peroxisome fission (Koch et al., 2004). In contrast, clusters of elongated tubular peroxisomes have been found on the ultrastructural level in the liver of *Pex11β* KO mice (Li et al., 2002b).

1.1.3. Enzyme composition and metabolic functions in peroxisomes

1.1.3.1. β-oxidation of fatty acids and fatty acid derivatives in peroxisomes

One of the most important functions of peroxisomes is the catabolism of fatty acids and fatty acid derivatives via β-oxidation in plant (Cooper and Beevers, 1969) and animal cells (Lazarow and De Duve, 1976). This process has been studied for more than 40 years. The β-oxidation can basically be understood as a cyclic process by which fatty acids are degraded from their COOH- terminal end. In each cycle the fatty acid carbon chain are shortened with two carbon atoms and one acetyl-CoA being released. The released acetyl-CoA unit can then be degraded in the citric acid cycle to produce CO_2 and H_2O. When comparing the β-oxidation enzymes in different species such as *Homo sapiens*, *Mus musculus* and *Rattus norvegicus* certain enzymes can be found: acyl-CoA oxidase (ACOX), DBP (D-bifunctional enzyme), LBP (L-bifunctional enzyme), SCPx (sterol carrier

protein X), thiolase A, thiolase B (Baumgart et al., 1996a; Baumgart et al., 1996b; Dieuaide-Noubhani et al., 1996). The enzymes involved in the peroxisomal β-oxidation vary depending on the types of fatty acids and different species (Figure. 6.), possess different substrates specificity and vary between species, organs, tissues and cell types (Baumgart, 1997).

Generally, the structural understanding of the peroxisomal β-oxidation system for an acyl-CoA ester is comparable to that of mitochondria and consists of four subsequent steps: (I) oxidation to a 2-*trans*-enoyl-CoA compound (dehydrogenation in mitochondria), (II) hydration of the double bond, (III) a further dehydrogenation and (IV) thiolytic cleavage (Wanders et al., 2010). In peroxisomes, step I is catalyzed by acyl-CoA oxidases producing H_2O_2 during substrate conversion. In contrast the first step of the β-oxidation in mitochondria is catalyzed by acyl-CoA dehydrogenases (ACADs).
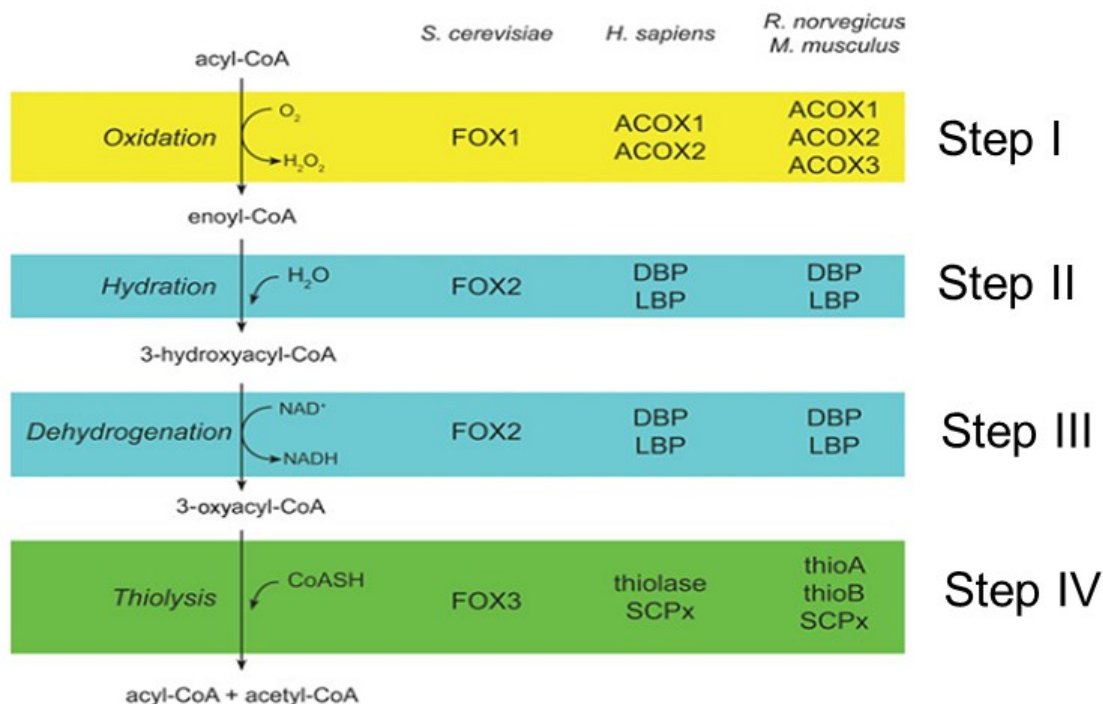
Figure.6. The enzymes involved in each step of the peroxisomal β-oxidation depend on which compound the enzyme reacts with and the different species. The graph was modified from (Visser et al., 2007).

Three types of ACOX enzymes have been discovered in mammals and have been found to work on different targets. ACOX1, also named Palmitoyl-CoA oxidase, is specific for straight-chain fatty acids such as VLCFA and eicosanoids (Baumgart et al., 1996b). The ACOX2 and ACOX3, also named trihydroxycoprostanoyl-CoA oxidase and pristanoyl-CoA oxidase, specifically react with the CoA-esters of bile acid intermediates and 2-methyl branched-chain fatty acids, such as pristanoyl-CoA (Baumgart et al., 1996a).

In comparison to rodents, the human gene of *ACOX3* which is expressed at very low level is not functional, whereas the mRNA and proteins level of the *ACOX1* and *ACOX2* genes are expressed similarly in rodents and man. In humans ACOX2 is involved in the degradation of pristanic acid and bile acid (Vanhooren et al., 1997), dihydroxycholestanoic acid (DHCA) and trihydroxycholestanoic acid (THCA), which is 3-methyl-branched fatty acids and bile acid intermediates (Figure 7) (Baumgart et al., 1996a).
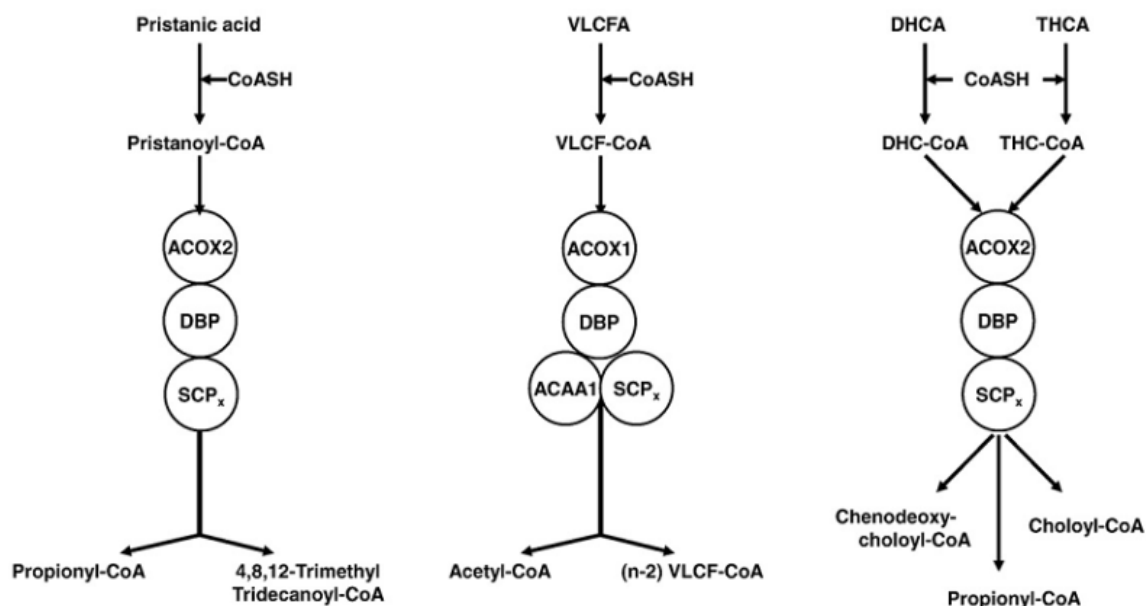
Figure.7. Enzymology of the peroxisomal β-oxidation systems involved in the oxidation of pristanic acid, VLCFA and DHCA/THCA in human (Wanders et al., 2010).

The peroxisomal β-oxidation steps II and III, the hydration of the double bond and the dehydrogenation are carried out by multifunctional proteins (MFPs). The enzymatic activity of enoyl-CoA hydratase and 3-hydroxyacyl-CoA dehydrogenase, by which the enoyl-CoA-esters of VLCFA, pristanic acid, DHCA, and THCA are further metabolized depend on the structure of the fatty acids. Two types of MFPs have been discovered in peroxisomes, such as the MFP2 for pristanic acid and the bile acid intermediates which contain a 2-methyl branch in the carbon chain, whereas the substrates with a straight carbon chain can react universally with both MFP1 and MFP2 (Dieuaide-Noubhani et al., 1997; Van Veldhoven).

Depending on the substrate, two types of enzymes are involved in the step IV of thiolytic cleavage in peroxisomal β-oxidation. (Figure. 7.) The first type of enzyme was found to be involved in the thiolytic cleavage in the liver of rats. Thiolase A and Thiolase B that can act on straight chain ketoacyl-CoAs (Hijikata et al., 1990). The second type of enzyme is the sterol carrier protein X (SCPx) which has

much broader substrates specificity. It catalyzes the cleavage of both straight chain and 2-methyl ketoacyl-CoAs due to its thiolase activity (Antonenkov et al., 1997). In particular, SCPx can react with the 3-keto-acyl-CoA-esters of pristanic acid, DHCA and THCA during peroxisomal β-oxidation (Figure.7.) (Seedorf et al., 1994).

1.1.3.2. The etherphospholipid synthesis in peroxisomes

The biogenesis of etherphospholipids is processed successively in peroxisomes and the ER. The synthesis consists of three steps. The first two steps take place in the peroxisome and are catalyzed by peroxisomal enzymes (Singh et al., 1989; Wanders, 2004b). The first Step: the compound dihydroxyacetonephosphate (DHAP), now named glyceronephosphate (GNP), is converted to acyl-DHAP. This step is catalyzed by the dihydroxyacetone phosphate acyltransferase (DHAPAT or GNPAT). During the second step this product is further converted to alkyl-DHAP, which is catalyzed by alkyldihydroxyacetone phosphate synthase (ADHAPS or AGPS) (Wanders, 2004b). The last step takes place both in the peroxisome and the ER and contains the production of alkylglycerol-3-phosphate (alkyl-G-3P). This step is catalyzed by the enzyme alkyl/acyl-DHAP NAD(P)H oxidoreductase. At the end of the third step the further conversion to plasmogens takes place in the ER (Brites et al., 2004).

The importance of etherphspholipids for cell survival lies in their contribution to biophysical properties of cell membranes. Moreover, etherphospholipids can trap ROS molecules to protect the cell membrane against damage caused by lipid peroxidation (Karnati and Baumgart-Vogt, 2008). One important feature of etherphospholipids is the vinyl ether bond which is especially important for ROS trapping (Brites et al., 2004). Two peroxisomal enzymes DHAPAT (or GNPAT) and ADHAPS (or AGPS) are known to be crucial for etherphospholipid biosynthesis. Brites et al. have determined that patients with deficiencies of either DHAPAT(GNPAT) or ADHAPS(AGPS) lack the etherphospholipid synthesis (Brites et al., 2004).

1.1.3.3. The cholesterol synthesis in peroxisomes

Peroxisomes play a major role in isoprenoid and cholesterol biosynthesis. This fact underlines the importance of this organelle for cells. Especially cholesterol is very abundant in lipid rafts, harboring various functionally different signaling receptors.

There are three strong reasons to recognize that peroxisomes are essential and major cell organelles for the synthesis of isoprenoid and cholesterol. Firstly, acetyl-CoA derived from peroxisomal β-oxidation of very long-chain fatty acids and medium-chain dicarboxylic acids is preferentially channeled to cholesterol synthesis inside the peroxisomes (Kovacs et al., 2007). Secondly, peroxisomal enzymes, in particular the isopentenyl diphosphate delta isomerase (IDI1), mevalonate kinase (MVK), phosphomevalonate kinase (PMVK) and mevalonate pyrophosphate decarboxylase (MPD), can catalyze conversion of mevalonate to farnesyl diphosphate (FPP), which is an essential step for isoprenoid and cholesterol synthesis. The conversion of FPP to lanosterol is believed to occur in the ER (Kovacs et al., 2002; Kovacs et al., 2007). Last but not least, the literature also reveals that peroxisomes play a vital role in the maintenance of cholesterol homeostasis (Kovacs et al., 2004).

1.1.3.4. Metabolism of reactive oxygen and nitrogen species in peroxisomes

Interestingly, lipid and reactive oxygen species (ROS) metabolisms are tightly related to each other, thus the peroxisome could be involved in the role of "metabolic signaling" (Karnati and Baumgart-Vogt, 2008) to regulate osteoblast (OB) differentiation and functions. According to the latest literature, more and more peroxisomal functions in the production and degradation of ROS and reactive nitrogen species (RNS) have been found (Fransen et al., 2012). Further, it has been realized that peroxisomes play a critical role in cell metabolism in addition to mitochondria. The peroxisomal enzymes involved in the production and scavenging of ROS (pro-and antioxidative enzymes) shown in the table below (Table.2.).

Table.2. **Enzymes which generate ROS and antioxidative enzymes in mammalian peroxisomes (Antonenkov et al., 2010; Fransen et al., 2012). The Mn-superoxide dismutase (SOD2) used to be recognized as the peroxisome antioxidant enzyme, until it has been found that it is actually located solely within the mitochondrial matrix (Karnati et al., 2013).**

| Enzymes in mammalian peroxisomes that generate ROS | | | Antioxidative enzymes in mammalian peroxisomes | |
Enzyme	Substrate	ROS	Enzyme	Substrate
Palmitoyl-CoA oxidase	Long- and very long-chain fatty acids, dicarboxylic fatty acids, glutaryl-CoA	H_2O_2	Catalase	H_2O_2
Pristanoyl-CoA oxidase	2-Methyl-branched fatty acids	H_2O_2	Peroxiredoxin I	H_2O_2
Trihydroxycoprostanoyl-CoA	Bile acids intermediates	H_2O_2	Peroxiredoxin V (PMP20)	H_2O_2
Urate oxidase	Uric acid	H_2O_2	Cu/Zn-superoxide dismutase (SOD1)	$O_2^{\cdot-}$
L-α-hydroxyacid oxidases	Glycolate, lactate, medium- and long chain 2-hydroxyacids	H_2O_2	Epoxide hydrolase	Epoxides
Polyamine oxidase	*N*-acetyl spermine/spermidine	H_2O_2	Soluble glutathione S-transferase (member of kappa family)	Hydroperoxides
Pipecolic acid oxidase	L-Pipecolic acid	H_2O_2	Membrane bound ('microsomal') glutathione S-transferase	Lipid hydroperoxides
Sarcosine oxidase	Sarcosine, L-proline	H_2O_2		
D-amino acid oxidase	D-isomers of neutral and basic amino acids	H_2O_2		
D-aspartate oxidase	D-isomers of acidic amino acids	H_2O_2		
Xanthine oxidase	Hypoxanthine, xanthine	$O_2^{\cdot-}$		
NO synthase, inducible	L-arginine	$\cdot NO$		

Actually, ROS are mostly generated by mammalian peroxisomes which contain various enzymes called FAD (or FMN)-dependent oxidases. ROS are byproducts from functional catalytic activities of these enzymes, such as the H_2O_2 that is generated during the conversion of their substrates. As shown in Table.2. H_2O_2 is the most popular type of ROS present in mammalian peroxisomes. Further types of ROS such as the superoxide radicals and NO produced by xanthine oxidase or the inducible form of nitric oxide synthase have also been found in functioning peroxisomes (Angermüller et al., 1986; Loughran et al., 2005).

In addition to the formation of ROS due to peroxisomal catalytic functional activities that could potentially damage the cell and initiate an alteration of cell signaling, peroxisomes can also function as an antioxidant defence system to maintain the oxidative homeostasis within and outside of the organelle due to their enzyme content of a variety of antioxidant enzymes. Especially Catalase is the most potent and fast enzyme degrading H_2O_2. Functional peroxisomes retains abundant amounts of various, I and V, SOD1, Epoxide hydrolase and glutathione S-transferase Peroxiredoxin (Table.2.) to decompose of ROS. Catalase and peroxiredoxins are targeted to the peroxisome via a modified PTS1 signaling peptide and are present in the peroxisomal matrix of most mammalian cells. Moreover, Catalase is typical peroxisomal matrix enzyme that metabolizes H_2O_2 in a parallel with variety of substrates, such as ethanol, methanol, phenol and nitrites by its peroxidative activity (Oshino et al., 1973).

1.1.3.5. Summary on the enzyme composition and metabolical functions of the peroxisome

Peroxisomal metabolic functions and the peroxisomal enzymes involved in these functions are summarized in blue schematic diagram in Figure.8.
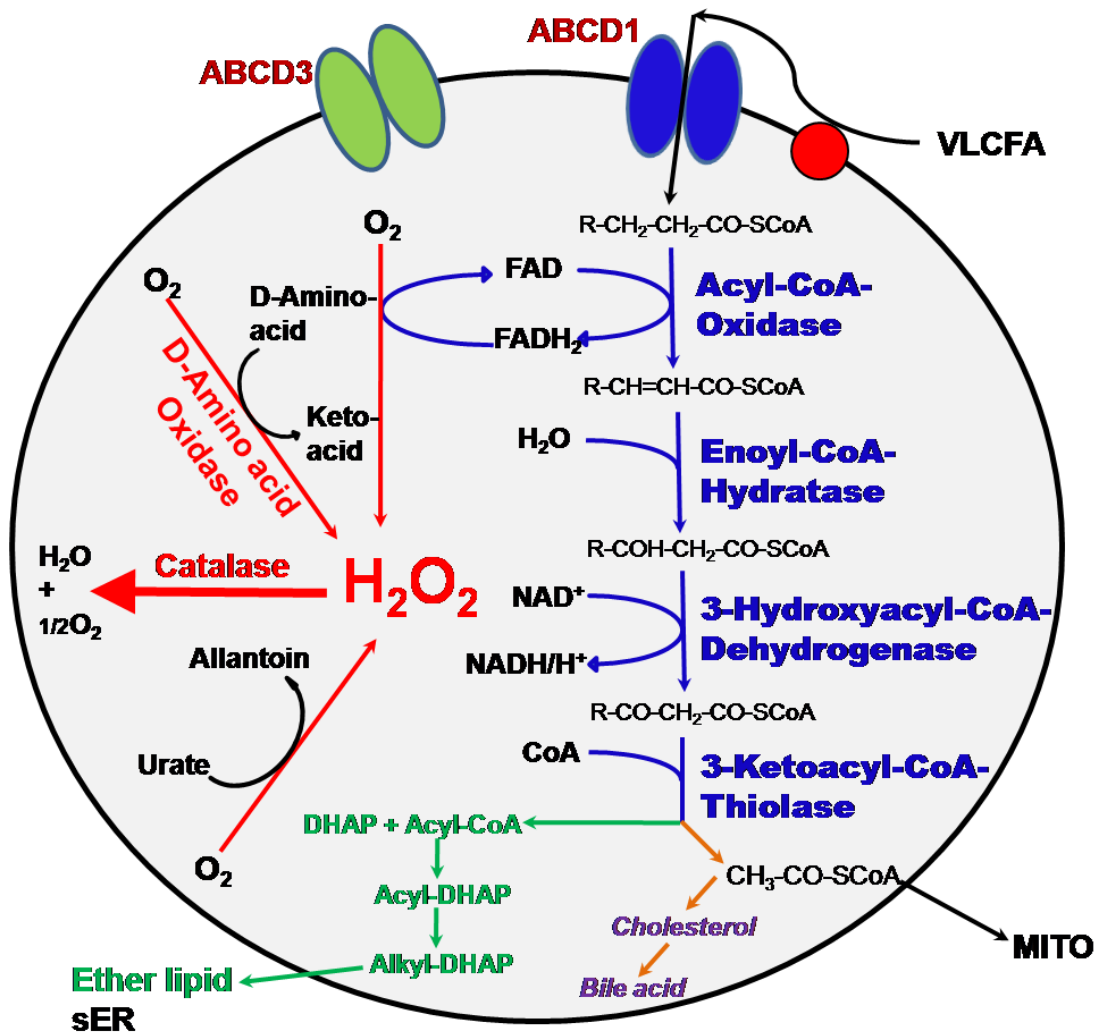
Figure.8. This scheme depicts the general functions of peroxisomes, including H$_2$O$_2$ metabolism, β-oxidation of distinct lipid derivatives as well as the synthesis of cholesterol and etherlipids. The picture was designed and provided with courtesy by Prof. Dr. Baumgart-Vogt.

1.2. Peroxisome biogenesis disorders

1.2.1. The peroxisome biogenesis disorders and human diseases

Peroxisome biogenesis disorders (PBDs) are defined as human diseases caused by the absence or deficiency in peroxisome biogenesis. PBDs are autosomal recessive diseases that arise from mutations in *PEX* genes that encode peroxins, required for the normal biogenesis of peroxisomes (Distel et al., 1996; Gould and Valle, 2000). Mutations in peroxins directly disrupt the apparatus required for the import of matrix proteins into the peroxisome containing a PTS1 or PTS2 peroxisomal targeting signal. Zellweger syndrome (ZS), neonatal adrenoleukodystrophy (NALD), and infantile Refsum's disease (IRD) represent a clinical continuum of autosomal recessive disease, called the disease of the Zellweger spectrum, with ZS being the most severe and IRD being the mildest form of the phenotypic spectrum (Maxwell et al., 2003). ZS is a multiple congenital anomaly syndrome and the patients show craniofacial abnormalities, including a high forehead, hypoplastic supraorbital ridges, epicanthal folds, midface hypoplasia, and a large anterior fontanel, accompanied by eye abnormalities, neuronal migration defects, hepatomegaly, and chondrodysplasia punctate(Steinberg et al., 2006; Wilson et al., 1986). Children with ZS exhibit typical skeletal deformations (Figure.9.), defects in the central nervous system, kidney cysts, liver cirrhosis, and adrenal insufficiency. Up to now, no curative treatment and therapy methodology are available for ZS patients and most of them survive less than a year(Gould and Valle, 2000).

Figure.9. Children with ZS exhibit skull deformities, a low nose saddle, hypertelorism, migrognathia and low ears. (Courtesy of Prof. R.J.A. Wanders, Amsterdam, Netherlands).

Another type of a peroxiosomal biogenesis disorder with disruption of peroxisomal function protein is the PEX7 deficiency which causes rhizomelic chondrodysplasia punctata (RCDP) type 1 (Heymans et al., 1985; Purdue et al., 1999). The RCDP shows a severe bone phenotype, the patients suffer from shortened long bones (humerus and femur) and shortened proximal limbs(Agamanolis and Novak, 1995; Braverman et al., 1997; Motley et al., 1997; Purdue et al., 1997; Shimozawa, 2007).

1.2.2. Animal models for peroxisome biogenesis disorders

Animal models for ZS have been developed through targeted disruption of the *Pex2* (Faust and Hatten, 1997) *Pex5* (Baes et al., 1997), *Pex11β* (Li et al., 2002b) and the *Pex13* (Maxwell et al., 2003) genes. All four knockout animals exhibit many of the organ abnormalities typical of ZS, including hypotonia and impaired neocortex and cerebellar neuronal migration and maturation and die at or shortly after birth. In this dissertation, two of the animal models were used and will be described in the following. Newborn pups with the typical ZS phenotype of mouse lines are shown in Figure.10. and 11.

The function of PEX13 in docking complex for matrix protein import has been described in chapter 1.1.2.3.
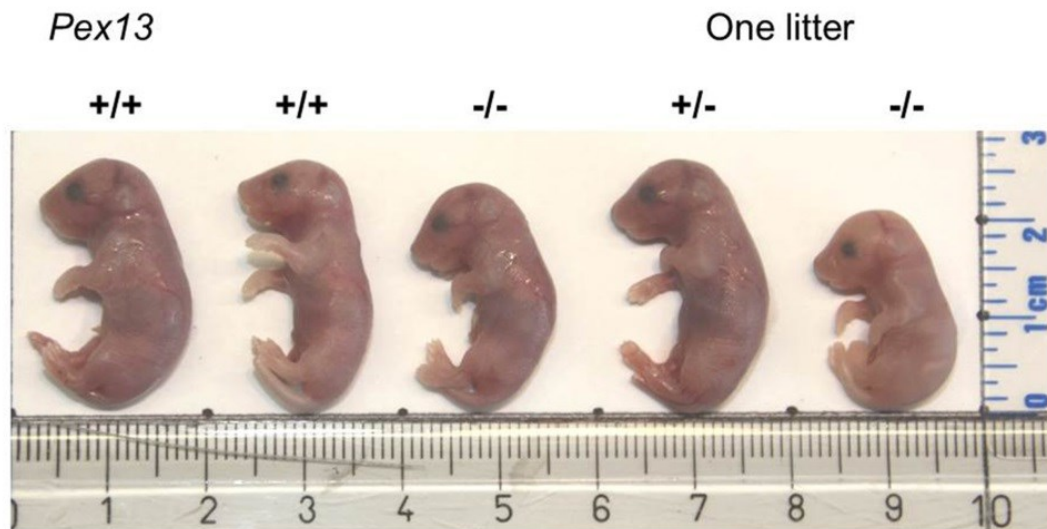
Figure.10. Appearance of new born pups with *Pex13* KO exhibiting a typical Zellweger phenotype (Picture was taken in our laboratory, prior to the picture the new born pups were scanned with flat-panel volumetric computed tomography**).**

The mouse mutant model with general *Pex13* disruption was generated by exon2 deletion in embryonic stem cell (ES) cells via the Cre/LoxP system. Pex13 mice exhibit many of the features of ZS patients, including intrauterine growth retardation, hypotonia, abnormal peroxisomal metabolism, and neonatal lethality. This phenotype is associated with defective peroxisome biogenesis and matrix import (Maxwell et al., 2003).

Compared to the *Pex13* knockout animal model, another ZS mouse model is the *Pex11β* knockout mouse which showed despite hardly altered biochemical peroxisomal matrix, the typical ZS phenotype, including hypotonia, a developmental delay, growth defects and a neuronal migration defect (Figure.11.).
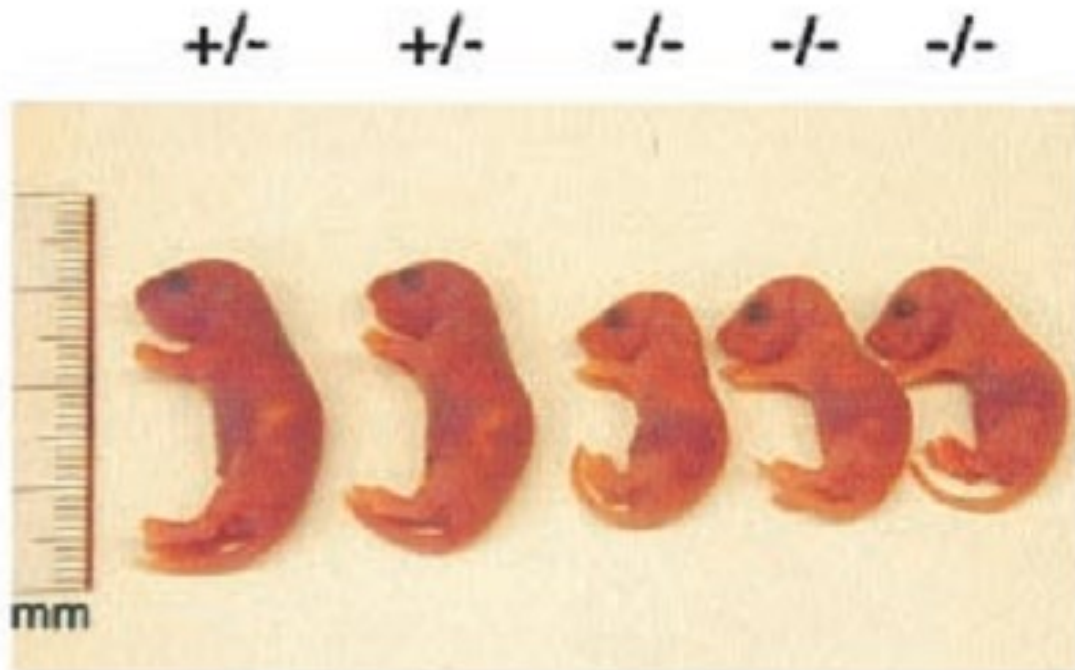
Figure.11. Appearance of new born pups of *Pex11β* KO Mice, exhibiting stronger growth retardation phenotype than *Pex13* KO mice with Zellweger syndrome. One litter of newborn mice with Pex11β gene heterozygous (+/-) and homozygous (-/-) offspring are depicted, the pups were anesthetized to take the picture.(Li et al., 2002b).

In *Pex11β* KO mice, peroxisomes proliferation is detective, but organelles are present and functional as matrix proteins are imported normally. Despite this fact, the animals exhibit the typical morphological alterations of Zellweger syndrome (Li et al., 2002b). Interestingly, the peroxisomes in the animal models only show mild defects in their peroxisomal metabolical functions (Li et al., 2002b), even though in the literature before the assumption was made that the ZS pathogenesis in other animal models was caused by pathological defects in the VLCFA accumulation or plasmalogen deficiency.

1.3. Cells of the bone and their role in bone remodeling and the pathogenesis of osteoporosis

1.3.1. The major types of bone cells and functions

The bone cells, the organic matrix and mineral phase are three major components of the bone. Mineralized mature bone is made up by hydroxyapatite which is the crystallized state of calcium phosphate precipitation. This mineralized structure provides in the compressive strength and rigidity of mature bones. Three major types of cells, osteoclasts, osteoblasts and osteocytes with distinct functional features, are the key components of mammalian bone (see Figure 12). These cells play important role in the formation of the skeletal elements during embryogenesis and regulate homeostasis of dynamic bone remodeling in adult bones. Further a mineral phase and a significant amount of extracellular matrix are necessary for the osteogenesis. The ossification and bone remodeling are developmental precisely cooperated interplay process involved by different transcription factors and signaling proteins. Thus, dysfunctions or dysregulation of it can result in a number of human diseases, such as cleidocranial dysplasia and osteoporosis (Lian et al., 2004).
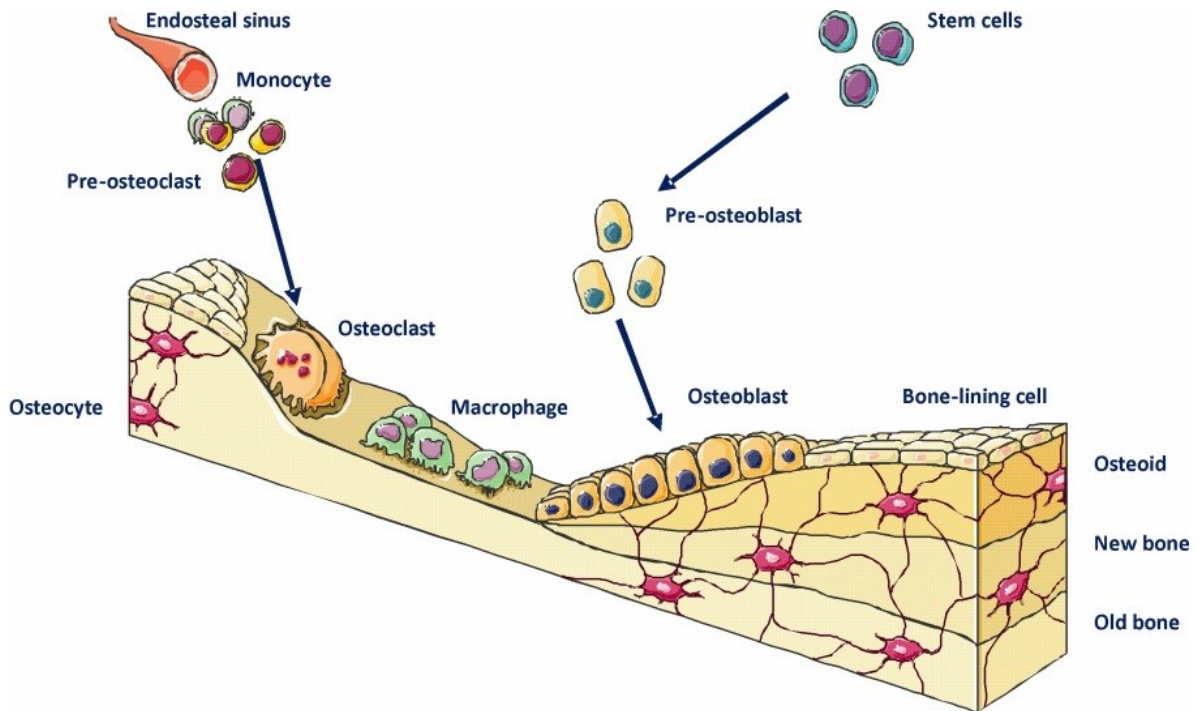
Figure.12. Schematic representation of the functional structures and locations of the three main types of bone cells: osteoblasts, osteocytes and osteoclasts, and the role of these 3 basic cell types in the bone remodeling process (Ewa, 2011).

The osteoblasts derive from mesenchymal stem cells (MSC) differentiation and synthesize the bone matrix (see section 1.3.2.1).

The osteocytes are normally recognized as the mature or post matured forms of osteoblasts that become trapped within calcified bone. The osteocytes play critical role in the osteogenic response to the stimuli of mechanical stress on bone. The bone remodelling process can be initiated by osteocytes with production of chemical messenger cascades once the physical strains have been sensed by it (Lanyon, 1992).

The osteoclasts are differentiated from precursors of the monocyte macrophage lineage. To date their morphological identity is characterized by an efficient multinucleate cell, featured with uncertain lifespan and ultimate fate. The osteoclast degrades bone by attaching to a bone matrix surface and by secreting chloric acids and enzymes which can absorb the anorganic and organic components of bone matrix. Osteoclast absorb to the surface in a manner of

mobilizing themselves from one eroding pit of mineralized surface to another site (Suda et al., 1992).

1.3.2. Osteobiogenesis, osteoblast differentiation and functional alterations

1.3.2.1. The differentiation process of osteoblast and osteoblast maturation stage markers

As mentioned above, the mature and functioning osteoblast originally are differentiated from MSC. However the whole differentiation process consists of several stages. Each stage can be identified by detecting of the expression levels of marker proteins. Early stage markers include the collagen, type I, alpha 1 and 2 (*Col1a1 and Col1a2*) and master regulator runt-related transcription factor 2 (Runx2) which decreases in expression in mature osteoblast. Further mature stage makers among others are osterix (Osx) and Bone γ-carboxyglutamic acid-containing protein (*Bglap*=osteocalcin) (Table. 3.). These marker proteins can be used as an indicator for the OB differentiation process. For instance, the expression of many middle-mature stage markers, particularly osteopontin (Opn) and integrin-binding sialoprotein (Ibsp), are abundant in the pre-osteoblast indicating the pre-mature differentiation of pre-osteoblasts occurred.

Table.3. The summary of the osteoblast differentiation stages and expression of marker proteins with schematic representation.

Stage	Osteoblast Progenitor	Early stage Pre-osteoblast	Pre-osteoblast	Mature osteoblast	Osteocyte
Markers	Col1a1 Col1a2 Runx2	Runx2 ALP	Runx2 OPN IBSP	IBSP OPN OSX	BGLAP OSX

1.3.2.2. Oxidative stress, age-related osteoblast differentiation delay and bone loss

It has been known that loss of bone mass with advancing age in mice is caused by a decline in the abundance of osteoblasts and is associated with increased oxidative stress and decreased canonical Wnt signaling. The secreted proteins bind either to the Frizzled receptor, or the low density lipoprotein receptor-related protein 5 (LRP5) and LRP6 co-receptors, resulting in an increasing level of β-catenin by preventing its degradation by the proteasome (Bodine, 2008; Glass and Karsenty, 2006a, b; Rodda and McMahon, 2006). It also has been found that age-related increased lipid oxidation product 4-hydroxynonenal (4-HNE) as well as an increased expression peroxisome proliferator-activated receptor-γ (PPARγ) were associated with bone loss in the skeleton (Almeida et al., 2009).

The model of the suppression of β-catenin via an oxidized lipid-activated ROS/FoxO/PPARγ/β-catenin cascade was established to demonstrate the afore mentioned mechanism (see section 1.3.1 and Figure.13.). There are two consequences of the oxidation of Polyunsaturated fatty acid (PUFA) generated by ROS and lipoxygenases which increase the oxidative burden of the skeleton via the generation of 4-HNE. Firstly, oxidative stress activates the forkhead box O (FoxO) family of transcription factors, which in turn attenuate β-catenin/T-cell factor (TCF)-mediated transcription because of competition between FoxO and TCF for a limited pool of β-catenin, leading to derepression of *PPARγ* transcriptional capability. Secondly, oxidized PUFAs activate PPARγ with the oxidation products as ligand and active the PPARγ transcriptional activity. For both of the consequences, the activation of PPARγ will result in decrease of osteoblastogenesis and increase of adipogenesis (Almeida et al., 2009).

Via this cascade, lipid oxidation contributes to the decline in osteoblast number and bone formation that occurs with aging by attenuating the canonical Wnt signaling required for the differentiation and survival of osteoblasts (Almeida et al., 2009).
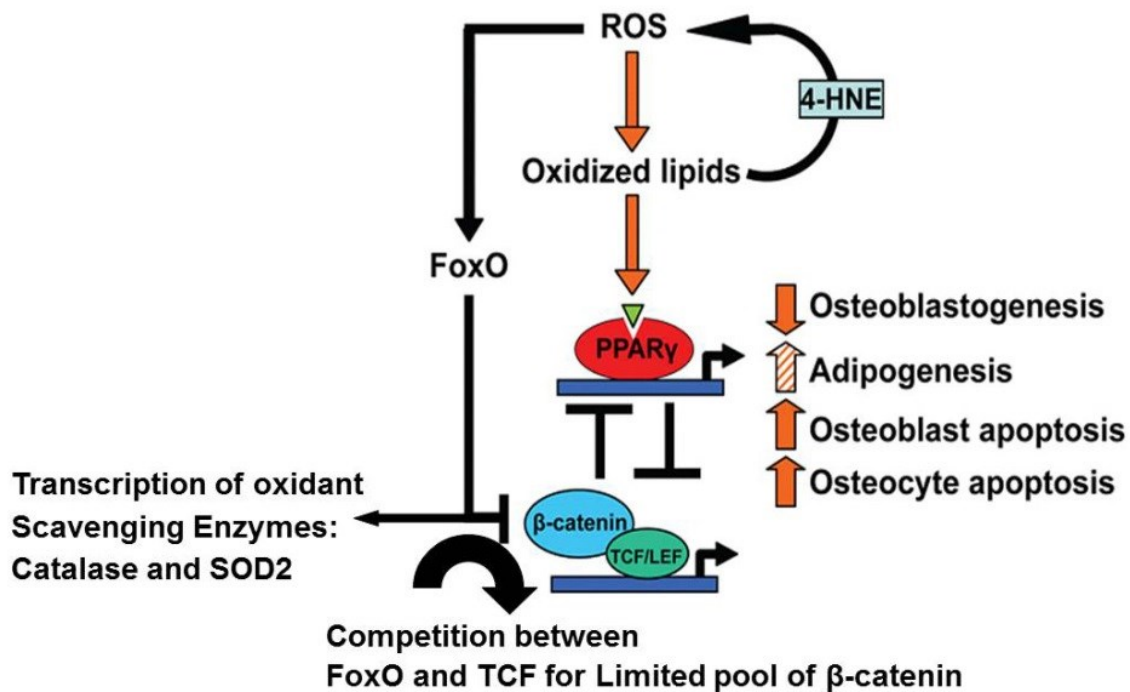
Figure.13. Suppression of β-catenin by an oxidized lipid-activated ROS/FoxO/PPARγ/β-catenin cascade, leading to a decreased bone formation. Graph modified from (Almeida et al., 2009).

Regarding the facts, oxidative stress compromises the functions of canonical Wnt signaling in the regulation of OB differentiation from MSC with the negative role of PPARγ in this circumstance. The activation of this cascade contributes to the osteoblast differentiation defect and the loss of bone with age. Because the activation of PPARγ regulates the proliferation and the quantity of peroxisomes in a positive manner, we hypothesize that peroxisomes at least partially play a role in maintaining the homeostasis between oxidative stress, lipid ligands and osteoblastogenesis.

1.3.2.3. Regulation of the bone absorption by osteoblast via the RANKL/OBG system
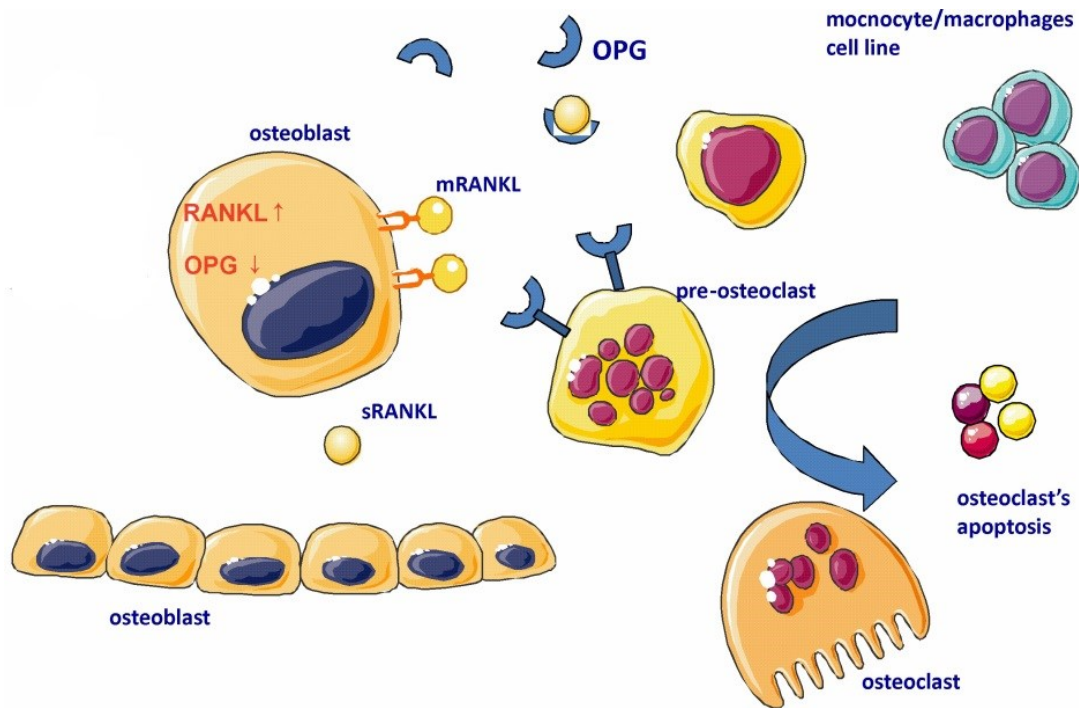
Figure.14. The role of osteoblasts in the mechanism of pre-osteoclast differentiation via osteoprotegerin (OPG) on the receptor activator of nuclear factor κ-B ligand (RANKL) mechanism. OPG can trap and neutralize of RANKL which activate osteoclasts by its receptor RANK(Ewa, 2011).

In addition to osteoblasts that promote the formation of bone, another key player in adult bone homeostasis is the osteoclasts (Harada and Rodan, 2003). The multinucleate cells derive from precursors of the monocyte–macrophage lineage (Boyle et al., 2003). These osteoclast cells can degrade bone tissue efficiently by removing its mineralized matrix and breaking up the organic bone structure (Boyle et al., 2003). Therefore, the amount of adult bone tissue is highly dynamically maintained by the remodeling process, which is in turn controlled by the interplay of osteoclasts and osteoblasts. This remodeling provides the adult bone with a mechanism for self-repair and adaptation to stress. Consequently, the differentiation and proliferation of osteoblast and osteoclast progenitor cells

significantly influences the reabsorption and formation of bone. Although the mechanisms of osteoblast and osteoclast differentiation are different with distinct progenitors, the differentiation and functions of them are strongly regulated by cytokine interactions with these two types of bone cells(Khosla, 2001). Two cytokines are expressed and released from osteoblasts. The macrophage colony-stimulating factor (M-CSF) and receptor activator of NF-κB ligand (RANKL) are essential for the genesis of osteoclasts (Figure.14.). The RANKL binds the membrane-anchored receptor activator of the nuclear factor κB (RANK), on the surfaces of both osteoclast progenitors and mature osteoclasts, inducing the activation of the nuclear factor of activated T cells cytoplasmic 1 (NFATc1) and promoting the osteoclastogenesis (Khosla, 2001; Nakashima and Takayanagi, 2011). The RANKL/RANK cascade can be blocked by osteoprotegerin (OPG), a cytokine and a soluble decoy receptor of RANKL produced by osteoblasts that prevents RANKL from binding to RANK, thus limiting osteoclast formation(Khosla, 2001). Therefore, the extent of proliferation and differentiation of osteoclast progenitors in bone and even the bone mass are determined by the relative concentrations of RANKL and OPG (Boyce et al., 2012).

1.4. Bone phenotype and peroxisomal phenotype in the *Sirt1* KO mouse model

Sirtuins are highly conserved NAD^+-dependent protein deacetylases and/or ADP-ribosyltransferases that can extend the lifespan of several animal models. The mammalian Sir2 ortholog, SIRT1, is known to be a global deacetylase that deacetylates many transcriptional factors and cofactors, playing an important role in aging and disease (Guarente, 2011; Imai et al., 2000; Li and Kazgan, 2011). Recent studies have shown that SIRT1 is a key regulator of bone development and remodeling. For instance, SIRT1 transgenic mice are protected from age-induced bone loss (Herranz et al., 2010). Conversely, SIRT1 heterozygous female mice display a reduction in bone mass due to decreased bone formation and increased marrow adipogenesis (Cohen-Kfir et al., 2011). Moreover, specific

deletion of SIRT1 in mesenchymal stem cells leads to decreased MSC differentiation to osteoblasts and chondrocytes, as well as a reduction in cortical bone thickness and trabecular volume in mice (Simic et al., 2013). A few pathways have been proposed to explain the observed role of SIRT1 in bone development and remodeling, such as deacetylation and activation of β-catenin, a Wnt signaling molecule involved in the self-renewal and differentiation of mesenchymal stem cells (Ling et al., 2009). However, SIRT1 could potentially affect bone homeostasis partially through other signaling pathways, particularly the PPARs. PPARs, including PPARα, β/σ, and γ, belong to the nuclear receptor superfamily. The PPARs form heterodimers with the retinoid X receptor (RXR), on function as lipid sensors through the direct binding of a variety of natural lipids and synthetic agonists, such as peroxisome proliferators, to the ligand-binding domain. Upon lipid binding, each of these receptors activates the transcription of a family of genes involved in lipid homeostasis, including many peroxisomal enzymes and proliferating proteins, thereby modulating systemic energy metabolism in response to nutrient availability (Shulman and Mangelsdorf, 2005).

In this dissertation, using primary osteoblast and osteoblast cell line, as well as SIRT1 knockout mouse model, I could show that SIRT1 regulates osteoblast differentiation and functions in part through the modulation of peroxisomal function. Loss of SIRT1 leads to pre-mature differentiation of pre-osteoblasts and impairs peroxisome biogenesis and function and further results in abnormal bone development in mice.

In addition to the peroxisome proliferator-activated receptor γ-coactivator 1α (Pgc -1α), Sirt1 has been found to regulate the activity and/or transcription of protein kinase B, mammalian target of rapamycin (mTOR) , FoxO 1 and 3a and myogenic determination factor, all of which are central players in the regulation of the energy status in skeletal muscle via actions on catabolic and anabolic signaling (Ryall, 2012).

2. Aims of the study

The strong calcification of cartilage in the patella and the growth plate, as well as ossification defect inducing and bone deformation in ZS patients, suggest that the peroxisome may play a very important role in ossification and bone development(Qian, 2010a): Previous research in our laboratory has revealed that the numerical abundance and the enzyme composition in all distinct cell types of the skeleton are significantly different and are increased as long as OB are approaching to maturation (Qian, 2010a). Moreover, peroxisome are very abundant in proliferating and even more abundant in hypertrophic cartilage of growth plates(Qian, 2010a). Therefore, we hypothesized that the peroxisomes play an important role in maintaining the homeostasis of bone cell ROS and lipid metabolism, the dysfunction of peroxisomes should be induced by peroxisome biogenesis deficiency, moreover should result in accumulation of lipids and ROS leading in consequences to lipid toxicity and increased oxidative stress. By these mechanisms, bone mineralization could be delayed by OB differentiation and maturation defect. To test these above hypotheses, the aims of my research were:

1. To investigate whether peroxisome deficiency would interfere with OB differentiation and maturation and how the normal functions of OB is disturbed by the peroxisome defect in using primary OB cells isolated from the calvaria of *Pex11β* and *Pex13* KO mice model.

2. To investigate the different mechanisms resulting in the osteoblast differentiation delay or osteoblast dysfunction induced by *Pex11β* and *Pex13* deficiency.

3. Since the SIRT1 control lipid metabolism via PGC1α and regulates PPAR functions and thus peroxisome genes are regulated by these nuclear receptors (Li, 2013), therefore, *Sirt1* KO/WT animals and *Sirt1* KO/WT OB were used to characterize the alteration induced in stem cell recruitment, ossification, and mice OB differentiation. A major focus has been laid in

characterizing the peroxisomal compartment and related gene expression in the *Sirt1* KO animal model.

3. Materials and Methods

3.1. General Materials used in the laboratory

3.1.1. Chemicals for the general application of molecular and morphological experiments

The chemicals used in this thesis with corresponding suppliers are listed in Table.4.:

Table.4. The chemicals used in experiments

Chemicals	Company name
Acrylamide	Roth, Karlsruhe, Germany
Agarose LE	Roche, Grenzach-Wyhlen, Germany
Alizarin Red S	Fluka, Neu-Ulm, Germany
Ascorbic acid	Sigma, Steinheim, Germany
Bradford reagent	Sigma, Steinheim, Germany
Bromophenol blue	Riedel-de-Haën, Seelze, Germany
Calcium chloride	Merck, Darmstadt, Germany
Ciprofibrate	Sigma, Steinheim, Germany
Citric acid	Merck, Darmstadt, Germany
Di-Potassium hydrogen phosphate	Merck, Darmstadt, Germany
Ethanol	Riedel-de-Haën, Seelze, Germany
Ethidium bromide	Fluka, Neu-Ulm, Germany
Ethylene diamine tetraacetic acid (EDTA)	Fluka, Neu-Ulm, Germany
Ethylene glycol-bis (2-aminoethylether)-N,N,N′,N′-tetraacetic acid (EGTA)	Fluka, Neu-Ulm, Germany

Glycine	Roth, Karlsruhe, Germany
Glycerol	Sigma, Steinheim, Germany
β-glycerolphosphate	Sigma, Steinheim, Germany
Hydrogen peroxide	Merck, Darmstadt, Germany
4-(2-Hydroxyethyl)-1-piperazineethanesulfonic acid (HEPES)	Roth, Karlsruhe, Germany
Ketamin	Bayer, Leverkusen, Germany
L-Glutamate	Cambrex BioScience, MD, USA
Mowiol 4-88	Polysciences, Eppelheim, Germany
3-[N-Morpholino]-propanesulfonic acid (MOPS)	Serva, Heidelberg, Germany
N-ACETYL-L-CYSTEINE	Sigma, Steinheim, Germany
N-Propyl-gallate	Sigma, Steinheim, Germany
Paraformaldehyde (PFA)	Sigma, Steinheim, Germany
Penicillin/Streptomycin	PAN Biotech, Aidenbach, Germany
Phenylmethanesulfonyl fluoride (PMSF)	Serva, Heidelberg, Germany
Ponceau S	Serva, Heidelberg, Germany
Potassium dihydrogen phosphate	Merck, Darmstadt, Germany
Potassium hydroxide	Fluka, Neu-Ulm, Germany
Rotiphorese Gel 30	Roth, Karlsruhe, Germany
RNaseZap	Sigma, Steinheim, Germany
Sodium carbonate	Merck, Darmstadt, Germany
Sodium chloride	Roth, Karlsruhe, Germany
Sodium hydrogen carbonate	Merck, Darmstadt, Germany
Sodium hydroxide	Merck, Darmstadt, Germany
Sucrose	Merck, Darmstadt, Germany
Sodium dodecyl sulphate (SDS)	Sigma, Steinheim, Germany

Tetramethylethylenediamine (TEMED)	Roth, Karlsruhe, Germany
Trishydroxymethylaminomethane (Tris)	Merck, Darmstadt, Germany
Triton X-100	Sigma, Steinheim, Germany
Trypan blue	Sigma, Steinheim, Germany
Tween 20	Fluka, Steinheim, Germany
Uranyl acetate	Merck, Darmstadt, Germany
Xylene	Merck, Darmstadt, Germany

3.1.2. Laboratory general instruments

All instruments used for the experimental parts of this thesis are summarized with appropriate supplier in Table.5. and listed in alphabetical order:

Table.5. Laboratory general instruments used in experiments listed by alphabetical order.

Type of Instruments	Manufacturer
AGFA Horizon Ultra Colour Scanner	AGFA, Mortsel, Belgium
Biocell A10 water system	Milli Q-Millipore, Schwalbach, Germany
Biofuge Fresco	Heraeus, Hanau, Germany
Biofuge Pico	Heraeus, Hanau, Germany
Bio-Rad electrophoresis apparatus (Sub Cell GT) system	Bio-Rad, Heidelberg, Germany
Dish washing machine (G 78 83 CD)	Miele, Gütersloh, Germany
Cary 50 Bio-UV-visible spectrophotometer	Varian, Darmstadt, Germany
Gel-Doc 2000 gel documentation system	Bio-Rad, Heidelberg, Germany
Flat–panel volumetric computed tomography (Obert et al., 2005)	GE medical systems, Milwaukee, WI
Fraction collector Heidolph pump drive 5101	Heidolph Instruments, Schwabach, Germany

Hera cell 240 incubator	Heraeus, Hanau, Germany
Hera safe, clean bench KS-12	Heraeus, Hanau, Germany
Ice machine, Scotsman AF-100	Scotsman Ice Systems, Vernon Hills, IL, USA
I Cycler PCR machine MiQ2 optical module	Bio-Rad, Heidelberg, Germany
Leica DMRD fluorescence microscope	Leica, Bensheim, Germany
Leica DC 480 camera	Leica, Bensheim, Germany
Leica TP1020 embedding machine	Leica, Nussloch, Germany
Leica TCS SP2 confocal laser scanning microscope	Leica, Nussloch, Germany
Leica SM 2000R rotation microtome	Leica, Nussloch, Germany
Microwave oven MB-392445	LG, Willich, Germany
Mini-Protean 3 cell gel chamber	Bio-Rad, Heidelberg, Germany
Microtome stretching water bath Type 1003	Vieth Enno, Wiesmoor, Germany
Multifuge 3 SR centrifuge	Heraeus, Hanau, Germany
Oven HERAEUS T 5050 EKP	Heraeus, Hanau, Germany
pH meter E163649	IKA, Weilheim, Germany
Pipettes	Eppendorf, Hamburg, Germany
Potter-Elvehjem homogenizer 8533024	B.Braun, Melsungen, Germany
Power supply - 200, 300 and 3000 Xi	Bio-Rad, Heidelberg, Germany
Pressure/Vacuum Autoclave FVA/3	Fedegari, Albuzzano, Italy
Pump Drive PD 5001	Heidolph Instruments, Schwabach, Germany
Sorvall Evolution RC centrifuge	Kendro, NC, USA
SmartspecTM 3000 spectrophotometer	Bio-Rad, Heidelberg, Germany
T25 basic homogenizer	IKA, Staufen, Germany

Thermo plate HBT 130	Medax, Kiel, Germany
Thermo mixer HBT 130	HLC, BioTech, Bovenden, Germany
Trans-Blot SD semi dry transfer cell	Bio-Rad, Heidelberg, Germany
TRIO-thermoblock	Biometra, Göttingen, Germany
Ultra balance LA120 S	Sartorius, Göttingen, Germany
Ultra Turrax T25 basic homogenizer	Junke & Kunkel, Staufen, Germany
Vortex M10	VWR International, Darmstadt, Germany
Water bath shaker GFL 1083	GFL, Burgwedel, Germany

3.1.3. The General materials for cell culture

The General materials and the all the cell culture medium used for cultivation of primary osteoblast and MC3T3-E1 cells are listed alphabetically in Table.6.:

Table.6. General materials for cell culture listed with notice of corresponding suppliers

General materials and culture medium	Company name
Cover slips	Menzel-Gläser, Braunschweig, Germany
Culture dish (35mm)	BD Biosciences, Heidelberg, Germany
Culture dish (60mm)	BD Biosciences, Heidelberg, Germany
Fetal bovine serum	Thermo Fisher Scientific, Schwerte, Germany
Filter tips and canules	Braun, Melsungen, Germany
Microtome blade A35	Feather, Köln, Germany
Minimum essential Medium (MEM) α medium	Invitrogen, Karlsruhe,Germany
Molecular weight markers (DNA, RNA)	Fermentas, St.Leon-Rot, Germany
N-Acetyl-L-cysteine	Sigma, Steinheim, Germany
Multi-well cell culture plates (12 wells)	BD Biosciences, Heidelberg, Germany
Nylon meshes (100, 20 and 10µm)	Bückmann, Mönchengladbach, Germany
Penicillin-Streptomycin	Life technology, Darmstadt, Germany

3.2. Experimental animals

3.2.1. *Pex11β* KO and *Pex13* KO animals in Germany

All experimental animals of the *Pex11β* and *Pex13* mouse line were maintained under specific pathogen free (SPF) conditions in the Central Animal Facility of the Justus Liebig University. The *Pex11β* KO and *Pex13* KO mice with C57BL/6J background were generated by crossbreeding of the heterozygous adult mice (Li et al., 2002b; Maxwell et al., 2003). The genotyping of these animals was performed by using genomic DNA isolated from tissue sampled mouse tails. The pregnancy of heterozygous female mice was calculated according to the identification of a visible vaginal plug (=E0.5). All experimental mice were delivered to the animal operation room in our laboratory at days E19 of the fetuses.

All animal experiments in my laboratory works were approved by the German Government Commission of Animal Care (Permission number: 471M1016 Peroxisomen G120/23).

3.2.2. *Sirt1* whole body KO mice experiment in the USA

General *Sirt1* knockout mice (*Sirt1* KO) and myeloid-specific *Sirt1* knockout mice (*Sirt1* Mac-KO) in C57BL/6 background were generated as described (McBurney et al., 2003; Purushotham et al., 2012; Schug et al., 2010). All animal experiments were conducted in accordance with guidelines of US NIEHS/NIH Animal Care and Use Committee.

3.3. Methods

3.3.1. Primary osteoblasts and MC3T3-E1 pre-osteoblast-like fibroblast cell line

3.3.1.1. Primary osteoblast cell isolation and culture

The pre-osteoblasts were isolated from calvariae of 19 day old embryos (E19) *Pex11β, Pex13* and *Sirt1* KO and WT mouse pups. After the fibrous tissue surrounding (periost) the bone was scraped off from the isolated calvariae, the whole bone was trimmed and cut into small pieces and transferred into 15 ml Falcon tubes, tissue was demineralized with 4 mM EDTA with shaking water at 37° C for 10 min, and washed thereafter with 1×Phosphate buffered saline pH 7.4 (PBS) solution (Millipore Darmstadt, Germany) for 5 min. The demineralization was repeated once more under the same condition. The demineralized bone pieces were further digested with collagenase 2 (PAA, Cölbe, Germany) at 37° C for 15 min. Five consecutive digestions were carried out. The first two digestions mainly contained fibroblasts which were discarded. The last 3 digestions were sieved through a polypropylene mesh with 200–297 μm^2 pore size into a 50 ml Falcon tube. Isolated pre-osteoblast were harvested with 5 min 100 xg centrifugation and cultured in α-MEM complemented with 2 mM Glutamin (Table.6.) containing 10% fetal bovine serum (Table.6.), 100 U/ml penicillin G and 100 µg/ml streptomycin at 37° C in a humidified atmosphere of 95% air and 5% CO_2. The following day, the medium was changed to remove any non-adherent cells. Thereafter, the medium was changed every two days. The purity of osteoblast isolated from mouse pups calvariae with this method was more than 95%(Qian, 2010a).

3.3.1.2. Cell culture of MC3T3-E1 pre-osteoblast-like fibroblast cell line

The MC3T3 cell line was established by Sudo originally and colleagues by isolation calvaria of C57BL/6 fetuses and was described to differentiate into mature osteoblast (Sudo et al., 1983). The non-transformed MC3T3-E1 cells were purchased from the Deutsche Sammlung von Mikroorganismen und

Zellkulturen (DSMZ, Braunschweig, Germany), kindly provided by Prof. Dr. Katrin Susanne Lips at University of Giessen Germany (En-Nosse et al., 2009). Cell cultures were maintained in the standard osteoblast medium α-MEM (Table.6.) supplemented with 10% fetal bovine serum (Table.6.), 100 U/ml penicillin G and 100 µg/ml streptomycin (Table.6.) at 37°C in a humidified atmosphere of 95% air and 5% CO_2.

3.3.1.3 Induction of pre-osteoblast maturation and osteoblast cell culture mineralization evaluation via Alizarin Red-S staining

After primary osteoblast isolation from *Pex13* KO and WT pup calvariae, the cells were cultured in osteoblast standard medium for 10 days. The cells were seeded in separate cell culture dishes at a density of 10^4 cells/cm^2 and the medium was changed to induce the differentiation of osteoblast. The α-MEM was supplemented with 10% fetal bovine serum (Table.6.), 100 U/ml penicillin G, 100 µg/ml streptomycin (Table.6.), 50 µg/ml ascorbic acid (Sigma, St. Louis, USA) and 10 mM β-glycerophosphate (Sigma, St. Louis, USA). The mineralization was evaluated with an Alizarin Red-S staining analysis which was carried out in an interval of 3 days up to 24 days calculated from the day of the cell isolation.

Prior to fixation of cells, the medium was removed and the cells were washed twice with PBS solution to completely remove red residues of medium. The washed cells were fixed with 95% ethanol for 15 min at room temperature (RT). After fixation, the cells were washed 3 times with distilled water. Finally the fixed osteoblast were stained by incubation with 0.1% Alizarin Red-S in Tris-HCl (pH 8.3) for 40 min at 37° C. During the incubation time, the progress of the staining was several times monitored by observing the samples with phase contrast microscope until the red staining of calcified extracellular matrix formation became visible and identifiable. To stop the staining process, the cells were washed 3 times for 5 min with distilled water. After the red residues were completely removed, the culture dishes containing stained cells were air-dried at

RT. After the culture dishes were completely dried, they were scanned with an ESPON perfection 1660 photo scanner.

3.3.2. Transfection of MC3T3-E1 cells and primary osteoblast

3.3.2.1. Transfection of MC3T3-E1 cells with Mus musculus *Pex11β* shRNA plasmids to knockdown the *Pex11β* gene expression.

To knockdown the *Pex11β* gene expression in MC3T3-E1 cells, the SureSilencing shRNA Plasmids for plasmid-based RNAi were purchased from Qiagen (Cat.336311 KM26107G). MC3T3-cells were transfected with Trans IT® LT-1 transfection Reagent purchased from Mirus (MIR2300) according to the standard protocol from the manufacturer Mirus for this reagent. 24 hours prior to each transfection, $5x10^5$ cells were seeded onto each well of 6-well plates. For each well, a mixture of lipofection solution was prepared by mixing 2 µl of Trans IT® LT-1 transfection reagent and 110 µl of DMEM serum free medium. After this lipofection solution was incubated at RT for 15 min, 1 µg of plasmid DNA was added and gently mixed. This final mixture was further incubated for 15 min at RT before transfection. Before transfection, for each well the old medium was replaced by filling with 2 ml of fresh standard osteoblast medium containing 10% FBS. The 100 µl of the final incubated lipofection solution with plasmid mixture complex was added drop wise. Meantime, the dispersal of the complex can be reached by swirling the plates. After transfection, to ensure the transfection efficiency, the transfected osteoblast cell cultures were incubated at 37 °C in the cell culture incubator for 48 hours prior to the application of the substances for either gene expression knockdown or Luciferase purposes.

Four types of plasmids which had been made by inserting different functional shRNA sequences (Table.7.) in the same plasmid backbone and one negative control plasmid which had been made by inserting a scrambled sequence into the expression vector was provided by the manufacturer for various cell types and conditions the sequences of which are listed in Table.7.

Table.7. The *Pex11β* shRNA plasmid sequences

Clone ID	Insert Sequence	Catalog No:	336311 KM26107G
1	CCACAACTGGCTTT GAAGTTT	**Marker gene :**	Green Fluorescent Protein (GFP)
2	GTACTTTGCCTGTG CAAGT	**Description**	*Peroxisomal biogenesis factor 11β*
3	TGCTTATGAGATTCG CCTATT	**Gene symbol**	*Pex11β*
4	TCTGAGCCTCGGAC GAAAGTT	**UniGene no:**	Mm.20901
Negative Control	GGAATCTCATTCGAT GCATAC	**RefSeq Accession no.:**	MN-011069

The screening of the *Pex11β* gene expression knockdown was performed by Semi-Quantitative polymerase chain reaction (RT-PCR) with the primer pair described in Table.8. For this purpose the isolated RNA from the transfected MC3T3 cells 48 hours after the transfection was transcribed in cDNA (see section 3.4.1). For further quantification of the knockdown of the *Pex11β* gene expression, the cDNA was further checked with the Quantitative RT-polymerase chain reaction (qRT-PCR) for quantification of the knockdown with the primers described in Table.8.

3.3.2.2. Transfection of MC3T3-E1 cells with *Sirt1* shRNA Lentivirus to generate a stable knockdown of the *Sirt1* gene

Mouse SIRT1 shRNA Lentiviral Particles (SantCruz SC-153192-v) and control shRNA Lentiviral Particle (SantCruz sc-108080) were used to transfect MC3T3-E1 cells according to the manufacturer's standard protocol (Santa Cruz Texas USA). The cells were transfected with a ratio of 2 infectious units/cell in supplemented medium containing 10% fetal bovine serum, 100 U/ml penicillin G and 100 µg/ml streptomycin, 5 g/ml polybrene (Sigma, St. Louis, USA). The medium was replaced the following day to remove the polybrene and cultured for

further experiments. The transfected cells were selected with 5 µg/ml Puromycin dihydrochloride (A1113803 Invitrogen) for 6 days. Thereafter culturing in non-selection medium for 2 days followed before the cells were processed for experiments.

3.4. Molecular biological experiments

3.4.1. RNA isolation from primary osteoblast and MC3T3-E1 cell culture and the reverse transcription to generate cDNA

Total RNA was isolated from primary osteoblasts and MC3T3-E1 cells by using the RNeasy Mini Kit®, according to the manufacturer's protocol (Qiagen, Heidelberg, Germany). The cells were collected and lysed directly from the cell culture dish by using cell Scrapers (Greiner bio-one541080) with 350 µl/well RLT buffer provided by the kit. The cell lysate was homogenized by directly transferring it to a QIAshredder spin column and centrifuging at a speed of 12,000x g for 2 min at room temperature (RT). Each RNA preparation was subjected to DNase I digestion to remove possible contamination of genomic DNA by using RNase-free DNAse set (Qiagen Cat 79254) by which the contaminated genomic DNA can be directly digested within RNeasy/QIAamp® columns. The quantity and integrity of the isolated RNA was assessed with the NanoDrop™ 8000 Spectro-photometer and RNA 6000 Nano LabChips (Caliper Life Sciences GmbH, Mainz, Germany). The isolated total RNA from primary osteoblasts and MC3T3-1 cells was reversely transcribed to cDNA. First-strand cDNA was synthesized from 1.0 µg of DNAse I-treated total RNA with oligo (dT) 12-18 primers using Superscript II reverse transcriptase (Invitrogen, Karlsruhe, Germany) according to the manufacturer's protocol.

3.4.2. Semi-quantitative polymerase chain reaction and agarose gel electrophoresis.

The PCR reaction mix contained the 450 ng template cDNA, 10 mM dNTPs, 1 unit Taq DNA polymerase and $10\times$ PCR buffer (Eppendorf, Hamburg, Germany). PCR reaction was performed in the Bio-Rad iCycler C1000 (Bio-Rad

Laboratories, München, Germany) with the following parameters: denaturation at 95°C for 2 min; followed by 32-45 cycles of denaturation at 95°C for 30 s, annealing at 50-65°C for 1 min, extension at 72°C for 1 min; and a final extension at 72°C for 7 min.

The target gene expression results were determined by the analysis of the RT-PCR product size via agarose gel electrophoresis. For this purpose, a 2% agarose gel, containing 0.5 µg/ml ethidium bromide electrophoresis in 1 x TAE buffer was casted. For each RT-PCR reaction, 10 µl of the product was stained with SYBR® Gold (Bio-Rad) and loaded on the gel and run at voltage of 90 V for 60 min. After the electrophoresis, the gel was photographed with UV light using the Gel-Doc 2000 documentation system from Bio-Rad Laboratories (München, Germany). The size of the RT-PCR products was measured by comparing to the bands of a 100bp DNA Ladder GeneRuler (100 bp) or 1000 bp ladder (Fermentas). Gene expression was analyzed by comparing the intensity and thickness of the gene of interest to that of 28S rRNA (reference gene) which was run in parallel on the same agarose gel. All primers for RT-PCR experiments are listed in alphabetical order in Table.8. depicting also the annealing temperature used for the PCR and the size of amplified product.

Table.8. RT-PCR primer pairs

Gene names	Forward primer(5'-3')	Reverse primer(5'-3')	$T_m(° C)$	Product (bp)
Abcd1	GAGGGAGGTTGGGGAGGCAGT	GGTGGGAGCTGGGGATAAGG	65	465
Abcd3	CTGGGCGTGAAATGACTAGATTGG	AGCTGCACATTGTCCAAGTACTCC	64	523
Catalase	ATGGTCTGGGACTTCTGGAGTCTTC	GTTTCCTCTCCTCCTCATTCAACAC	64	833
FoxO1	GGGAGAATGTTCGCTTTCTGGT	CCACCTCATCAGGCACTTCTC	56	662
FoxO3	CACTGAGGAAAGGGGAAATGGG	TGGGGTCCCACAGGCTCAAAAG	58	540
FoxO4	TTGTGCCTAGAAGAGAGTGCTG	ATTTGACACACTTCCCCACTCC	54	531
Ho-1	GCACTATGTAAAGCGTCTCCACGAG	CCAGGCAAGATTCTCCCTTACAGAG	65	610
Nrf2	CCACTGGTTTAGCCATCTCTCC	GTGGACATTAGCCCTTCCAAAC	64	364
Pex11β	GTATGCCTGTTCCCTTCTCG	CTCGGTTGAGGTGACTGACA	65	216
Sirt1	GGTAGAGCCTGCATAGATCTTCA	TGGCAGTAATGGTCCTAACTGGG	62	512
Sirt2	CCATGACCTCCCGCAGGACAGCG-	GGGTCCCCAGGAAAGGGAGCCTA	69	505
Sirt3	GTGCCCCGACTGCTCATCAATCG	CCGATCAACATGCTAGATTGCCC	55	523
Sirt4	CACCCGGTCTGACGATTTGGCTT	CCGTGTTAGCTATTGCTCCTGCC	64	483
Sirt5	TTGCTGCGACCTCACGTGGTGTG	GGAAGGACTTGACAGCCTCTTCC	65	505
Sirt6	GGGGACTGAGCCCAGGTTTGCAT	CTTCTGGGAGCCTGGGGCCCTTA	67	494
Sirt7	TATCCTAGGAGGCTGGTTTGGCA	GGAGGCTTAGTTAGATTCTCCCT	59	503
28srRNA	CCTTCGATGTCGGCTCTTCCTAT	GTGGACATTAGCCCTTCCAAAC	65	254

T_m = Annealing temperature; bp = base pairs.

All primers were designed to specially amplify the parts of cDNA sequences of the corresponding mRNA of interest. The primer design was achieved by published cDNA sequences using the Nucleotide Database of NCBI (http://www.ncbi.nlm.nih.gov/nucleotide/). The online software *"Primer3"* (http://frodo.wi.mit.edu) was used to analyse and select the most suitable primers which were standardized at a length of around 20-22 base pairs (bp). The "GC" content was kept around 40-60% out of total length of each primer and the annealing temperature (T_m) difference between forward and reverse primer of each primer pair was limited to less than 4° C to ensure the specific binding capacity. To prevent amplification of genomic DNA extron-spanning primers were designed. To ensure the specificity of each primer, BLAST searches against the EST and non-redundant mouse transcriptome databases (http://www.ncbi. nlm.nih.gov/blast/Blast.cgi) were applied to ensure no nucleotide matches at the 3' ends of each primer (Tanaka et al., 2012). All primers used in the experiments were synthetized by Eurofins MWG Operon Germany, and the PCR conditions

for each primer pair were optimized with a temperature gradient from 55-70°C on a BioRad iCycler prior to further experiments.

3.4.3. Quantitative real time-polymerase chain reaction

Quantitative real time-polymerase chain reaction (qRT-PCR) was performed using a SYBR Green PCR Master Mix (Applied Biosystems) with the IQ5® I cycler (Bio-Rad, Müchen, Germany) using the standard protocol provided by manufacturer (thermal cycling 94˚C for 3 min followed by 45 cycles at 94˚C for 30 s, T_m =60 °C for 45 sec and 72°C for 1 min.). The mRNA levels were normalized to the osteoblast differentiation stable references gene *Actb, Hmbs and Hprt1* (Stephens et al., 2011); the sequences of the primers used for the qRT-PCR are noted in alphabetical orders in Table.9.

Table 9. Sequences of the primers used for the qRT-PCR

Gene Name	Sense 5'-3'	Antisense 5'-3'
Abcd1	ACAGTGCCATCCGCTACCTA	ATGAGCTACTAGACGGCTTCG
Abcd3	TCAGAATGGGACGCTCATTGA	TGGCAGCGATGAAGTTGAATAA
Actb	CTCTGGCTCCTAGCACCATGAAGA	GTAAAACGCAGCTCAGTAACAGTCCG
Acox1	CCGCCACCTTCAATCCAGAG	CAAGTTCTCGATTTCTCGACGG
Acox2	ACGGTCCTGAACGCATTTATG	TTGGCCCCATTTAGCAATCTG
Acox3	TTCTAGTGCTGATTAACTGCCTG	AGAAACGAAACTGTGGTTCCAA
Alp	AGGGCAATGAGGTCACATCC	CACCCGAGTGGTAGTCACAAT
Bglap	ATGCTTCTCAGAGCCTCAGTC	TAGGCGGTCTTCAAGCCATA
Catalase	TGGCACACTTTGACAGAGAGC	CCTTTGCCTTGGAGTATCTGG
Col1a1	GCTCCTCTTAGGGGCCACT	ATTGGGGACCCTTAGGCCAT
Col1a2	AGCTTTGTGGATACGCGGAC	TAGGCACGAAGTTACTGCAAG
Hmbs	GAGTCTAGATGGCTCAGATAGCATGC	CCTACAGACCAGTTAGCGCACATC
Hprt1	GAGGAGTCCTGTTGATGTTGCCAG	GGCTGGCCTATAGGCTCATAGTGC
Ibsp	ACGGCGATAGTTCCGAAGAG	CTAGCTGTTACACCCGAGAGT
Mfp1	AATACAGCGATACCAGAAGCCA	CCAGCTCTAGTCCTCCTCCA
Mfp2	TTAGGAGGGGACTTCAAGGGA	TCGCCTGCTTCAACTGAATCG
Opn	GGTCAAAGTCTAGGAGTTTCCAG	CACCGCTCTTCATGTGAGAGG
Osterix	TCCCTGGATATGACTCATCCCT	CCAAGGAGTAGGTGTGTTGCC
Pex5	AATGCAACTCTTGTATCCCGAG	GGCGAAAGTTTGACTGTTCAATC
Pex11α	TCAACCGCGTGGTTTATTACA	CGCCCACCTTTGCCATTTC
Pex11β	GACGAAAGTTGCTACGCCTG	GCTCGGTTGAGGTGACTGAC
Pex11γ	CTAGTGGAACAATGCCCCAAC	AGGCCATACTGCTTAGTGTAGA
Pex13	TGGATATGGAGCCTACGGAAA	CGGTTAAAGCCCAAACCATTG
Pex14	GCCACCACATCAACCAACTG	GTCTCCGATTCAAAAGAAGTCCT
Pex19	GCAGCGATGCAAGTTCTCAG	CCACTTAACGTCTCCTTTAGGC
Runx2	CGGTGCAAACTTTCTCCAGGA	GCACTCACTGACTCGGTTGG
Pgc-1α	AACCAGTACAACAATGAGCCTG	AATGAGGGCAATCCGTCTTCA
Pparγ	GGAAGACCACTCGCATTCCTT	GTAATCAGCAACCATTGGGTCA
RANKL	CGCTCTGTTCCTGTACTTTCG	GAGTCCTGCAAATCTGCGTT

3.4.4. Osteoblast protein abundance analysis via Western blots

3.4.4.1. Whole cell lysate isolation for the western blot analysis of whole cell protein abundance

Total cell lysates of primary osteoblast or ME3T3-E1 cell cultures were isolated by using the Cell Lysis Buffer (10X) purchased from Cell Signaling (Cat. #9803) according to the standard protocol provided by the manufacturer. Before isolation, the medium was removed and the 5×10^5 cells were washed with PBS and cell number was counted. The final osteoblast total cell lysates were retained in 1x

cell lysis buffer which was diluted from original 10x cell lysis buffer solution containing 20 mM Tris-HCl (pH 7.5), 150 mM NaCl, 1 mM Na_2EDTA, 1 mM EGTA, 1% Triton×100, 2.5 mM sodium pyrophosphate, 1 mM β-glycerophosphate, 1 mM Na_3VO_4 and 1 µg/ml leupeptin, with Milli-Q water, containing 10% protease inhibitor mix M (SERVA, Heidelberg, Germany). The whole process of cell lysate isolation was done on ice.

3.4.4.2. Determination of the nuclear protein abundance in the nuclear fraction of osteoblast

After the cell medium had been removed, the osteoblast cells were washed with PBS to remove the residues from the medium, thereafter the cells were further trypsinized (Sigma, Steinheim, Germany) for 3 min at 37°C. To remove the trypsin the detached cells were washed once more with PBS. The nuclear protein isolation was carried out with the ProteoJET™ Cytoplasmic and Nuclear Protein Extraction Kit purchased from Fermentas LIFE SCIENCES (Cat. #K0311) using the standard protocol provided by the manufacturer. All the procedures were performed on ice or in the pre-cooled 4° C centrifuge. All solutions used for the protein extraction contained 10% protease inhibitor mix M (SERVA, Heidelberg, Germany).

3.4.4.3. Western blots

Before protein samples were separated by sodium dodecyl sulfate polyacrylamide gel electrophoresis (SDS-PAGE), the protein concentration of each sample was measured with the Bradford Assay using bovine serum albumin (BSA)(Roth, Karlsruhe, Germany) as standard (Bradford, 1976). 20 µg of the protein sample and 1 µl of dual color and unstained precision plus protein Standards® (Bio-Rad, Heidelberg, Germany) were loaded into the blots of a 12% SDS polyacrylamide gels. These gels were used for the electrophoresis and were made with the ingredients listed in Table.10.

Table.10. Solutions for four 12% SDS-polyacrylamide gels with combs with a thickness of 1.25 mm

Resolving gel buffer A	0.4% SDS 1.5 M Tris-HCl, adjusted to pH 8.8
Stacking gel buffer B	0.4% SDS, 0.5 M Tris-HCl, adjusted to pH 6.8 ，
Resolving gel (12%)	2 ml of ddH$_2$O, 10 ml of buffer A, 8 ml of 30% acrylamide,15 µl of TEMED, 130 µl of 10% APS
Stacking gel	5 ml of ddH$_2$O, 5 ml of buffer B, 1.25 ml of 30% acrylamide, 15 µl of TEMED, 130 µl of 10% APS
10X Sample buffer	3.55 ml ddH$_2$O, 1.25 ml 0.5 M Tris-HCl (pH 6.8), 2.5 ml 50% (w/v) glycerol, 2.0 ml 10% (w/v) SDS, 0.05 % bromophenol blue. Prior to use 50 ml β-mercaptoethanol has was added

The gel electrophoresis was carried out at stable voltage of 2.4 V/cm^2. After the sample proteins were separated by SDS-PAGE gel electrophoresis, they were blotted onto polyvinylidene fluoride (PVDF) membranes (Millipore, Schwalbach, Germany) with a Bio-Rad Trans-Blot® SD semidry transfer cell (Bio-Rad München, Germany) for 50 min at 90 mA constant current. Tris-buffered saline (TBS) containing 10% non-fat milk powder (Roth, Karlsruhe, Germany) and 0.05% Tween-20 (TBST) was used to block the nonspecific protein-binding sites on the membrane for 2 hours at RT. The incubation with the primary antibodies was carried out at 4° C with no shaking for overnight. After the incubation with the primary antibodies, the membranes were washed 5 times for 15 min with 1x TBST solution to completely remove residues of the primary antibodies. Thereafter, the membranes were incubated with alkaline phosphatase-conjugated secondary antibodies at RT for 1 hour. The bound antigen antibody complexes were visualized by chemiluminescence detection of alkaline phosphatase activity with the ImmunoStar^{TM} AP from Bio-Rad (München, Germany) as substrate. The chemiluminescence induced light was used for exposure with Kodak Biomax MR negative films (Kodak, Stuttgart, Germany). The films were developed according to the manufacturer's protocol. Finally the developed negatives were scanned with an AGFA scanner. The membranes were re-used to detect different target proteins by stripping and re-probing

several times with different primary antibodies. All Western blot analyses were performed in triplicates to produce stable repeatable results.

Table.11. The composition of all buffer solutions used for Western blots

10×Electrophoresis buffer	250 mM Tris, 2 M glycin + 1% SDS
20× Transfer buffer	Bis-Tris-HCl buffered (pH 6.4) polyacrylamide gel, NuPAGE transfer buffer (Invitrogen, Heidelberg, Germany)
10× TBS	0.1M Tris, 0.15 M NaCl in 1 l ddH$_2$O, adjusted to pH 8.0
10% Blocking buffer	10 g fat free milk powder in 1x TBST solution
1% BSA	10 g BSA in 100 ml 1x TBST + 0.05% Tween 20, pH 8.0
1× Washing buffer (TBST)	10 mM Tris/HCl, 0.15 M NaCl, 0.05% Tween 20, pH 8.0
Stripping buffer (500 ml)	62.5 mM Tris (pH 6.8), 0.2% SDS, 500 ml ddH$_2$O – 42°C water bath for 40 min with additional 500 µl β-mercaptoethanol

Table.12. Antibdies used for immunofluorescent stainings or Western blots

Peroxisomal antigens	Species AB raised in	Dilution	Supplier
Catalase (CAT), mouse	Rabbit, polyclonal	1:2000	
Peroxisomal biogenesis factor 13 (PEX13p), mouse	Rabbit, polyclonal	1:1000	Gift from Denis I. Crane, School of Biomol. Biophys. Sci., Griffith Univ., Nathan, Brisbane, Australia
Peroxisomal biogenesis factor 14 (PEX14p), mouse	Rabbit, polyclonal	1:4000	
ABC-transporter D3 (ABCD3), mouse	Rabbit, polyclonal	1:1000	Gift from Alfred Völkl, University of Heidelberg, Germany
Mitochondrial antigens			
Superoxide dismutase 2 (SOD2), rat	Rabbit, polyclonal	1:1000	Abcam Cat. no ab13533, Cambridge, UK
Osteoblast-specific antigens			
Osteopontin (OPN), mouse	Mouse, monoclonal	1:400	Santa Cruz Biotechnology Inc., Heidelberg, Germany, Cat. no: sc-21742
Runt-related transcription factor 2 (RUNX2), mouse	Rabbit, polyclonal	1:400	Santa Cruz Biotechnology Inc., Heidelberg, Germany, Cat. no:sc-10758
Antibody used for IF staining of *Sirt1* KO/WT paraffin embedded newborn mice.			
SIRT1	Rabbit, polyclonal	1:400	Cell Signaling #2028
Retinoic Acid Receptor Beta (PARβ)	Rabbit, polyclonal	1:400	Abcam 53161, Cambridge, UK
Antibody used for WB loading control			
Histone H3	Rabbit, polyclonal	1:1000	Cell Signaling #9715
Secondary Antibodies:			
Anti-Rabbit-IgG Alexa Fluor 488	Donkey, polyclonal	1:600	Molecular Probes/Invitrogen, Cat. no: A21206
Anti-Mouse-IgG Texas Red	Horse, polyclonal	1:200	Vertor laboratories, Inc, Burlingame, USA, Cat. no: TI-2000
Anti-Mouse IgG alkaline phosphatase	Goat, polyclonal	1:20,000	Sigma, Steinheim, Germany. Cat. no: A3562
Anti-Rabbit IgG alkaline phosphatase	Goat, polyclonal	1:20,000	Sigma, Steinheim, Germany. Cat. no: A3562

3.5 Morphological experiments

3.5.1. Indirect immunofluorescence stainings of primary osteoblasts

Primary osteoblasts grown on poly-L-lysine-coated coverslips were rinsed with 1×PBS (150 mM NaCl, 13.1 mM K_2HPO_4, 5 mM KH_2PO_4, pH 7.4) and fixed with 4% paraformaldehyde (PFA) in PBS (pH 7.4) for 20 min at RT. After fixation, the cells were washed three times with PBS. Thereafter, they were incubated for 10 min in PBS containing 1% glycine and for an additional 10 min in PBS containing 1% glycin and 0.3% Triton X-100 for permeabilization. After washing the cells with PBS, they were incubated for 30 min in PBS containing 1% BSA and 0.05% Tween 20 to block the nonspecific protein binding site. Thereafter, the coverslips with cells were incubated with primary antibodies overnight at 4°C in a moist chamber, followed by washing with PBS 3 times for 5 min the next morning. The incubation with the secondary antibodies was performed for 1 hour at RT. Nuclei were counterstained with Hoechst 33342 (2 µg/ml) and TOTO 3 iodide (Invitrogen). The solutions used in these experiments are described in Table.13.

Table.13. Solutions for immunofluorescence staining of primary osteoblast

Perfusion fixative solution	4% PFA in 1X PBS (150mM NaCl, 13.1mM K_2HPO_4 , 5mM KH_2PO_4), pH 7.4
Glycine (1%)	1g Glycine in 100ml of 1X PBS buffer
Glycin (1%) + Triton X-100 (0.3%)	1g Glycine in 100ml of 1X PBS buffer + 0.3ml Triton X-100
Blocking buffer- 1% PBSA + 0,05% Tween 20	To 2g BSA add 200ml of 1X PBS and 100µl of Tween 20
Mowiol 4-88 solution	Overnight stirring of 16.7 % Mowiol 4-88 (w/v) + 80ml of 1X PBS, add 40ml of glycerol, stir again overnight; centrifuge at 15,000 U/min for 1h and take off the supernatant and store at -20°C
Anti-fading agent (2.5%)	2.5g N-propyl-gallate in 50ml of PBS and 50ml of glycerol
Mounting medium	Mowiol 4-88 mixed with anti-fading agent in ratio of 3:1

3.5.2. Indirect immunofluorescence staining on Paraformaldehyde-fixed paraffin-embedded mouse tissue

Before 19 days old *Pex13* KO/WT mouse fetuses (E18.5) isolated by caesarian section from pregnant mice and 0.5 day old new born *Sirt1* KO/WT mouse pups were used in perfusion fixation. The perfusion fixation was carried out injecting 4% depolymerized paraformaldehyde (PFA) containing 2% sucrose in PBS (pH 7.4) through left ventricle of the heart using and further fixed by immersion at 4° C overnight. The fixed samples were paraffin-embedded (Paraplast, Sigma, St. Louis, MO, USA) using a Leica TP 1020 automated vacuum infiltration tissue processor(Nenicu et al., 2007). Sections (3 µm) were cut with a Leica RM2135 rotation microtome. The staining experiments were performed for 3 days as Table.14. described:

Table.14. The experiments procedures of .indirect immunofluorescence staining on PFA-fixed paraffin embedded mice tissue sections.

Time	Experiments procedures
Day 1	Deparaffinization: sections were placed into 50°C oven (Heraeus, Hanau, Germany) for overnight deparaffinization
Day 2	1. Deparaffinized with xylene (3x 5min) followed by rehydration in a series of ethanol (2x 99%, 96%, 80%, 70%, 50% ethanol, 2 min each time). 2. Antigen retrieval: sections were treated with trypsin and thereafter microwaved in TEG buffer (Table.15.) for 5-6min. 3. Blocking with 4% BSA and 0.05% Tween 20 in PBS at RT for 2 hours 4. Sections were incubated with primary antibodies (Table.12.) at RT for overnight.
Day 3	1. Sections were rinsed with PBS and thereafter 2. Sections were incubated with the secondary antibodies (Table.12.) at RT for hours 3. Nuclear staining

In parallel, negative controls were processed with an addition of PBS buffer instead of the first antibodies. Nuclei were visualized with Hoechst 33342 (2µg/ml) and TOTO-3 iodide (Molecular Probes/Invitrogen, Carlsbad, USA) for 10 min at RT. The solutions were used in these experiments were described in Table.15.

Table.15. Solutions for immunofluorescence stainings on PFA-fixed paraffin embedded mice tissue section.

Perfusion fixative solution	4% PFA in 1x PBS (150 mM NaCl, 13.1 mM K_2HPO_4, 5 mM KH_2PO_4), prior to use adjust to pH 7.4
10X PBS	1.5 M NaCl, 131 mM K_2HPO_4, 50 mM KH_2PO_4, prior to use adjust to pH 7.4
Trypsin (0.1%)	0.1 g trypsin in 100 ml of 1x PBS buffer, freshly prepared
TEG buffer	5 mM EGTA, 0.1 M Tris, pH 9.0
Blocking buffer-4% PBSA + 0,05% Tween 20	To 8 g BSA add 200 ml of 1x PBS and 100 µl of Tween 20
Dilution buffer- 1% PBSA + 0,05% Tween 20	To 2 g BSA add 200 ml of 1x PBS and 100 µl of Tween 20
Mowiol 4-88 solution	Overnight stirring of 16.7% Mowiol 4-88 (w/v) + 80 ml of 1x PBS, add 40 ml of glycerol, stir again overnight; centrifuge at 15,000 U/min for 1 h and remove the supernatant and store at -20° C
Anti-fading agent (2.5%)	2.5 g N-propyl-gallate in 50 ml of PBS and 50 ml of glycerol
Mounting medium	Mowiol 4-88 mixed with anti-fading agent in ratio of 3:1

Samples were analyzed by confocal laser scanning microscopy (CLSM) with a Leica TCS SP2 microscope (Leica Mikrosysteme Vertrieb GmbH, Wetzlar, Germany).

3.5.3. Apoptosis detection by terminal deoxynucleotidyl transferase dUTP nick end labeling

Apoptotic cells in *Pex11β* WT and KO osteoblast cell cultures were detected by the Terminal-deoxynucleotidyl-transferase dUTP nick end labeling (TUNEL) using the ApopTag® Fluorescein *in situ* Apoptosis Detection Kit (S7110 Millipore Schwalbach, Germany) according to the manufacturer's protocol. The basic principle of this method is that the 3'-OH ends of double-stranded or single-stranded DNA breaks can be enzymatically labelled in situ with nucleotides – in our case conjugated with digoxigenin (provided in Reaction Buffer 90417 Millipore) by the terminal deoxynucleotidyl transferase (TdT Enzyme 90418

Millipore). Thereafter, the digoxigenin-conjugated nucleotides can be bound by the anti-digoxigenin antibody labelled with Fluorescein (90426 Millipore). (Product information provided by Millipore for Kit S7110).Negative controls were done using 1×PBS (Millipore Darmstadt, Germany) solution instead of the TdT Enzyme from this Kit. Positive controls had been pre-treated with DNase I (0.1U/µl Deoxyribonuclease I, Amplification Grade Invitrogen Cat.18068-015); diluted in DNase I reaction buffer) for 2 min to artificially simulate DNA strand break induced apoptosis.

Primary cell cultures of osteoblasts isolated from three pairs of *Pex11β* WT and KO animals were analyzed for each genotype. For the quantification of the apoptosis rates in each cell culture TUNEL-positive cells in 500 randomly selected *Pex11β* WT and KO osteoblast were used. Quantification of TUNEL positive cells revealed a pronounced increase in number of apoptotic cells cell cultures from *Pex11β* KO will in comparison to WT mice (P≤0.001). Sample images were also analyzed by confocal laser scanning microscopy (CLSM) with a Leica TCS SP2 (Leica Mikrosysteme Vertrieb GmbH, Wetzlar, Germany).

3.5.4. Whole skeleton bone volume and bone density estimation using flat-panel volumetric computed tomography (fpvCT) of P0.5 mouse pups

Radiological analysis was applied on new born mouse pups (P0.5) for determination of skeleton size, bone volume and density by a flat-panel volumetric computed tomography (fpvCT for research only) developed by General Electric company (GE). All the techniques for this method were developed by Dr. Martin Obert from the Department of Neuroradiology from the Justus Liebig University of Giessen and were used in cooperation with our group already for scans of adult mice (Obert et al., 2005). The animal scanning and VCT image analysis accomplished by Dr. Martin Obert at the Department of Neuroradiology at the Justus Liebig University of Giessen. The advantageous workstation (Version 4.1, GE Medical Systems, USA) and a LINUX based dual 2.2GHz processor PC with 4GB RAM were needed for the reconstitution of the

data, by which the volume data were visualized as maximum intensity projection (Qian, 2010a). The relative bone volume of the scanned mouse pups were estimated by Dr. Obert's developed software (IDL, Version 6.0, RSI, Boulder, CO, USA)(Obert et al., 2005). Total of 13 P0.5 mouse pups including all genotypes (3 of *Pex13* WT pups, 5 of *Pex13* heterozygous (HE) pups and 5 of *Pex13* KO pups) were scanned with the VCT. To estimate the partial volume effects, each mouse was scanned 3 times with different position rotating on the phantom holder. To ensure that with used the scan parameter, data (density volume) are in the linear range, plastic straw filled with H_2O or aqueous solutions of 50, 100, 200, and 400 mg K_2HPO_4 per ml H_2O were scanned in parallel. One way ANOVA were used to compare the estimated bone volume between each genotype group of *Pex13* KO, WT and heterozygous.

3.6. Functional assay of protein DNA binding, biophysical methodology

3.6.1. Dual-Luciferase reporter gene assay to monitor transcriptional activities of markers of bone differentiation RUNX2 and FoxOs, PPARs

3.6.1.1. Transfection of MC3T3-E1 cells and primary osteoblasts with Dual-luciferase reporter assay plasmid

The reporter gene assay experiments were performed by using the Promega Dual-Luciferase Reporter Assay System using the manufacturer's protocol Promega (Cat. No: E1910). The Dual-Luciferase Reporter Assay plasmids and relevant control plasmids used for the transfection of MC3T3-E1 cells are listed in Table.16.

Table.16. Plasmids for Dual-Luciferase Reporter Assay

Plasmid name	Inset gene	Cat:	Function	Manufacturer
R19	RUNX2 recognizing DNA binding motif (Drissi et al., 2000)		Luciferase gene expression reporter assay	Dr.Hicham Drissi*
pGL3-6XDBE	6 copies of daf-16 family protein binding elements (Ambrogini et al., 2010)		Luciferase gene expression reporter assay	Prof.Dr. Boudewijn Burgering#
pGL3-Basic	Luciferase tag fused vector backbone	E1751	Luciferase gene expression reporter assay Negative control for R19 plasmid	Promega Mannheim Germany
p4xACO-Luc	PPAR-responsive element	Addgene 16533	Luciferase gene expression reporter assay	Addgene Cambridge MA USA
pBV-Luc	Luciferase tag fused vector backbone	Addgene 16539	Luciferase gene expression reporter assay Negative control	Addgene Cambridge MA USA
pRL-SV40	Renilla luciferase (Rluc) control reporter	E2231	Dual Luciferase assay internal control vectors	Promega Mannheim Germany

* Address: University of Massachusetts Medical School, Worcester, MA 01655-0106, USA.

Address: University Medical Center, Utrecht, Netherlands, plasmids was kindly provided to my colleague Guofeng Qian in our lab.

All transfections for the luciferase report gene assay were performed with the Trans IT® LT-1 transfection reagent purchased from Mirus (MIR2300) according to the standard protocol. The luciferase activity assay was carried out 48 hours after transfection.

For the transfection of one well (from a 6-wells plates) 1 µg of Luciferase functional plasmid containing the firefly luciferase as reporter gene was added to 100 ng Dual Luciferase assay internal control vectors pRL-SV40 (with Renilla luciferase) and 4 µl of Trans IT® LT-1 to perform Dual luciferase assays (Vijayan et al., 2011).

3.6.1.2. Sample preparation for Luciferase reporter gene assay

The transfected MC3T3-E1 cells were cultured in the 6-well cell culture plates for 48 hours after the transfection and the luciferase assay measurements were

performed according to the standard protocol of the manufacturer Promega. The growth medium was carefully removed from the cell culture and the cells were rinsed with 1x PBS solution to completely remove the rest of the medium. 150 µl of 1x strength of luciferase cell culture lysis buffer which had been made by mixing 4 volumes of sterile water and 1 volume of the luciferase cell culture lysis reagent (CCLR) (5X provided within the kit Promega Cat. No: E1910), was added to each well of a 6-well plate and the plates were gently shaken for 10 s to ensure that the complete surface was covered with lysis buffer. The total cell lysates were collected by scrapping cell culture dishes and transferring the lysate into reaction tubes. Before the luciferase activity measurement, all samples were incubated on ice for 15 seconds, completely mixed by vigorously vortexing for 15 s and finally harvested by centrifugation at a speed of 13000× g for 30 s at RT.

3.6.1.3. Luciferase activity measurement.

Prior to the measurement, the luminometer (BERTHOLD Technologies Lumat LB 9507) was primed using the luciferase assay reagent (base line) which was mixed completely and equilibrated at RT before use. The sequence of measurement was programmed so that the luciferase enzyme activity was read by a 2 s measurement delay followed by a 10 s measurement. For each measurement, 50 µl of the cell lysate was dispensed into the luminometer tubes. In each respective measurement, luciferase activity measurement reading was programmed to automatically adjust to work in a linear range. For the output of the results, relative light units of luciferase activity were normalized to the values per mg protein of the samples.

3.6.2. Biophysical Methodology to determine cell cycle of primary osteoblasts

The determination of cell cycle using Fluorescence-activated cell sorting applied in flow cytometry (FACS) were performed in collaboration with Dr. Carl Bortner in the Flow Cytometry Center of Signal Transduction Laboratory, NIEHS, USA.

3.6.2.1. DNA Analysis to determine osteoblast cell cycles using Becton Dickinson FACSort flow cytometer

The basic principle of the Becton Dickinson FACSort flow cytometer method is utilizing ethanol to fix the osteoblast cells and permeabilize the membrane, followed by using Propidium Iodide (PI), which is a DNA-binding fluorochrome dye intercalating in the double-helix.(Geary et al., 1982; Harty-Golder and Braylan, 1982). The interfering signal from unspecific staining of double-stranded RNA can be eliminated by Ribonuclease-A (RNase).

3.6.2.2. Osteoblast cell culture fixation

Osteoblasts were cultured in a 6-well cell culture dish as a 75% confluent monolayer. After the cells were trypsinized, they were washed and re-suspended in 500 µl PBS and chilled well on ice. After 15 min incubation, the cold cell suspensions were gently pipetted into clear 12x75 mm polystyrene Falcon tubes containing 500 µl of ice cold 70% ethanol which had been pre-cooled and mixed by forcing air bubbles through the suspension with plastic pasteur type transfer pipettes. The cell suspension was topped off to approximately 2-3 ml with agitation by adding additional ice cold 70% ethanol. All mixtures remained on ice for another 15 min and the final volume was adjusted to 5 ml with ice cold 70% ethanol and the cells were stored at -20° C overnight.

3.6.2.3. Debris removal

Before the PI staining step, the debris in the osteoblast cell suspension was removed by using Fetal or newborn bovine serum (FBS). 1 ml of ice cold FBS was carefully transferred onto the underlay of the Falcon tube and centrifuged at 300 xg for 3 min. After centrifugation, the liquid phase was carefully removed without disturbing the pellet and the attached debris was carefully removed from the side of tubes by using a cotton swab. After all debris had been completely removed, the pellet was washed once in 3 ml of 1x PBS prior to DNA staining.

3.6.2.4. RNA removal and DNA staining

The cell pellet was re-suspended in 1 ml of 1x PBS containing 1000 units of highly purified RNase (Cat # M4265, Promega Corporation, Madison, WI, USA). After the suspension was completely mixed by vortexing, the mixture was incubated in 37 º C water bath for 15 min for the RNA digestion. Thereafter, the tubes were removed from the water bath and the cells were further incubated in 20 μg/ml PI (Cat #4170, Sigma-Aldrich, St. Louis, MO, USA) in this 1x PBS. The mixture was completely mixed by vortexing and an incubation at RT for 30 min followed. Prior to FACS analysis, the final cell suspensions were pipetted through a nylon monofilament mesh screen with 44 micron openings to remove large multicellular aggregates common in ethanol-fixed preparations. Thereafter, the analysis at the flow cytometer was performed.

The analysis was carried out using a Becton Dickinson FACSort flow cytometer and CELLQuest software (Becton Dickinson Immunocytometry Systems, San Jose, CA). Individual cells (7,500 per experimental sample) were selected by gating on a PI area versus width dot plot to exclude cell aggregates and debris. The cells were excited using a 488 nm argon laser and emission was detected at 585 nm. The data was analyzed using Modfit software for Mac version 2.0.

3.6.3. Flow cytometric analysis of ROS in *Sirt1* gene shRNA knockdown MC3T3-E1 cells

The principle behind dichlorodihydrofluorescein diacetate (H$_2$-DCFDA) dye (Invitrogen C10422) for the detection of the intracellular generation of ROS in osteoblast is that the fluorescent ROS-modified H$_2$-DCFDA byproduct dichlorofluorescein, which is produced after oxidation and cleavage by cellular esterases, can be detected with the flow cytometer. After the osteoblast cells were treated with 10 mM of heme oxidase for 30 minutes, 1×10^6 cells were counted and further incubated with medium containing 15 µM H$_2$-DCFDA for 30 min at 37°C. Before the ROS levels of these osteoblasts were detected with FACScalibur flow cytometer, samples were completely washed for three times

with 1x PBS at RT. The levels of ROS-oxidized DCFDA fluorescent signals were determined with the FACSCalibur flow cytometer. DCF-detectable (FL1-H) fluorescent signals were displayed as histograms and ratios of signals versus control data were calculated using mean fluorescence intensity (Naidu et al., 2009; Vijayan et al., 2011).

3.7 Numerical data presentation and statistical analysis

The numerical data are presented as bar charts whereby each column of bar charts represents the mean value for biological replication of 3 times in each group. The error bars of each column represent the values of standard error (SE) of each experimental group. Student t-test for paired values and ANOVA test for multi-paired values were applied to evaluate the difference in significance between and within experimental groups, the significances of differences were indicated as *(P≤0.05), **(P≤0.01) and ***(P ≤0.001) compared with the corresponding basal value of the WT.

4. Results:

4.1. Part I: The *Pex11β* gene KO causes peroxisomal dysfunction, resulting in osteoblast differentiation delay and severe cell signaling alterations

4.1.1. *Pex11β* KO in primary osteoblasts and *Pex11β* gene knockdown via *Pex11β* shRNA in the MC3T3-E1 cell line

4.1.1.1. *Pex11β* gene deficiency primary osteoblasts

Primary osteoblasts from the calvariae of *Pex11β* KO mouse pups were isolated. To confirm that the *Pex11β* gene expression was knocked out a qPCR with specific primers was performed. On the basis of the mRNA level of the *Pex11β* gene the KO was evaluated. As is shown in Figure.15. the basal value of the *Pex11β* mRNA in *Pex11β* KO osteoblast is completely diminished than in WT primary osteoblasts.

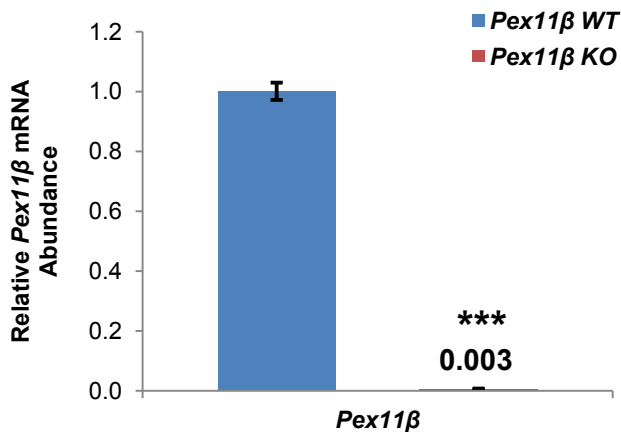
Figure.15. The *Pex11β* gene expression was completely diminished in osteoblast cells isolated from *Pex11β* KO mice. Total RNA of WT osteoblasts and *Pex11β* KO osteoblasts were analyzed for the expression of the *Pex11β* gene via qRT-PCR.

4.1.1.2. *Pex11β* gene deficiency in MC3T3-E1 cells

The *Pex11β* dysfunction in MC3T3-E1 cell line was generated by knocking down the *Pex11β* gene expression with shRNA plasmids with different functional sequences (see Table.7.). To evaluate the effects of these plasmids on diminishing the *Pex11β* gene expression level, a RT-PCR and qRT-PCR were performed with the total RNA isolated from the MC3T3-E1 cells 48 h after transfection (Figure.16.). With these methods strong variation of *Pex11β* knockdown was observed by using the 4 different *Pex11β* shRNA plasmids. A significantly reduced expression of the *Pex11β* gene could be detected in the MC3T3-E1 cells transfected with plasmid 1,3,4. The highest down-regulation was obtained with plasmid 3 whereas the plasmid 2 induced a *Pex11β* mRNA stabilization (increased *Pex11β* band).
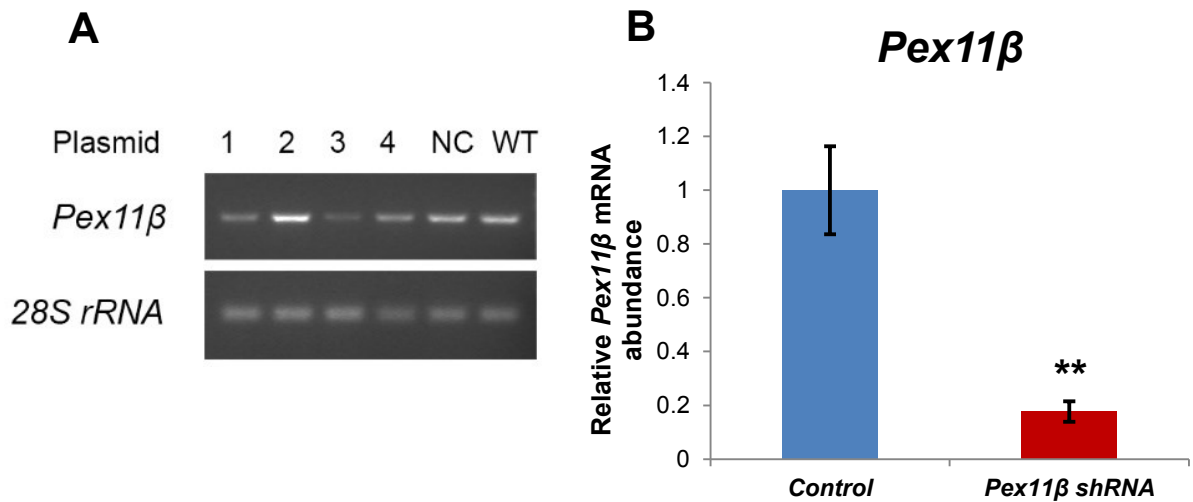
Figure.16. Different *Pex11β* plasmids show distinct effect on the *Pex11β* mRNA expression level. The expression of the *Pex11β* gene was significantly diminished in *Pex11β shRNA* transfected ME3T3-E1 cells. A: Total RNA of negative control (NC), wild type control (WT) and transfected MC3T3-E1 cells with *Pex11β* shRNA knockdown plasmids were analyzed for the expression of the *Pex11β* gene by semi-quantitative PCR. Four shRNA knockdown plasmids (1-4) were compared with a negative control plasmid NC and cells which were not transfected (WT). **B**: In the best knockdown group, total RNAs of the negative control and of MC3T3-E1 cells transfected with the *Pex11β*

gene shRNA knockdown plasmid 3 were analyzed to determine the relative expression levels of the *Pex11β* gene by qRT-PCR (82% knock down).

4.1.2. The *Pex11β* gene KO results in dramatically decreasing the expression level of the peroxisomal functional enzymes

It has been known that the abundance of the PEX11β protein can strongly influence peroxisome proliferation(Li et al., 2002a). To determine the effects of *Pex11β* knockout on the expression of other peroxisome biogenesis genes, qPCRs were performed with the samples of total RNA isolated from *Pex11β* WT/KO primary osteoblast and the *Pex11β* knockdown MC3T3-E1 cells (Figure.17.and 18.).
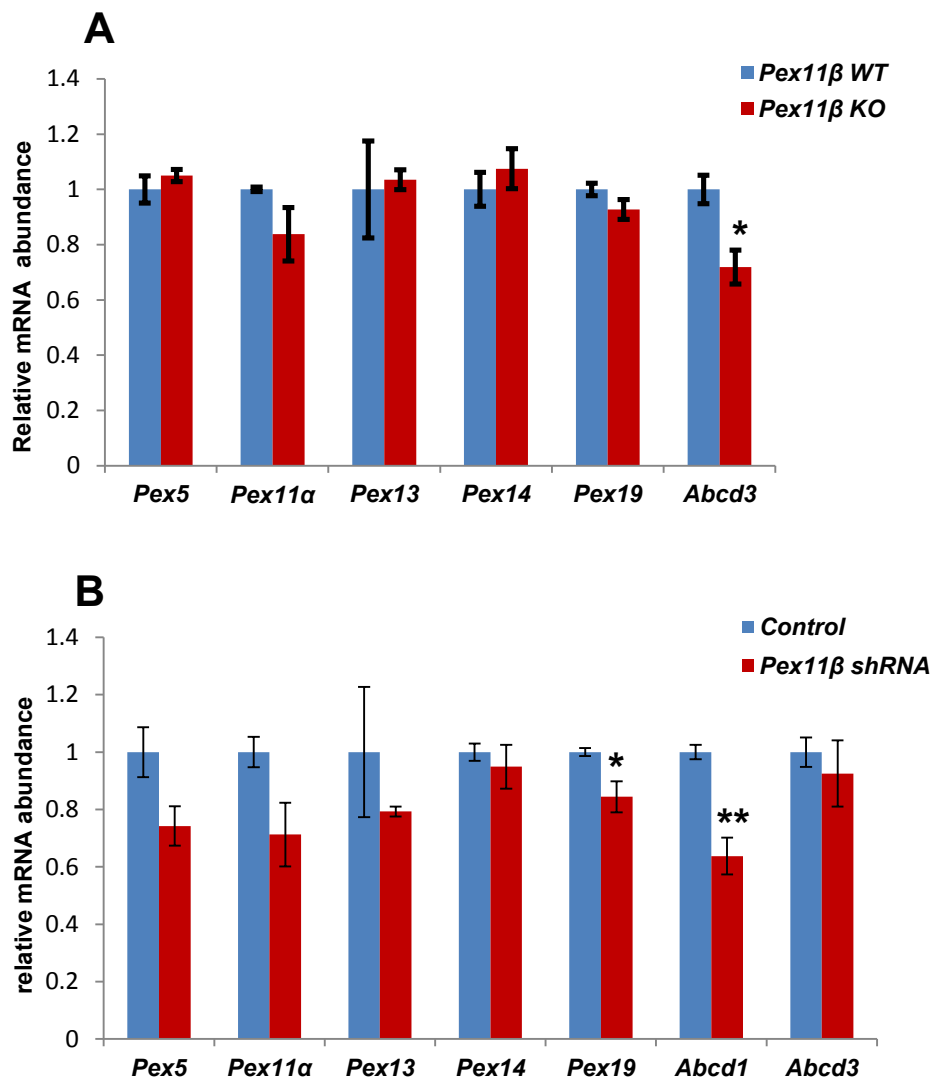
Figure.17. The expression levels of peroxisome biogenesis genes are not significantly changed compared to the WT levels, whereas the PMP protein was down regulated in *Pex11β* KO osteoblast cells and *Pex11β* shRNA knockdown MC3T3-E1 cells. A: Total RNA of WT and *Pex11β KO* primary osteoblasts were analyzed for the expression level of important peroxisome biogenesis genes via qRT-PCR. **B:** Total RNA of *Pex11β gene* shRNA knockdown plasmids and corresponding control plasmid transfected MC3T3-E1 cells were analyzed to determine the expression levesl of important peroxisome biogenesis genes via qRT-PCR.

The results of the qRT-PCR demonstrate that the expression levels of most of the peroxisome biogenesis genes are not altered significantly via the chronic

causal KO (Figure.17.A) and ones slightly with the acute knockdown (Figure.17.B) of *Pex11β*. Most of the changes in the gene expression occurred in *Abcd3* which encodes a membrane transporter that functions as a channel for metabolic β-oxidation substrates, such as VLCFA. This result suggests the peroxisomal β-oxidation functions possibly may have been interfered by *Pex11β gene* deletion.
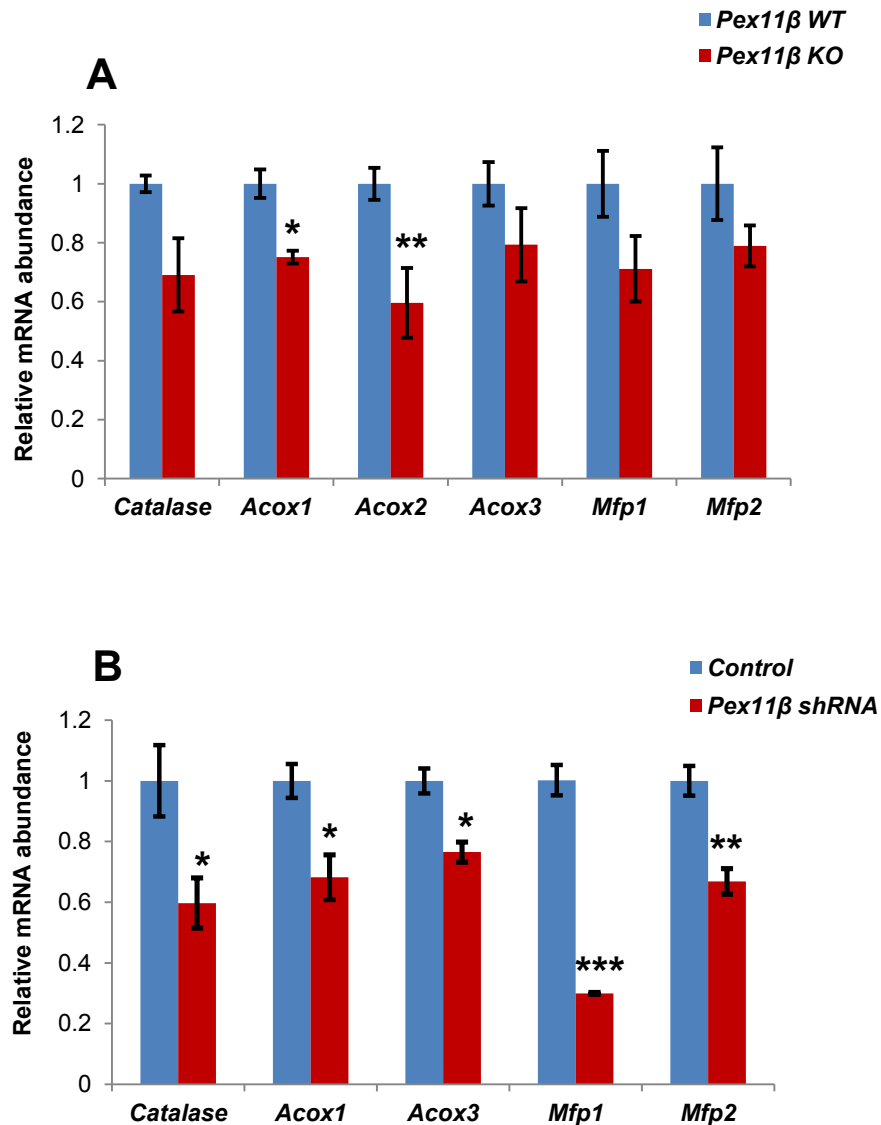
Figure.18. The gene expression of most peroxisomal enzyme is significantly decreased in *Pex11β* KO osteoblast and *Pex11β* shRNA knockdown MC3T3-E1 cells. A: Total RNA of WT control and *Pex11β KO* osteoblasts were analyzed to determine the expression levels of important peroxisomal antioxidant and β-oxidation

enzyme genes by qRT-PCR. **B:** Total RNA of *Pex11β* gene shRNA knockdown plasmids and corresponding control plasmid transfected MC3T3-E1 cells were analyzed to determine the expression levels of important peroxisomal antioxidant and β-oxidation enzyme genes by qRT-PCR.

The qRT-PCR results revealed that the gene expression levels of fatty acid β-oxidation enzymes, especially *Acox1* and *Acox2*, were significantly decreased in the *Pex11β* KO osteoblast (Figure.18.A). In the MC3T3-E1 cell line acute knockdown also the mRNAs for most peroxisomal β-oxidation enzymes are reduced whereas in the chronic *Pex11 β* knock out only *Acox1* and *Acox2* are diminished. Furthermore, the down-regulation of β-oxidation enzymes in *Pex11β KO* osteoblast also has been confirmed on the protein level via western blot which were previously performed in our laboratory: in particular the Thiolase, as well as the lipid transporter ABCD3 in the peroxisomal membrane were down-regulated (Qian, 2010a). Therefore, the β-oxidation function of the peroxisome was disturbed through the *Pex11β* gene deletion in osteoblast, which probably results in the accumulation of lipids together with their metabolic and toxic effects in *Pex11β KO* osteoblast.

4.1.3. Osteoblast differentiation and maturation were severely altered in the primary osteoblast cells culture with *Pex11β* KO

Previously, it has been shown that primary osteoblast with a *Pex11β* KO are much less matured compared to WT osteoblast. We have observed that the typical middle stage of osteoblast maturation marker OPN and the later stage osteoblast cell maturation marker BGLAP (Tanaka et al., 2012) are reduced present in *Pex11β* KO osteoblast compared to the WT osteoblast, both in vitro and vivo. More interestingly, in further experiments, we found that the differentiation and maturation delay caused by *Pex11β* deficiency mainly occurred in the later stage of pre-osteoblast, mature osteoblast, as the following figure 19 shows. The expression levels of osteoblast differentiation marker genes can be used for indicating progressing steps of osteoblast differentiation and maturation. Our group also has found that the middle stage and maturation

marker protein OPN and BGLAP were decreased in *Pex11β* KO osteoblast (Qian, 2010a), whereas the osteoblast progenitor marker *Col1a1* and *Col1a2* gene expression levels were not significantly changed in *Pex11β* KO osteoblast compared to WT. Therefore, the delay in *Pex11β* KO osteoblast starts only after the osteoblast progenitor stage at the maturation stage of early-osteoblast.

The delay of osteoblast differentiation might not be the only reason why *Pex11β* KO animal exhibit reduced ossification and bone value. Therefore we have investigated whether there are other abnormal phenotypes in *Pex11β* KO osteoblast that might affect ossification(Qian, 2010b).
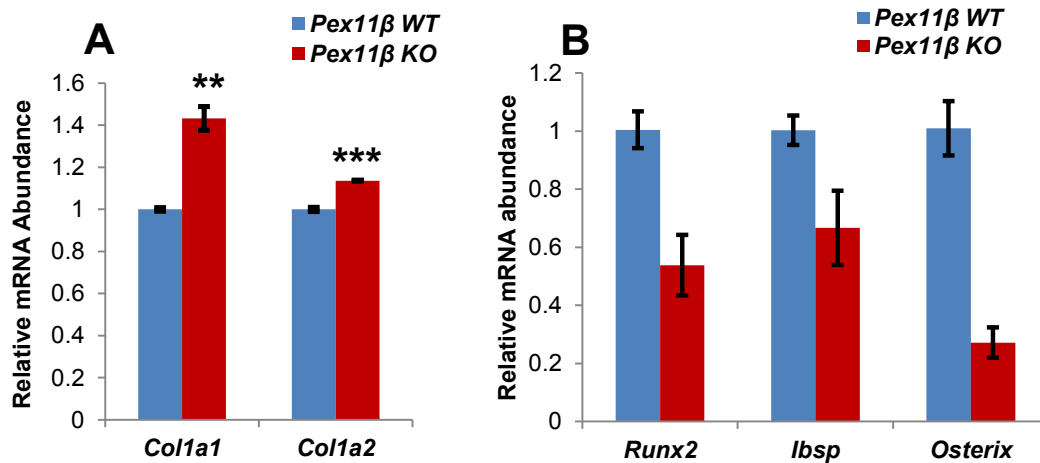
Figure.19. The *Pex11β* KO osteoblast exhibit a delay in the differentiation process indicated by the expression level of osteoblast differentiation stage markers. **A:** Total RNA of WT and *Pex11β KO* osteoblast were analyzed to determine the expression levels of osteoblast progenitor markers *Col1a1* and *Col1a2* via qRT-PCR; **B:** Total RNA of *Pex11β KO* osteoblast and WT were analyzed to obtain the expression levels of the pre-osteoblast marker Runx2, mature osteoblast marker *Ibsp* and osteocyte marker *Osterix* via qRT-PCR**.**

4.1.4. The DNA binding functions of key nuclear receptors regulating the osteoblast differentiation and function were significantly altered in *Pex11β KO* osteoblasts

4.1.4.1. The *Pex11β* shRNA knockdown in MC3T3-E1 cell culture coordinates the results of primary osteoblast cells and lead to significant decrease of differentiation and maturation

To further confirm the results of differentiation delay of *Pex11β* KO osteoblast, the model of *Pex11β* shRNA knockdown in MC3T3-E1 cell was used. The .expression levels of osteoblast differentiation markers of the early middle and maturation stage (Figure.20.) are dramatically decreased in the *Pex11β* shRNA knockdown in MC3T3-E1 cells in the very similar manner as the ones in *Pex11β* KO primary osteoblast (Figure.19.). Therefore, this cell line was used to measure gene transcriptional activity using the luciferase reporter gene assays (Figure.21.-23).
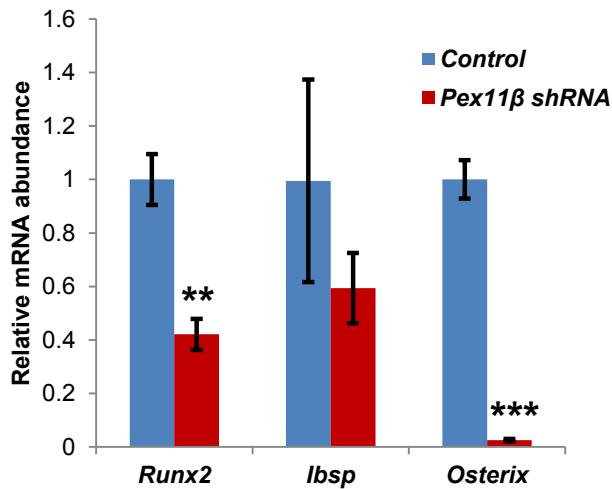
Figure.20. The *Pex11β* shRNA knockdown in MC3T3-E1 cells also exhibit a delay in the differentiation process indicated by the expression level of osteoblast differentiation stage markers. Total RNA of MC3T3-E1 cells transfected with *Pex11β* gene shRNA knockdown and control plasmids were analyzed to determine the expression levels of the pre-osteoblast marker Runx2, mature osteoblast marker *Ibsp* and osteocyte marker *Osterix* via qRT-PCR. The columns are the mean ± SE for n=3

experiments in each group, student t test for paired values compared with the corresponding basal value of the WT/control was used.

4.1.4.2. Significant decrease of the DNA binding activity of FoxOs in osteoblast with *Pex11β* shRNA knockdown.

Previous research on the skeleton revealed the importance of the regulator forkhead box1 (FoxO1) which is indeed a regulator of redox balance in osteoblast (Almeida et al., 2009; Ambrogini et al., 2010; Tanaka et al., 2012). FoxO1 belongs to the winged helix/forkhead family of transcription factors. which share a highly conserved 110-amino-acid DNA-binding domain, also known as forkhead box or winged–helix domain (Obsil and Obsilova, 2011). This balance was clearly decreased in *Pex11β* KO in osteoblast; in particular, the level of FOXO1 protein was reduced in *Pex11β* KO osteoblasts compared with WT(Qian, 2010a).
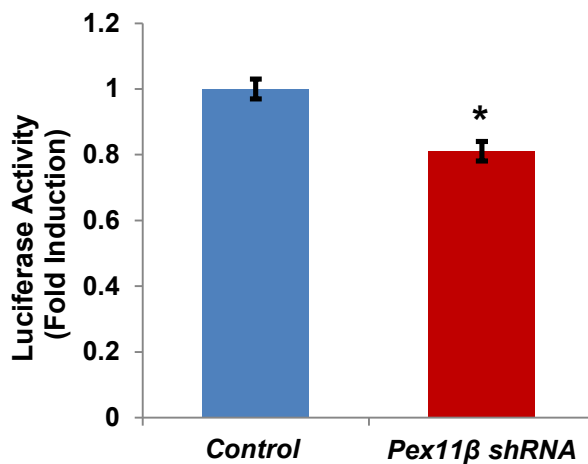
Figure.21. The FoxO protein DNA binding capability was slightly decreased in *Pex11β* shRNA knockdown ME3T3-E1 cells. ME3T3-E1 cells after *Pex11β* shRNA knockdown and control cells were transfected with the pGL3-6xDBE FoxO response element luciferase reporter plasmids (Ambrogini et al., 2010). 24 hours after transfection, cell extracts were collected and assayed for luciferase activity.

4.1.4.3. Increase of the activity of the PPAR response element (PPRE) in *Pex11β* KO osteoblast compared with WT

Previous research in our lab had revealed that the PPARγ protein level was dramatically increased in *Pex11β KO* osteoblast which was determined by Western blots using the whole cell lysate of *Pex11β* KO and WT osteoblast (Qian, 2010a). Activation of the PPARγ can result in the differentiation of the mesenchymal stem cells into adipocytes instead of the osteoblast progenitors (Almeida et al., 2009) and this activation can be triggered by the binding of PPAR and agonists. The activated PPARγ can bind the PPRE to switch on the specific gene expressions that regulate the mesenchymal stem cell differentiation (Almeida et al., 2009; He et al., 1999).
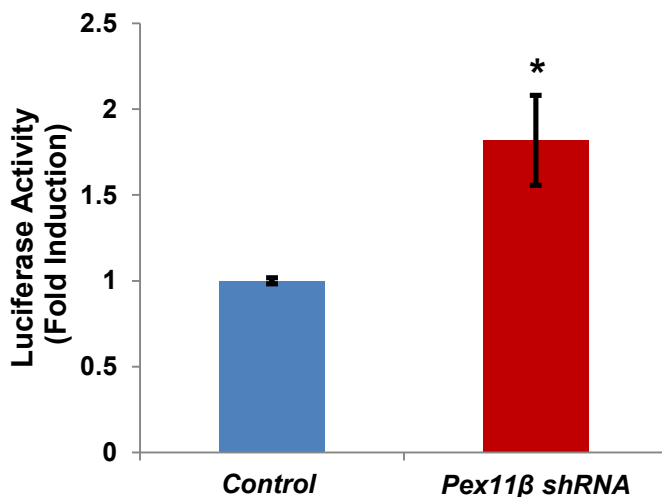
Figure .22. The PPARs response element (PPRE) is considerably more activated in *Pex11β* shRNA kockdown ME3T3-E1 cells compared to the control group (WT). ME3T3-E1 *Pex11β* shRNA knockdown cells and control cells were transfected with luciferase reporter vectors (plasmid p4xACO-Luc).24 hours after the transfection; cell extracts were collected and assayed for luciferase activity.

4.1.4.4. Significant decrease of the Runx2 DNA binding activity in *Pex11β* KO osteoblast

RUNX2 is an important transcription factor in osteoblast progenitors, pre-osteoblasts and even in chondrocytes by regulating the expression of several bone and cartilage genes and is essentially required for the bone formation *in vivo* (Drissi et al., 2000). The RUNX2 DNA binding function is based on the affinity to specific motifs localized in the promoter region of some important genes regulating bone cell differentiation and bone formation, including *Runx2* itself thus being self-regulated in part by a "negative feedback (Drissi et al., 2000). RUNX2 determines the lineage of osteoblast from multipotent mesenchymal cells, enhances osteoblast differentiation at an early stage, and inhibits osteoblast differentiation at a late stage (Komori, 2002). In the *Pex11β* shRNA knockdown osteoblast, RUNX2 DNA binding capability was considerably altered (Figure.23.). A decrease of approximately 20% in the reporter gene activity was observed and later stage differentiation was delayed in the *Pex11β* shRNA knock down cells.
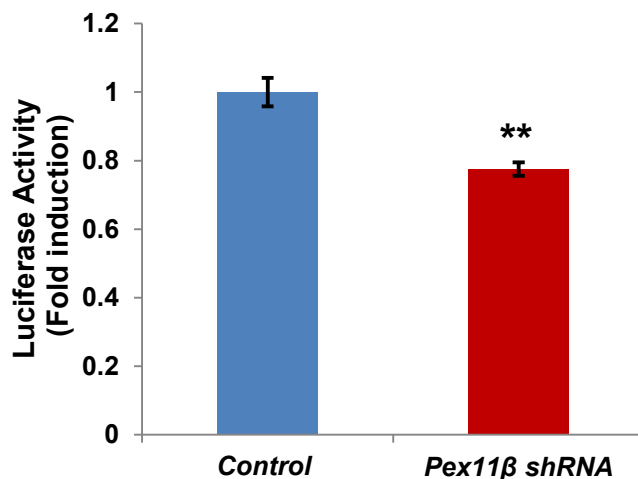
Figure.23. The Runx2 response element activity is decreased in *Pex11β* shRNA knockdown ME3T3-E1 cells. ME3T3-E1 *Pex11β* shRNA knockdown and control cells were transfected with the luciferase reporter vector (plasmid

R19 as described in "*Materials and Methods*"). 24 hours after the transfection, cell extracts were collected and assayed for luciferase activity.

4.1.5. Significantly higher amount of apoptosis of primary *Pex11β KO* compared to WT osteoblasts.

To quantify the apoptotic osteoblast, a TUNEL assay was performed using *Pex11β* KO/WT primary osteoblast. The number of apoptotic osteoblast in the *Pex11β* KO model was significantly higher in comparison to the WT (Figure.24.). The TUNEL staining results revealed that apoptosis was considerably increased in the *Pex11β* KO osteoblast cell culture, which suggests that the osteoblast function might be disturbed strongly by possibly increasing oxidative stress due to peroxisome dysfunction in *Pex11β KO* osteoblast cells. Furthermore, this result also suggests that some critical cellular signaling pathways that attenuate to the osteoblast differentiation and maturation, such as FoxOs and PPAR signaling pathways might be also altered by the increase in oxidative stress in *Pex11β* KO osteoblast. Therefore, several functional assays to determine the altered activity of these signal pathways were performed by using *Pex11β* the shRNA knockdown MC3T3-E1 cell model.
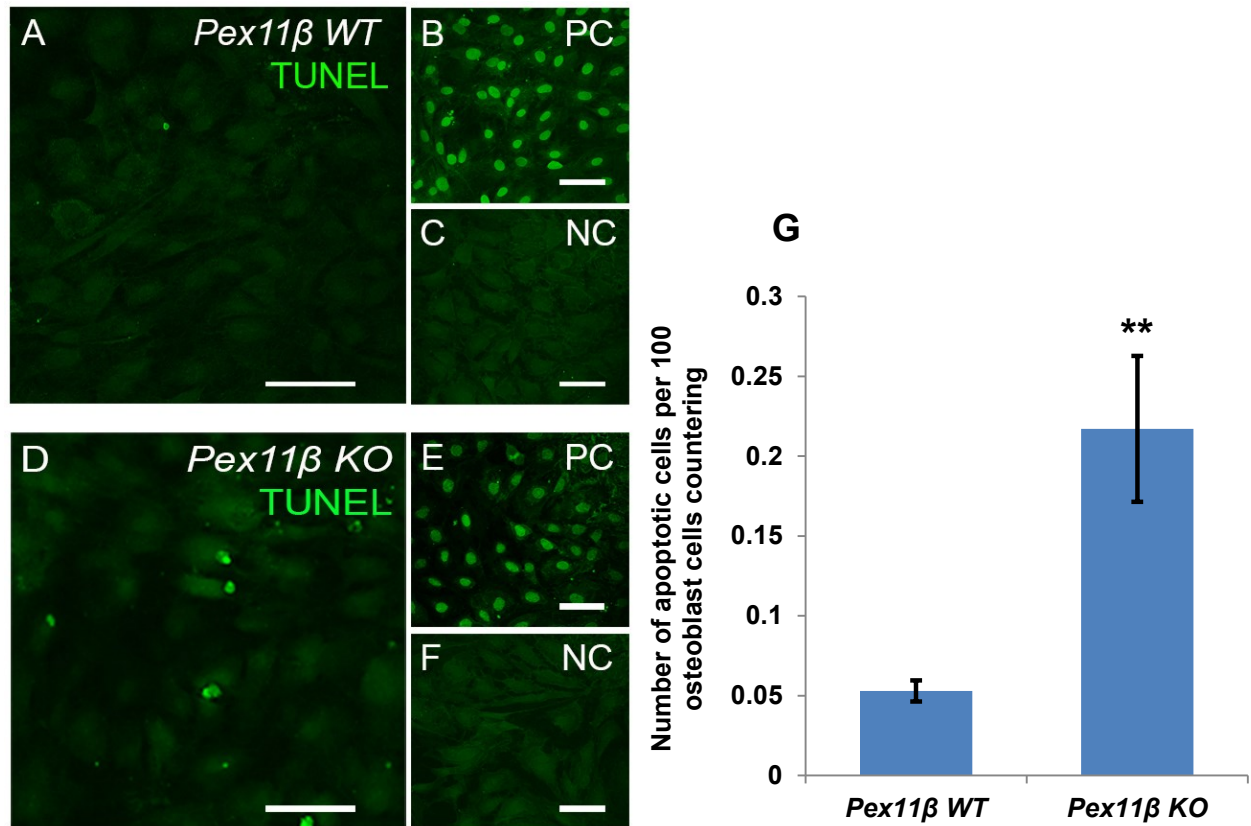
Figure.24. Increased number of apoptotic osteoblast present in primary *Pex11β* KO osteoblast cell culture compared to WT. Apoptotic cells in *Pex11β* WT and KO osteoblast cell cultures were detected using the ApopTag® Fluorescein *in situ* Apoptosis Detection Kit (S7110 Millipore GmbH, Schwalbach, Germany) by direct TdT-mediated dUTP-biotin nick end labeling (TUNEL)**,** utilizing an anti-digoxigenin antibody conjugated with Fluorescein molecule according to the manufacturer's protocol (**A** and **D).** The number of apoptotic nuclei was (right picture G) increased in *Pex11β* KO cell cultures **(D)** in comparison to the WT cell cultures **(A)**. **B and E**: Positive controls (PC) had been pre-treated with 0.1U/µl DNase I for 2 min to artificially induce DNA strand break. **C and F:** Negative controls (NC) were done using 1×PBS solution instead of the TdT Enzyme from this Kit. (see section 3.5.3) **G**: Osteoblasts isolated from 3 pairs of *Pex11β* WT and KO animals were analyzed. For the quantification of the apoptosis rates in each of the 3 cell cultures, TUNEL-positive cells in 500 randomly selected *Pex11β* WT and KO osteoblasts were counted. Quantification of TUNEL positive cells revealed a pronounced increase in the number of apoptotic cells in *Pex11β KO* cell culture in comparison to WT cells (P<0.001). Bars represent 50 µm.

4.1.6. Strong disruption of the cell cycle and proliferation rate in *Pex11β* KO osteoblast

Previous results also showed the weaker transcriptional function of FoxO in *Pex11β* KO osteoblast cells (Figure.21.) (Sanchez et al., 2014; Sang et al., 2014). Therefore, it could be hypothesized, that the cell cycle of *Pex11β* KO osteoblast cells should be altered compared to the WT. Wherefore we applied a FACS experiment.

The FACS results of cell revealed that the S-phase and the G2/M phase of the *Pex11β* KO osteoblasts were extended. Statistically, more *Pex11β* KO osteoblast in cell culture were in the S-phase and the G2/M phase and less in the G1 phase compared to the WT cells in cell culture. However, when the osteoblasts were cultured with differentiation enhancing medium and osteoblasts differentiation was promoted, even less *Pex11β* KO osteoblasts were found in the S-phase started to decrease dramatically after 4 and 7 days of induction compared to WT osteoblast (Figure.25.)
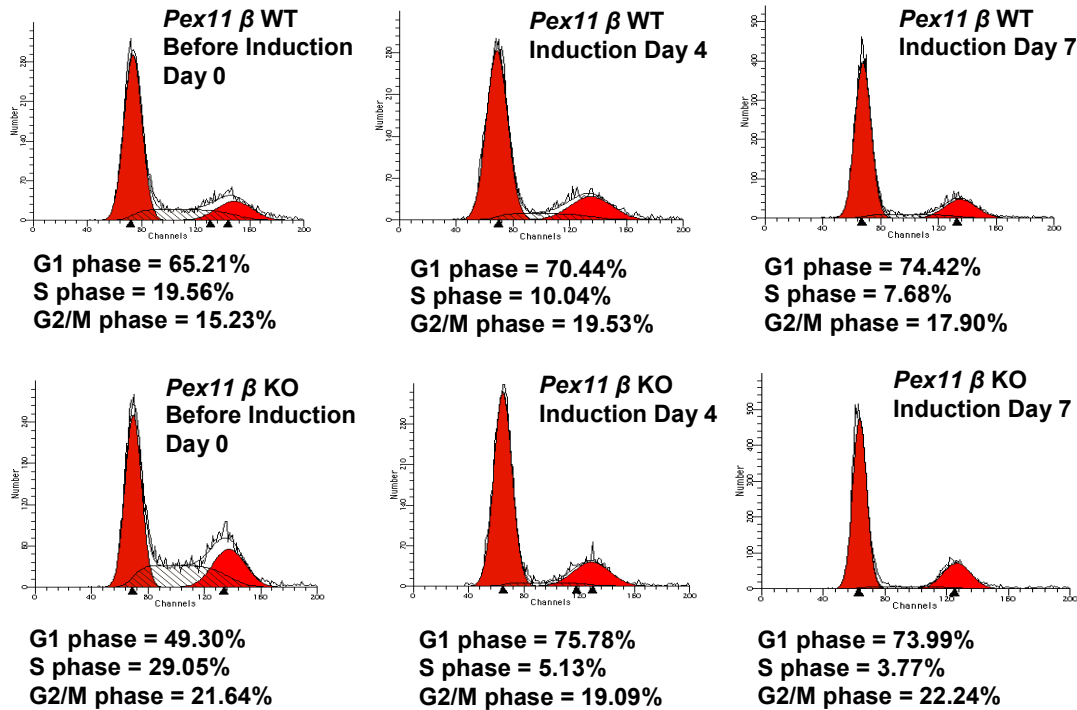
Figure.25. FACS analysis of cell cycle of *Pex11β* KO in comparison to WT osteoblasts. Percentage of cells in different phase are indicated below the graph. Cell cycles of *Pex11β* KO osteoblast were strongly altered compared to *Pex11β* WT osteoblasts, and this alteration was diminished when the osteoblasts were cultured in osteoblasts differentiation enhance medium from day 0 (induction start).

By numeric analysis, the reason for the decrease in the number of *Pex11β* KO osteoblasts in the S-phase appears to be because of an interference in the G2/M phase checkpoint by the *Pex11β* gene deletion and because more *Pex11β* KO osteoblasts in the S-phase went through the checkpoint and were arrested in the G2 phase. The checkpoint at the boundary between the G2 and M phase of the cell cycle (G2/M) can regulate entry into mitosis. In many organisms, this checkpoint surveys DNA damage and cell size and is controlled by both the activation of mitotic cyclin-dependent kinases (Cdks) and the inhibition of an opposing phosphatase, protein phosphatase 2A (PP2A). Misregulation of mitotic entry can often lead to oncogenesis or cell death (Han et al., 2010).

4.2. Part II: The *Pex13* KO caused peroxisomal biogenesis defect result in the interference with the antioxidative response, osteoblast differentiation and maturation

4.2.1. *Pex13* KO mice (P0.5) exhibit a delay in the ossification process

Previous results of a doctoral student in the Baumgart-Vogt group showed, that *Pex13* KO mice develop an obvious bone phenotype much later than *Pex11β* KO mice. Indeed, E19 *Pex11β* KO mouse fetuses display defects in ossification and skeletal deformation (Qian, 2010a), whereas E19 *Pex13* KO mouse fetuses do not yet display significant differences in ossification and skeletal formation. Therefore we analyzed older P0.5 *Pex13* KO/WT mouse pups which were used to determine the bone development. The results are depicted in Figure 26. With the help of the VCT analysis, it was shown that in comparison to *Pex13* WT and *Pex13* heterozygous (HTZ) mice, the skeletal differentiation of *Pex13* KO mice was altererd, displayed by much smaller size of the pups and significantly less bone volume due to delayed ossification. In particular, the size of the skull in *Pex13* KO mice is relatively smaller and the long bones such as tibiae, ribs, femora are shorter, indicating both intramembranous and endochondral ossification defects in *Pex13* KO mice (Figure.26.).
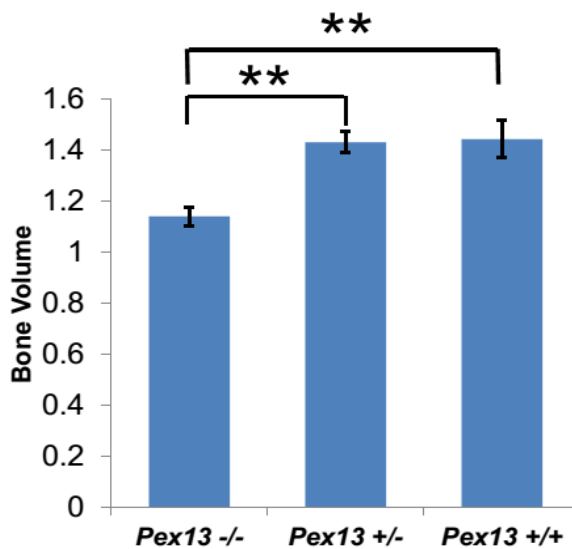
Figure.26. *Pex13* **KO pups are smaller; the bone volume is significantly decreased and the ossification delayed compared to WT pups. A:** Newborn *Pex13* KO pups (P 0.5) were scanned with a VCT. Significant difference are observed by comparing ossification center in the *Pex13 KO* animals (e.g. in ossification coxal and paws or skull). **B:** Relative bone volume (g/cm^3) estimated via VCT scanning revealed that the bone volume of the *Pex13* KO mice is significantly reduced in comparison to *Pex13* WT and *Pex13* HTZ mice.

Compared to *Pex11β* KO mice*,* it seems that the ossification defect of *Pex13* KO mice is initiated in a later stage of development, probably caused by a decreased capability of osteoblast mineralization. Therefore, a minimization staining experiment was performed using osteoblast isolated from *Pex13* KO mice in compared to WT mice. The following Figure.27. depicts the results. The differentiation enhancing medium can stimulate and speed up the pre-osteoblast differentiation to mature state osteoblast with full functional mineralization capacity which is indicated by the synthesis and secretion of osteocalcin (BGLAP) protein (Figure.28.D). The mineralization staining revealed that less calcium hydroxyapatite containing osteoid was formed in the *Pex13* KO cells compared to *Pex13* WT cells under the same cell culture conditions. This result suggests that differentiation and maturation processes are significantly delayed in *Pex13* KO osteoblast.
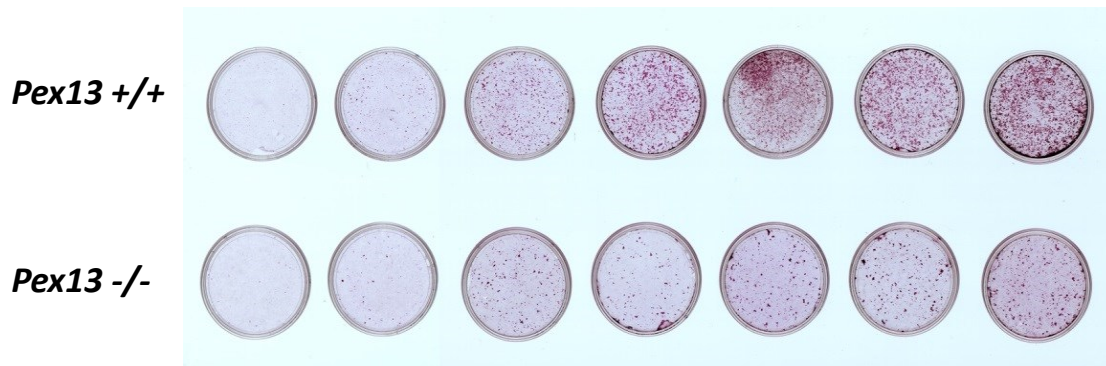
Figure.27. Mineralization staining was performed to detect the synthesized matrix at various stages of osteoblast differentiation in *Pex13*KO versus WT osteoblasts in cell culture. The differentiation medium was added to the cell culture starting at day 10 after the primary osteoblast isolation. Osteoblasts were cultured for 9 days (28-10=18) in the differentiation enhancing medium, calcium-rich deposits can be stained with Alizarin red S staining to evaluate the progress of bone formation of mature state osteoblasts in cell culture (Gregory et al., 2004). The *Pex13* KO osteoblast cell culture was stained less by Alizarin red S.

To further confirm the delay of *Pex13* KO osteoblast differentiation, the gene expression level of osteoblast differentiation and maturation markers were determined with qRT-PCR (Figure.28.). Interestingly, compared to the delay in differentiation of *Pex11β* KO osteoblasts starting at middle stage, the differentiation delay of *Pex13* KO osteoblast started from the osteoblast progenitor stage, which was the earliest stage of osteoblast isolated from the calvariae of mouse pups of *Pex13* KO. Throughout the lifespan of osteoblast until the osteocyte stage, the differentiation process is significantly delayed. Specifically, in the pre-osteoblast stage and middle stage of osteoblast differentiation compared to WT, the delay is indicated by a strongly reduced gene expression level of osteoblast differentiation stage markers for osteoblast progenitors markers (A) *Col1a1* and *Col1a2*, (B) pre-osteoblast markers *Alp and Runx2,* (C) middle stage osteoblast differentiation markers *Ibsp* and *Opn,* (D) osteoblast maturation markers *Osterix* and *Bglap* (Figure.28.)*.*
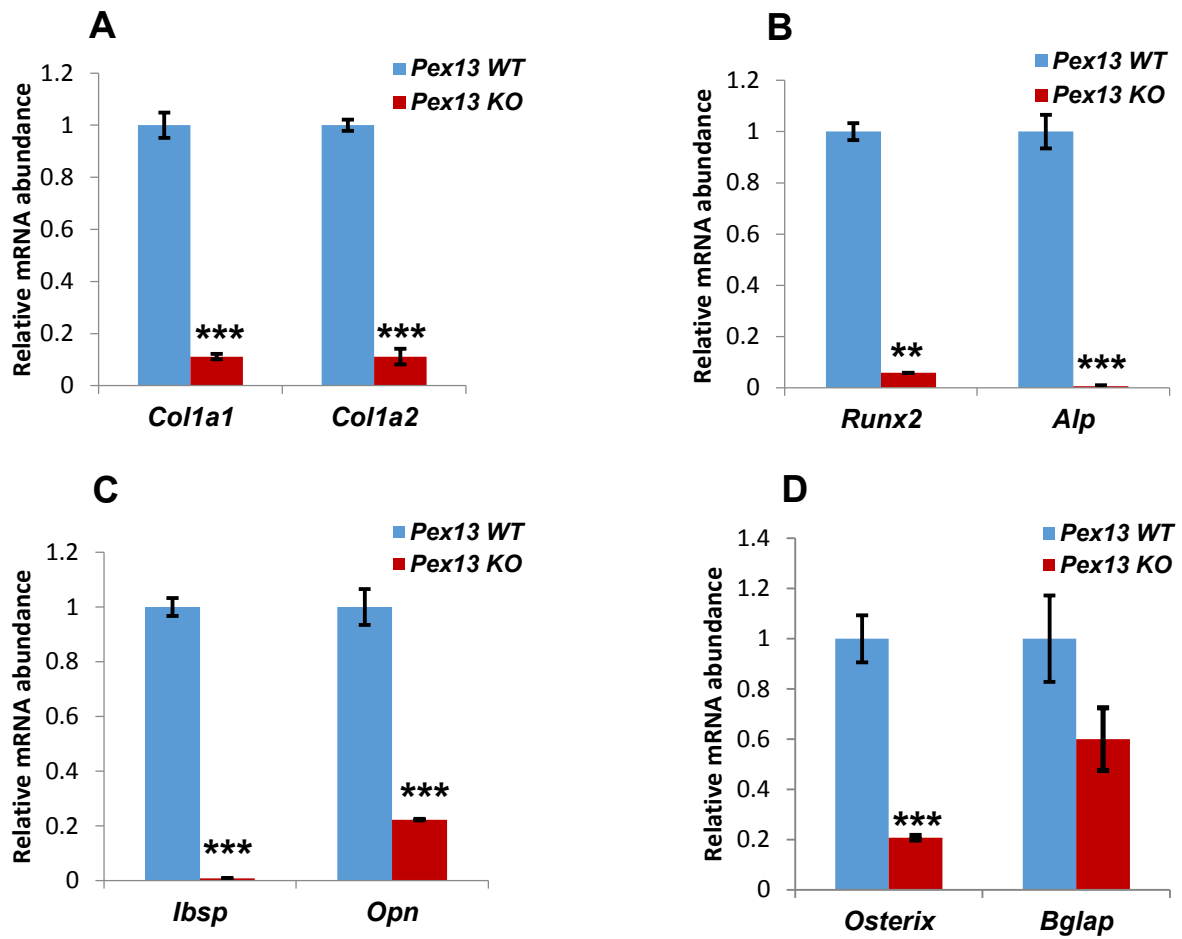
Figure.28. Delayed differentiation and maturation of osteoblast from calvariae of *Pex13* KO mice. Total RNA of wild type (WT) control and *Pex13* KO osteoblast was analyzed to determine the expression levels of mRNA for osteoblast progenitor and mature osteoblast markers. **A**: osteoblast progenitor markers *Col1a1* and *Col1a2*; **B**: Pre-osteoblast markers *Alp and Runx2*; **C:** osteoblast middle stage marker *Opn* and *Ibsp*; **D**: osteoblast maturation markers *Osterix* and *Bglap* via qRT-PCR.

4.2.2. Peroxisomal biogenesis genes and the osteoblast differentiation process were disturbed

The expression levels of peroxisome biogenesis genes and metabolic matrix enzymes genes are decreased in *Pex13* KO osteoblast. It has been observed that the *Pex13* KO mice lack morphologically intact peroxisomes and display a defect in the import of matrix proteins containing either type 1 or type 2 targeting signals (Maxwell et al., 2003). To determine, how peroxisome biogenesis and metabolic genes are altered by the *Pex13* gene deletion in osteoblast, qPCRs were performed to analyze the expression levels for peroxisome related genes. The results are depicted in Figure.29. The expression levels of almost all peroxisomal biogenesis (except for *Pex11α*) and functional enzyme genes were dramatically reduced in *Pex13* KO osteoblast compared to WT.
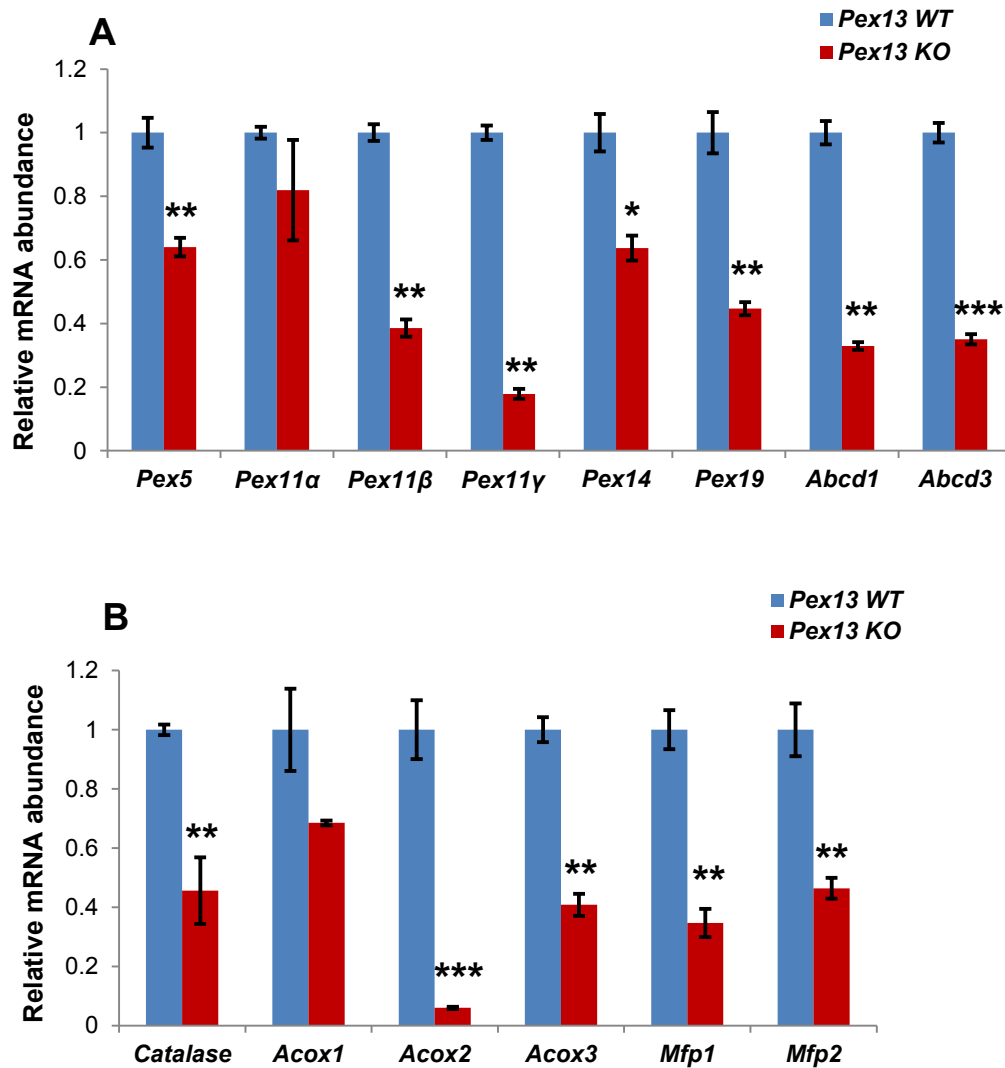
Figure.29. Peroxisome related gene expression is strongly reduced in *Pex13* KO osteoblast. A: Total RNA of WT control and *Pex13 KO* osteoblasts was analyzed to determine the expression levels of important peroxisomal biogenesis genes and **B:** genes of peroxisomal matrix enzyme genes by qRT-PCR.

4.2.3. The oxidative response is stimulated by oxidative stress in the bone cells of *Pex13* KO mice due to peroxisomal dysfunction

Alteration of mitochondria morphology and indication for oxidative stress has been described in the *Pex5 KO* mouse model by Baumgart and colleagues (Baumgart et al., 2001). However, no information on alteration of mitochondria

due to peroxisomal knockout was described in osteoblast or other bone cells. A nice indicator of mitochondrial oxidative stress is the elevation of SOD2, which has been exclusively localized to mitochondria, by our group, in comparison to previous report that allocated this enzyme also to the peroxisomal membrane(Singh et al., 1999)

The excellent anti-SOD2 antibody was used in this thesis to detect potential activation of the antioxidative response in mitochondria of *Pex13* KO osteoblast (Figure.30.).
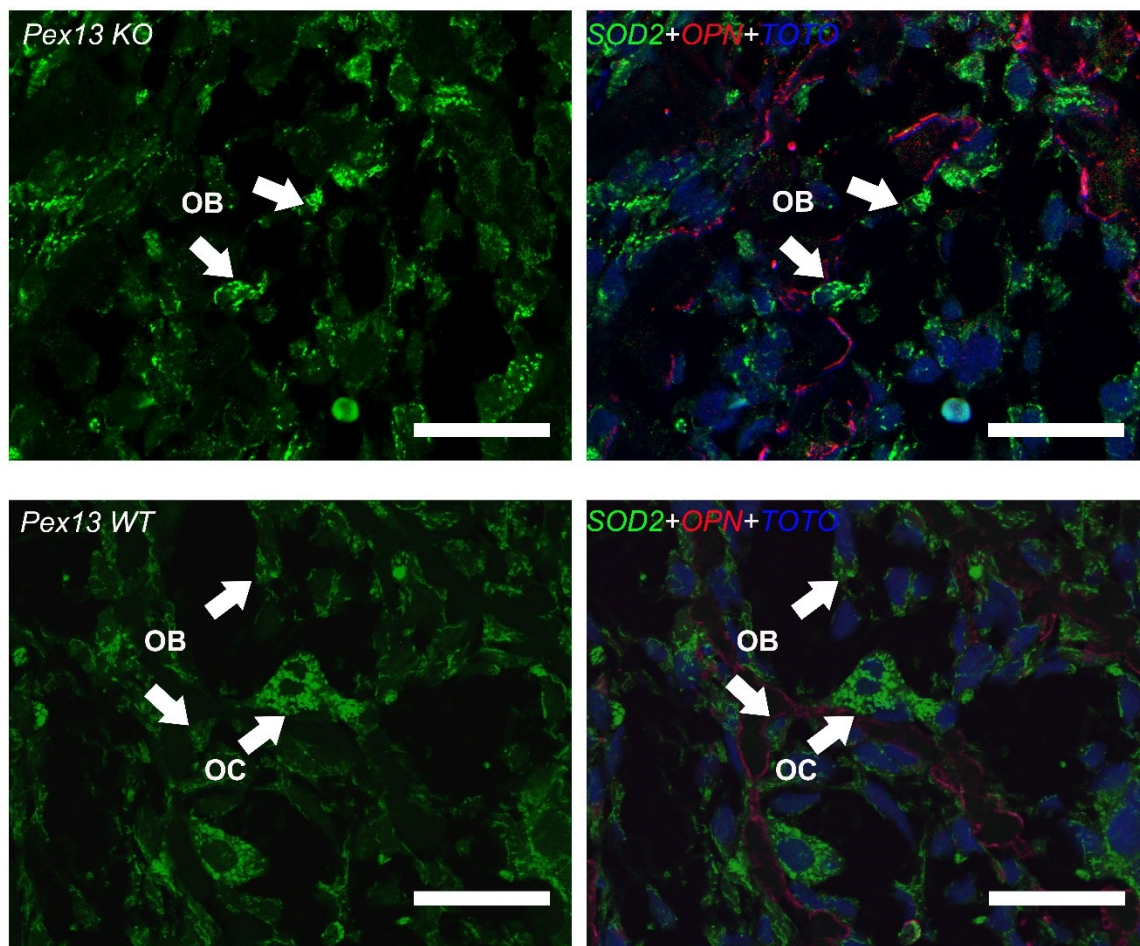
Figure.30. The mitochondrial antioxidant enzyme SOD2 is increased in *Pex13 KO* osteoblast. Double immunofluorescence labelling of paraffin sections of the mandibular bone of *Pex13* KO and *Pex13* WT mouse sections with antibodies against SOD2 and OPN. The red fluorescence (OPN) indicates the differentiated osteoblast (indicated by the arrows). Strongest green fluorescenct (SOD2) are mitochondria more prominent in

Pex13 KO osteoblast. In the WT animal SOD2 staining and mitochondria are most prominent in osteoclast (OC), whereas osteoblasts are hardly stained for SOD2. Bars represent 50 μm.

Under normal conditions, SOD2 in osteoclast mitochondria are most labelled, and osteoblasts only show minor labelling. Indeed, highly elevated SOD2 levels were found in the osteoblast of *Pex13* KO mice. The elevation of SOD2 might be explained by a higher ROS production within the mitochondria or a higher cytoplasm ROS level due to the *Pex13* KO.

To further test this hypothesis, an experiment with the induction of the antioxidant N-Acetyl-Cysteine (NAC) to the cell culture was designed. In particular, this rescue experiment was designed to the antioxidant N-Acetyl-Cysteine (NAC) to treat the *Pex13* KO osteoblast cell cultures in order to eventually compensate the response effects caused by increased oxidative stress in *Pex13* KO osteoblast (Figure.31.).
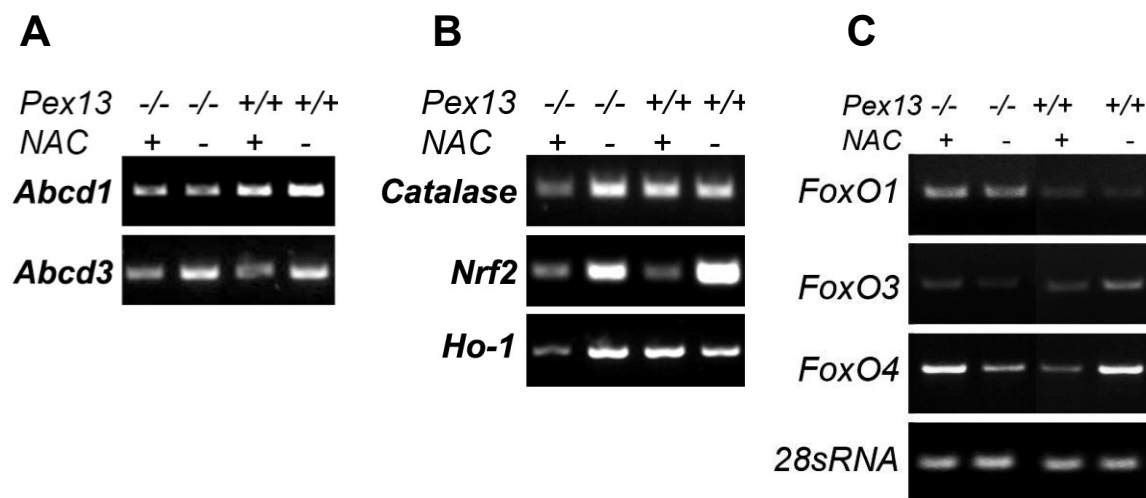
Figure.31. The reaction to N-Acetyl-Cysteine is different in *Pex13* KO and WT osteoblast. Oxidative stress in *Pex13* KO osteoblast can be partially rescued by treatment with antioxidant drug N-Acetyl-Cysteine (NAC). Total RNA was isolated from wild type (WT) control and *Pex13* KO osteoblast cell cultures which were treated with osteoblast medium containing 5 mM N-Acetyl-Cysteine (NAC) for 3 days. The total RNA was analyzed to determine the expression levels of mRNA for **A:** peroxisomal

membrane transporters *Abcd1* and *Abcd3;* **B:** antioxidative enzymes catalase, Heme oxygenase 1 (HO-1) and its regulator Nuclear factor (erythroid-derived 2)-like 2 (NRF2); **C:** important redox-sensitive transcriptional regulator of the FoxO family (members Foxo1, 3 and 4) in bone by semi-quantitative polymerase chain reaction (RT-PCR).

Considering the peroxisomal markers, the expression level of peroxisomal membrane protein ABCD1 were decreased in *Pex13* KO osteoblast, in both NAC treated and untreated situation. This result indicates that the presence of peroxisomes was decreased in *Pex13* KO osteoblast in this cell culture with drug treatment model (Figure.31.A). Interestingly, the expression level of peroxisomam antioxidative enzyme catalase was increased in the *Pex13* KO osteoblast and dramatically reduced when the ROS molecules were trapped by NAC drug. Whereas, antioxidant response regulator NRF2 expression level was decreased in *Pex13* KO and also decreased with NAC treatment in both *Pex13* KO and WT osteoblast. The NFF2 regulating antioxidant enzyme HO-1 expression were much decreased in NAC treated *Pex13* KO osteoblast, compared with the one in NAC treated *Pex13* WT osteoblast (Figure.31.B). Furthermore, within the 3 isoforms existing in osteoblast, FoxO1 expression level is much higher in *Pex13* KO osteoblast and also dramatically increased in NAC treated *Pex13* KO osteoblast (Figure.31.C). FoxO1 within the FoxO family is indeed an important regulator of redox balance in osteoblast and the catalase gene baseline transcription could be activated by FoxOs through oxidative stress and lipid peroxidation (Almeida et al., 2009; Ambrogini et al., 2010; Tanaka et al., 2012).

4.2.4. The DNA binding activity of the Runx2 nuclear receptor which regulates osteoblast differentiation and function was significantly attenuated in primary osteoblast of *Pex13* KO mice

As shown earlier in the *Pex11β* Chapter (4.1.5.4), the RUNX2 DNA binding capability was demonstrably altered, approximately 20% decrease i*n Pex11β* shRNA knockdown cells compared to control cells (Figure.23.) and only later stage differentiation was seriously delayed in the *Pex11β* KO osteoblast

compared with WT (Figure.19.).However, in the *Pex13* KO osteoblast, the RUNX2 DNA transactivation capability was decreased around 70% (Figure.32.) and the most severe differentiation delay occurred in the osteoblast-progenitor, early pre-osteoblast and middle stage of osteoblast differentiation in *Pex13* KO (Figure.28.) (Komori, 2008).
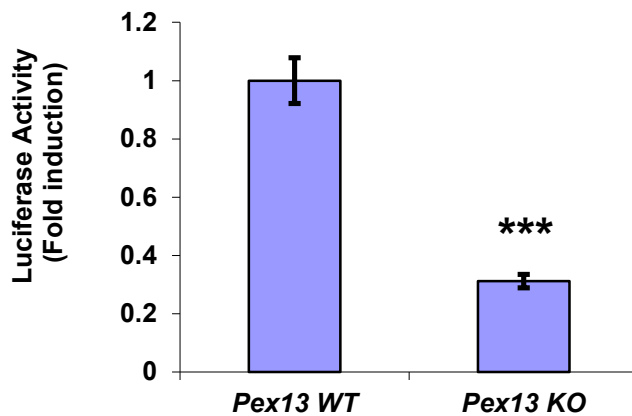
Figure.32. The activity of the Runx2 response element is decreased in *Pex13* KO primary osteoblast. *Pex13* KO and WT primary cells were transfected with the luciferase reporter vector plasmid R19. 24 hours after transfection, cell extracts were collected and assayed for luciferase activity.

4.3. Part III: SIRT1 deficiency impairs peroxisomal functions and promotes pre-mature differentiation of pre-osteoblasts and abnormal bone development in mice

The results in Figure.36. and 44. have been published in Molecular Cell with the pubmed ID PMID: 25155613

Shuang Tang, Gang Huang, **Wei Fan**, Yue Chen, James M. Ward, Xiaojiang Xu, Qing Xu, Ashley Kang, Michael W. McBurney, David C. Fargo, Guang Hu, **Eveline Baumgart-Vogt,** Yingming Zhao, and Xiaoling Li (2014) "SIRT1-mediated deacetylation of CRABPII regulates cellular retinoic acid signaling and modulates embryonic stem cell differentiation" Molecular Cell. 2014 Aug 20. pii: S1097-2765(14)00604-2. doi: 10.1016/j.molcel.2014.07.011.

The mammalian SIRT1 has been very well studied and it has been understood to be implicated in a variety of metabolic processes by its functions of central sensor of nutrient and energy metabolism (Li and Kazgan, 2011). The variety of metabolic activities of mammalian are modulated by activated SIRT1 through either direct protein deacetylation or indirect chromatin remodeling (Li and Kazgan, 2011). Since the SIRT1 control lipid metabolism via PGC1α and regulates PPAR functions and subsequently peroxisome genes are regulated by these nuclear receptors (Li, 2013), it can be believed vice-versa that the SIRT1 activity could possibly be altered by peroxisomal dysfunction caused by *Pex11* or *Pex13* gene deletions. Therefore, the levels of *Sirt1* gene expression and SIRT1 protein in *Pex11β* and *Pex13* KO animal models were determined with qPCR, WB and IF staining.

4.3.1. SIRT1 protein level is altered in primary osteoblast with peroxisomal deficiency
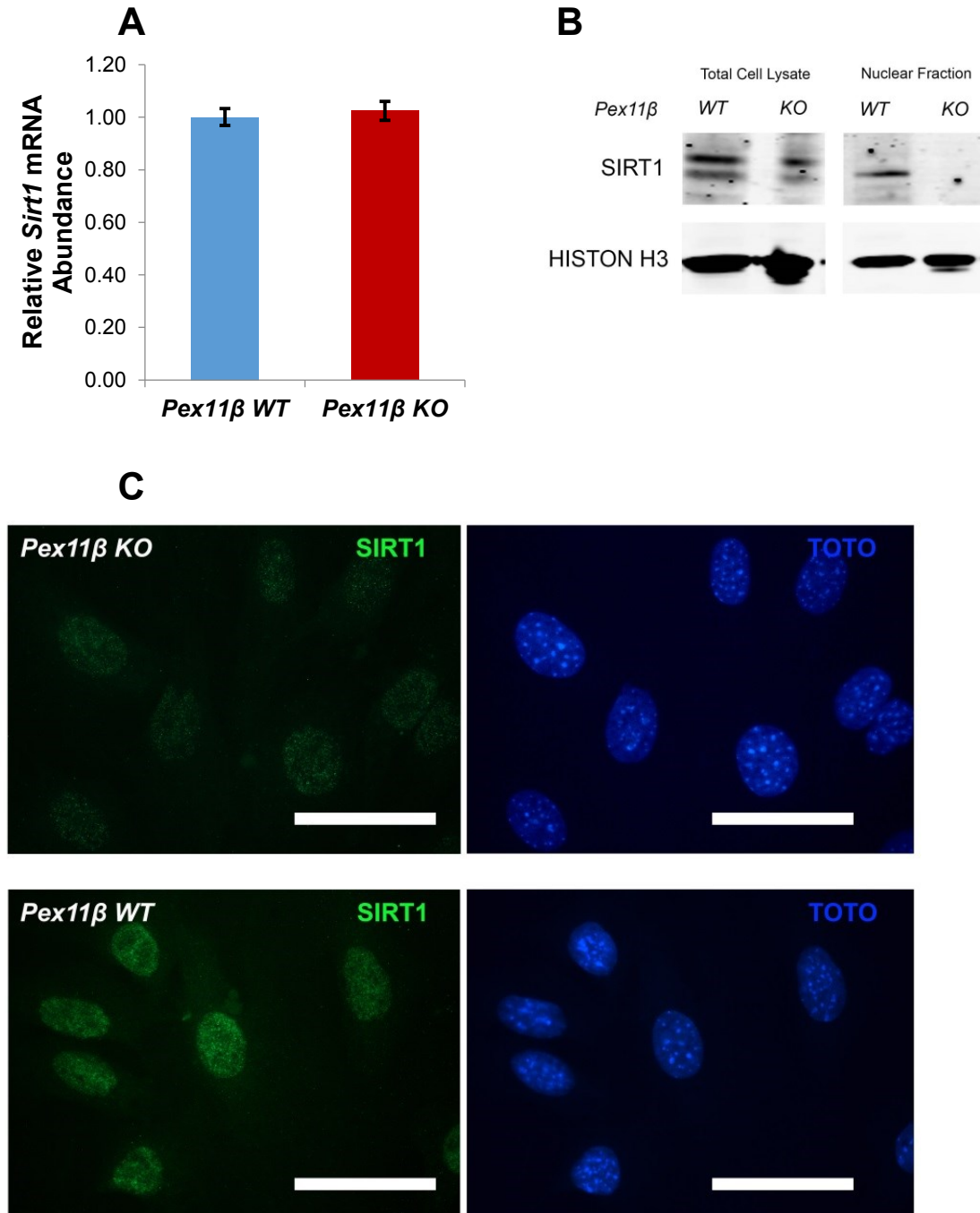
Figure.33. The SIRT1 protein content *Pex11β* KO primary osteoblasts, in particular in the nuclear fraction, is much lower than in WT osteoblasts, while there is no significant difference in *Sirt*1 gene expression. A: Total RNA of WT control and

Pex11β KO osteoblast were analyzed to identify the expression level of the *Sirt1* gene expression via qPCR. **B:** Comparative Western blot analyses to examine the SIRT1 protein content in total osteoblast cell lysate and the nuclear fraction. **C:** Immunofluorescence preparation to determine the SIRT1 protein content in *Pex11β* KO and WT primary osteoblasts Bars represent 50µm.

From the literature it is known that SIRT1 plays several roles in pathways that are related to bone development and remodeling, in particular, deacetylation and activation of β-catenin, a Wnt signaling molecule involved in the self-renewal and differentiation of mesenchymal stem cells (Ling et al., 2009). Previous research in our laboratory, also revealed that the delay of osteoblast differentiation was associated with an increase in oxidative stress and the cytoplasmic translocation of β-catenin caused by canonical Wnt signaling diminishment in *Pex11β* KO osteoblast (Qian, 2010a).
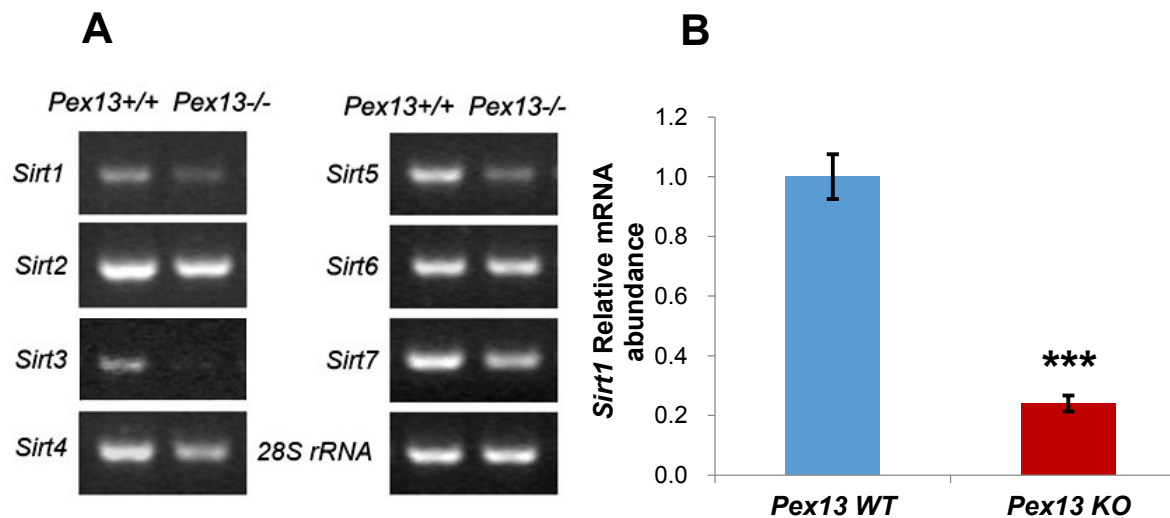
Figure.34. The Sirtuin genes including *Sirt1* expression are significantly lower in *Pex13* KO osteoblast compared to WT. A: RT-PCR results exhibit the alterations of mRNA levels of Sirtuin genes in *Pex13* KO osteoblasts. **B** Total RNA of *Pex13* KO/WT osteoblast was analyzed for the expression level of the *Sirt1* gene by qRT-PCR.

In contrast to *Pex11β* KO osteoblast, but also in osteoblasts with PEX13 deficiency the *Sirt1* mRNA was significantly downregulated. In these knockout cells, also the mRNA expression of other Sirtuin family members was analyzed.

Interestingly, especially the mitochondrial Sirtuin deacetylase mRNAs, the one for the *Sirt 3, 4* and *5,* were down-regulated in *Pex13* KO osteoblasts (Figure.34.A) (Haigis and Sinclair, 2010). Altogether suggests increase of mitochondrial stress in *Pex13* KO osteoblast cells and severe interferences with general acetylation of sirtuin substrates due to the peroxisomal deficiency. To summarize, both the SIRT1 protein nuclear region downregulation in the *Pex11β* KO osteoblast (Figure.33.) and the dramatically down-regulated *Sirt1* gene expression level in *Pex13* KO osteoblast (Figure.34.) may play important roles in the dysregulation of osteoblast differentiation and ossification defect due to peroxisome deficiency. Fortunately, a *Sirt1* KO animal was available for us through collaboration with the group Xiaoling Li at NIEHS USA. Therefore, in the following it was analyzed whether the *Sirt1* KO would also have an effect on the peroxisomal compartment and influence bone differentiation.

4.3.2. *Sirt1* KO in primary osteoblast and *Sirt1* ShRNA stable knockdown in the MC3T3-E1 cell line

Two osteoblast cell culture models were used to analyses the effect of a *Sirt1* defect on the osteoblast differentiation and peroxisome composition. Primary OB isolated from calvariae of P0.5 *Sirt1* KO/WT mice and *Sirt1* shRNA knockdown in MC3T3-E1 cells. The qRT-PCR and Western blot analysis verified the complete deletion of the *Sirt1* gene in primary osteoblasts and the decrease of SIRT1 protein abundance in MC3T3-E1 cells transfected with *Sirt1* shRNA. (Figure.35.).
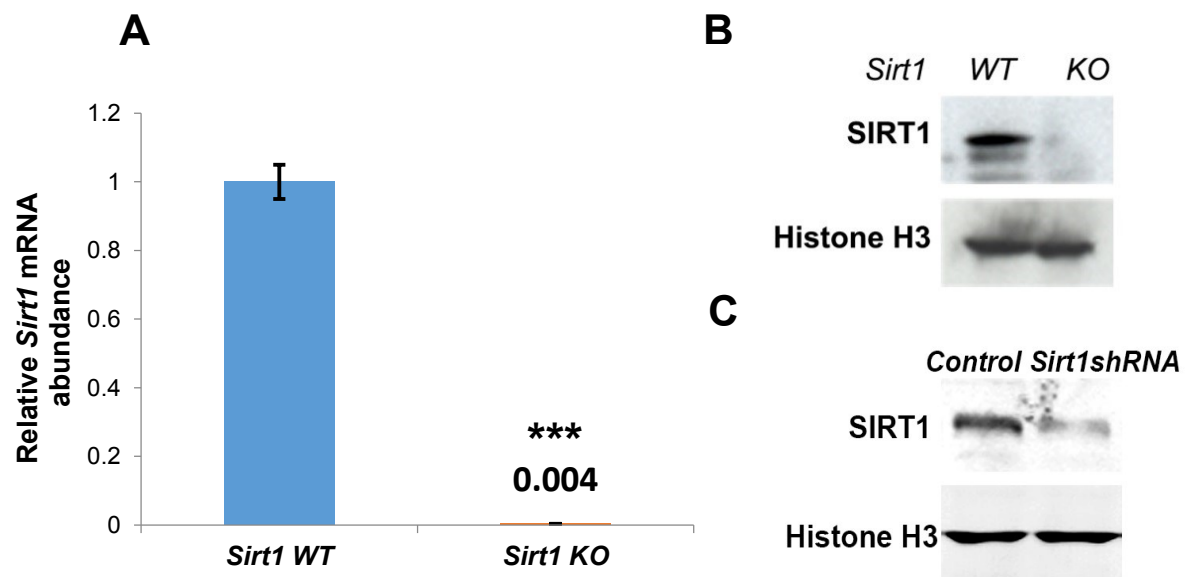
Figure.35. Verification of the absence of *Sirt1* in primary osteoblast and SIRT1 knockdown in shRNA transfected MC3T3-E1 cells. A: Total RNA of WT control and *Sirt1* KO osteoblast was analyzed for the expression level of the *Sirt1* level by qRT-PCR. **B:** Comparative Western blot analyses to examine the SIRT1 content in whole cell lysate of Sirt1 KO and WT primary osteoblast. The abundance of the Histone H3 was used as loading control. **C:** Comparative Western blot analyses to examine the SIRT1 protein content in whole cell lysate of *Sirt1* shRNA knockdown and control MC3T3-E1 cells.

In additional to biochemical experiments, the *Sirt1* KO was also confirmed in the immunofluorescence preparation of paraformaldehyde fixed paraffin-embedded tissue section of bone. Figure. 36. reveals the high specificity of the anti-SIRT1 antibody and clearly shows high level staining for SIRT1 in osteoblast of WT animal and no staining in *Sirt1* KO animal.
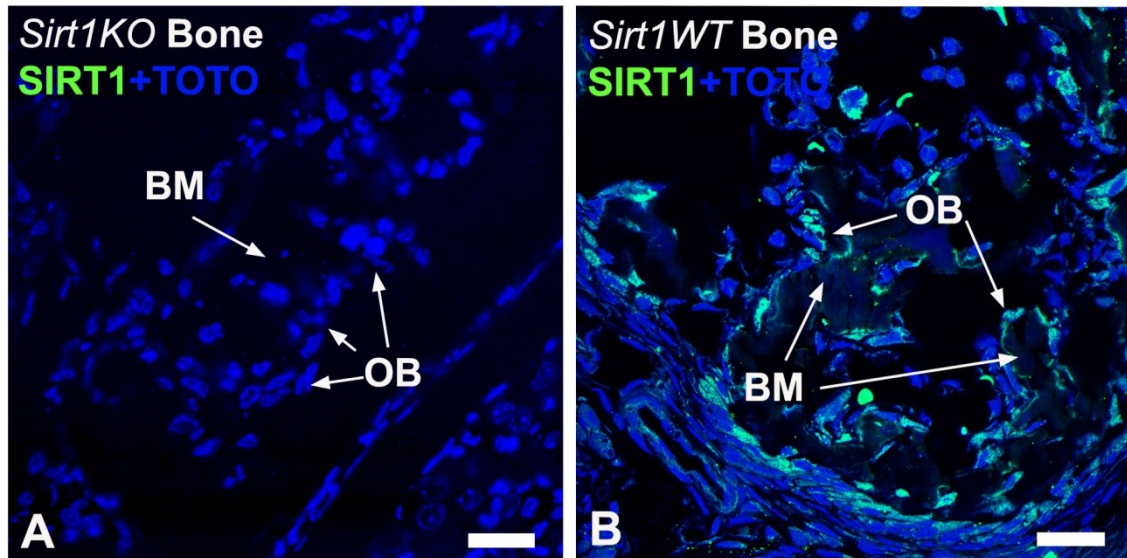
Figure.36. The SIRT1 protein is highly abundant in bone tissue of WT mice and absent in *Sirt1* KO mice compared to WT. Paraffin sections of *Sirt1* KO and WT P0.5 mouse pups were labeled with fluorescence-labelled antibodies against the endogenous SIRT1 protein (green). The pictures were taken at the calcified region bone matrix (BM) of the diaphysis of the femur in long bones isolated from *Sirt1* KO and WT P0.5 mouse pups. These results were published in collaboration study with X. Li (NIEHS, North Carolina, USA) Figure 7 B of Tang et al, Mol Cell 2014. Bars represent 50 µm.

4.3.3. Differentiation and maturation of osteoblasts were promoted from the pre-osteoblast stage in *Sirt1* KO osteoblast

As mentioned in a previous chapter (see 1.3.2.1), the expression levels of osteoblast differentiation stage markers are important parameters to evaluate the progression of osteoblasts differentiation. By using these parameters, the progress of differentiation of *Sirt1* KO osteoblast compared to WT was determined with qRT-PCR. Apparently, in comparison to peroxisome deficient knockout, the *Sirt1* KO osteoblast contain higher levels of mRNA of middle and later stage bone markers.
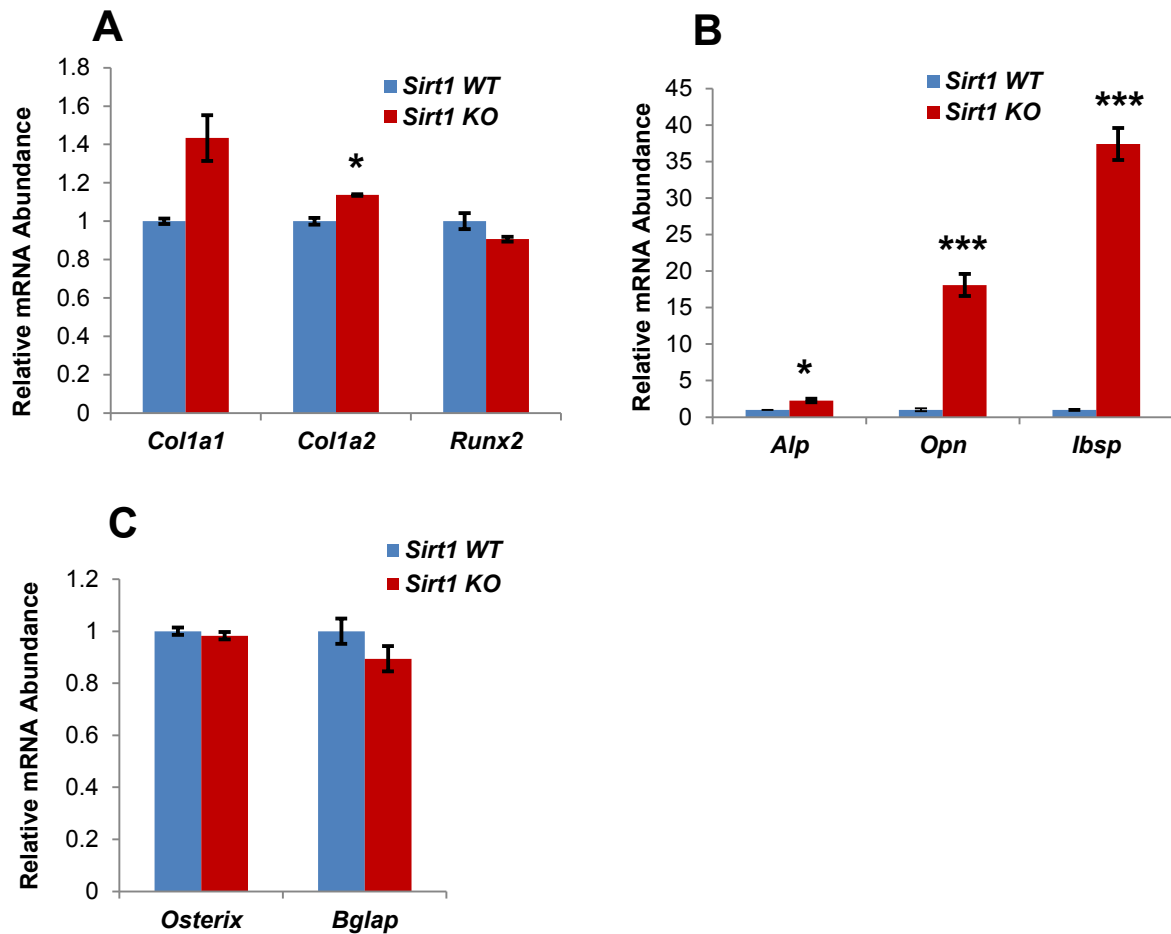
Figure.37. SIRT1 deficiency results in pre-mature differentiation pattern of OB. Total RNA of WT control and *Sirt1 KO* osteoblast was analyzed for the gene expression level of various mRNA bone marker proteins via qRT-PCR**:** KO of *Sirt1* in osteoblast leads to an increased expression of middle to mature osteoblast marker genes (*Alp, Opn* and *Ibsp*) compared to WT (B). In contrast, the expression levels of marker genes for osteoblast progenitors (A) and mature osteoblast (C) with a *Sirt1 KO* exhibit no significant change compared to WT.

Since OPN is the most accepted osteoblast middle stage marker, the endogenous OPN protein content was determined in *Sirt1* KO/WT osteoblast via IF staining (depicted in Figure.38.).
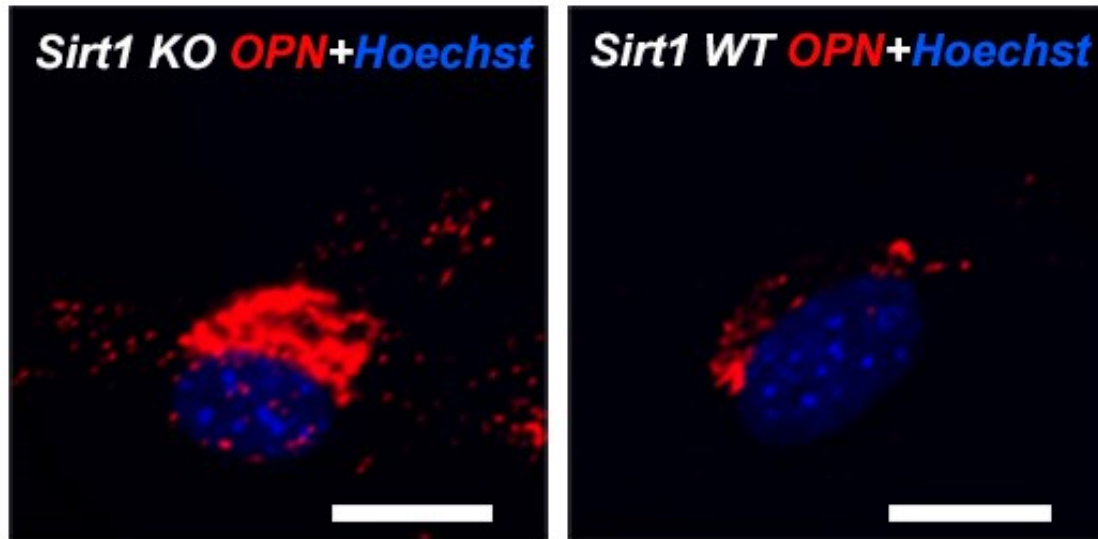
Figure.38.The osteoblast middle stage marker protein OPN is much more abundant in the *Sirt1* KO OB cells compared with WT osteoblast cells, IF staining for OPN in the organelles of the secretory pathway, e.g. ER, Golgi and secretory vesicles is enhanced in Sirt1 KO osteoblast. Bars represent 10 µm.

It has been published in the literature that specific deletion of SIRT1 in MSC leads to decreased in MSC differentiation into osteoblasts and chondrocytes, as well as a to reduction in cortical bone thickness and trabecular volume in mice (Simic et al., 2013). The above results revealed that the deletion of *Sirt1* gene actually also promotes the osteoblast differentiation solely in the middle stage of compared to the WT. Throughout the entire osteoblast differentiation process it can be assumed that SIRT1 actually plays dual roles in distinct differentiation stages: promoting differentiation from MSC stage to osteoblast progenitor stage and interfering differentiation from pre-osteoblast stage to maturation stage.

4.3.4. Peroxisome biogenesis and function were significantly attenuated in *Sirt1* KO osteoblast and in MC3T3-E1 cells with a *Sirt1* gene knockdown

In the literature, it has been shown that SIRT1 may mediate the effect of caloric restriction by affecting PPARγ, PGC1-α and FOXOs (Han et al., 2010), which are all strongly altered in *Pex11β* and *Pex13* KO osteoblast (described in section 4.1 and 4.2). Therefore, we also analyzed the gene expression levels coding for

protein involved in peroxisome biogenesis and peroxisomal metabolism. To analysis this hypothesis, enzyme genes in *Sirt1* KO/WT osteoblast were determined with qRT-PCR with total osteoblast RNA and IF staining of the tissue sections. The results of these experiments are depicted in figures 39-41.

The results presented in Figure.39. are very similar to the expression levels of the examined genes in *Pex13* KO osteoblast (Figure.29.). The mRNA expression levels for the peroxisome biogenesis genes (Figure.39.A) and the peroxisomal metabolic enzymes (Figure.39.C), even the peroxisome membrane transporter *Abcd1* and *Abcd3* (Figure.39.B) were dramatically diminished in *Sirt1* KO osteoblast compared to WT osteoblast. These results were further confirmed by the *Sitr1* shRNA knockdown in MC3T3-E1 cells.
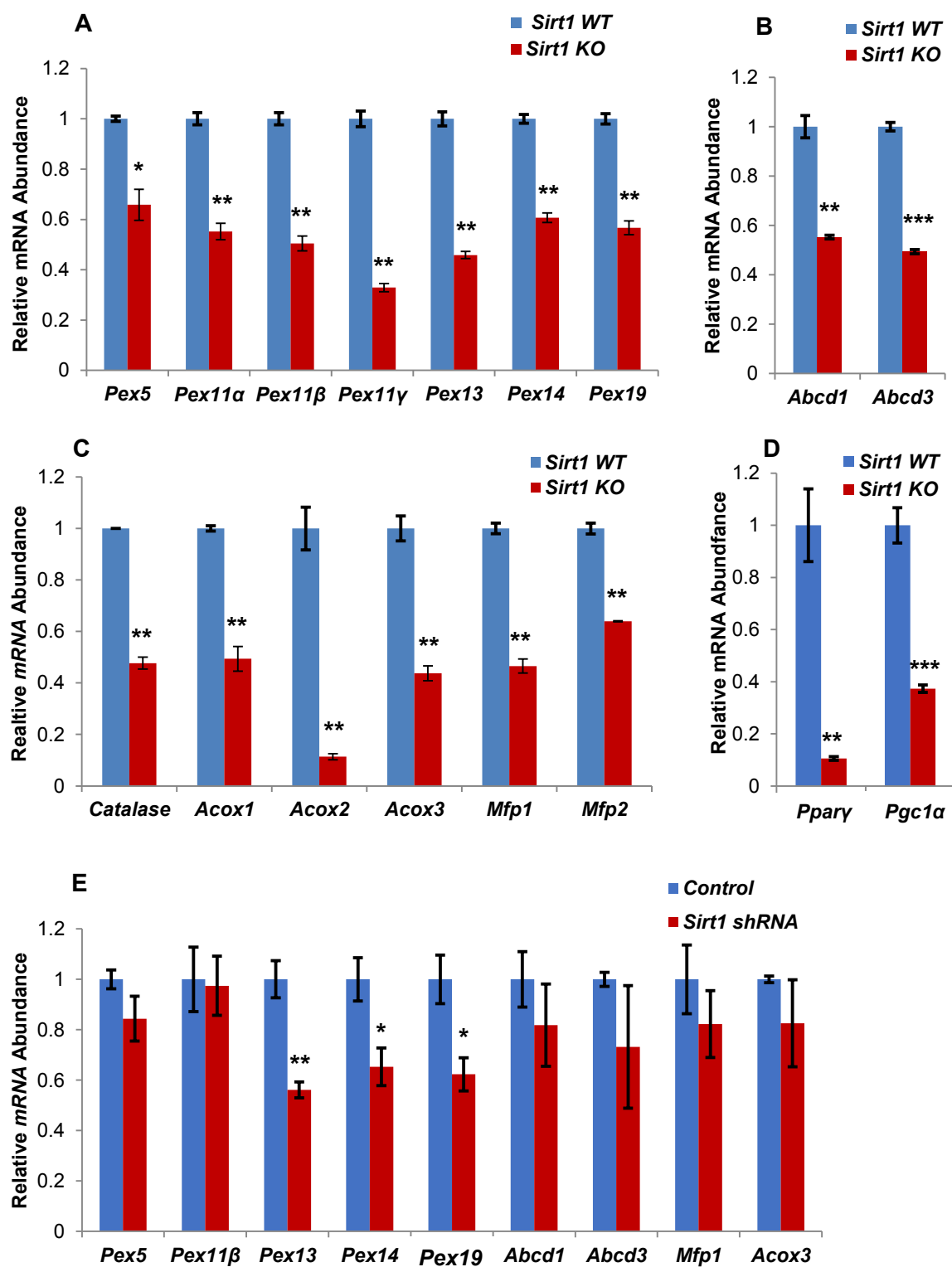
Figure.39. Knockout of *Sirt1* in primary osteoblast and knockdown in MC3T3-E1 cells induces comparable effects on the mRNA levels for peroxisomal related proteins. *Sirt1* KO osteoblasts showed decreased expression levels of mRNA for peroxisome biogenesis genes **(A)**, peroxisomal transporter **(B)** and peroxisomal metabolic enzymes **(C)**. *Sirt1* KO osteoblasts also exhibit strongly decreased *Pparγ* and *Pgc1α*. mRNA level (**D**).Moreover, a knockdown of the *Sirt1* mRNA in MC3T3-E1 cell leads to comparable effects**(E)**.

In addition to the observed mRNA alterations, also the number of peroxisome and the level of peroxisome protein were decreased (Figure.40.).
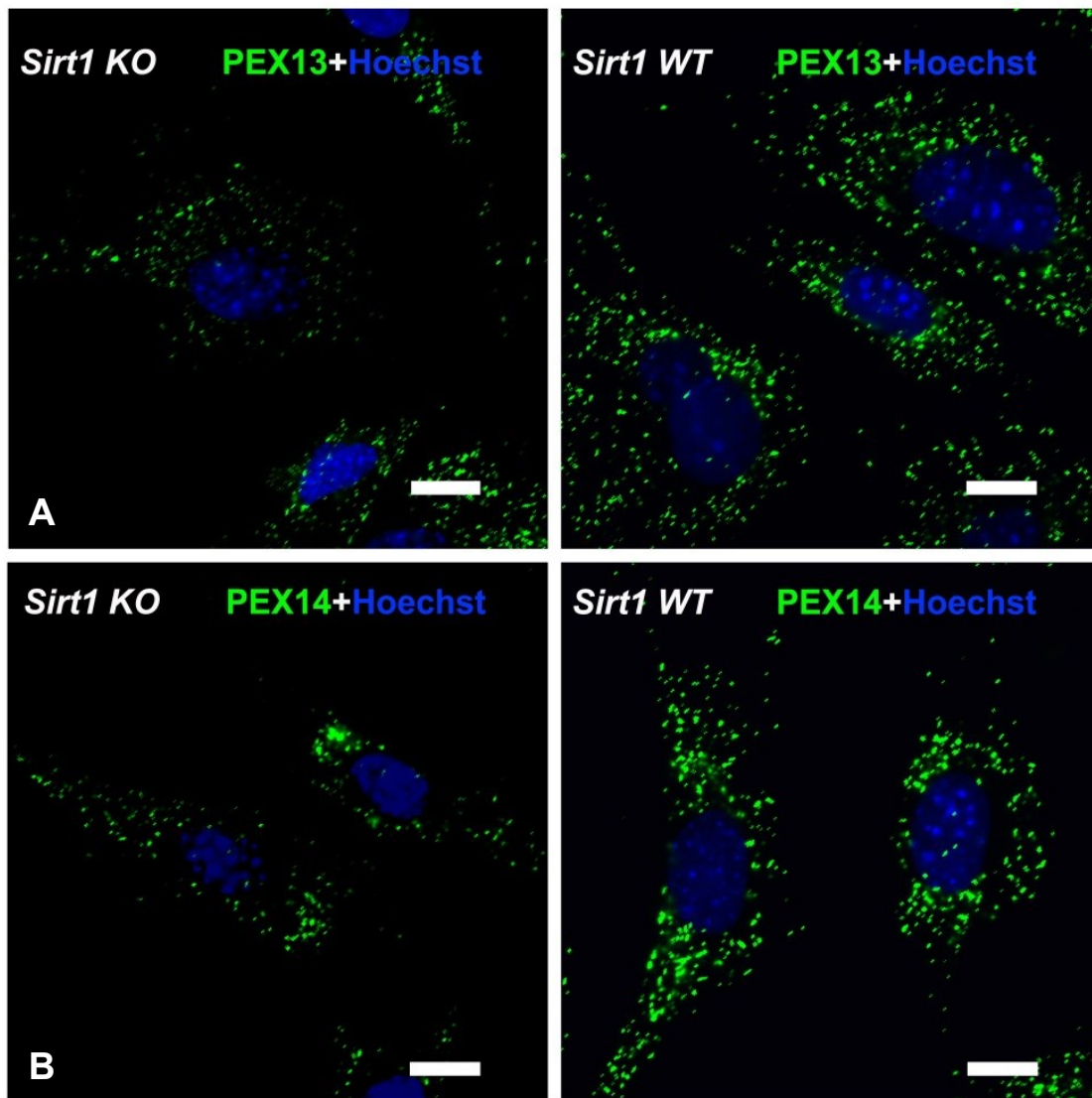
Figure.40. The abundance of the peroxisome biogenesis proteins PEX13 (A) and PEX14(B) are considerably decreased in *Sirt1* KO osteoblast compared to WT. Indirect IF staining was performed with primary rabbit antibodies against PEX13 and PEX14 and donkey anti-rabbit antibodies secondary labelled with Alexa 488 (green). Bars represent 10 µm.

Similar to the biogenesis proteins PEX13 and PEX14, also the protein level for catalase (CAT) and the peroxisomal transporter ABCD3.
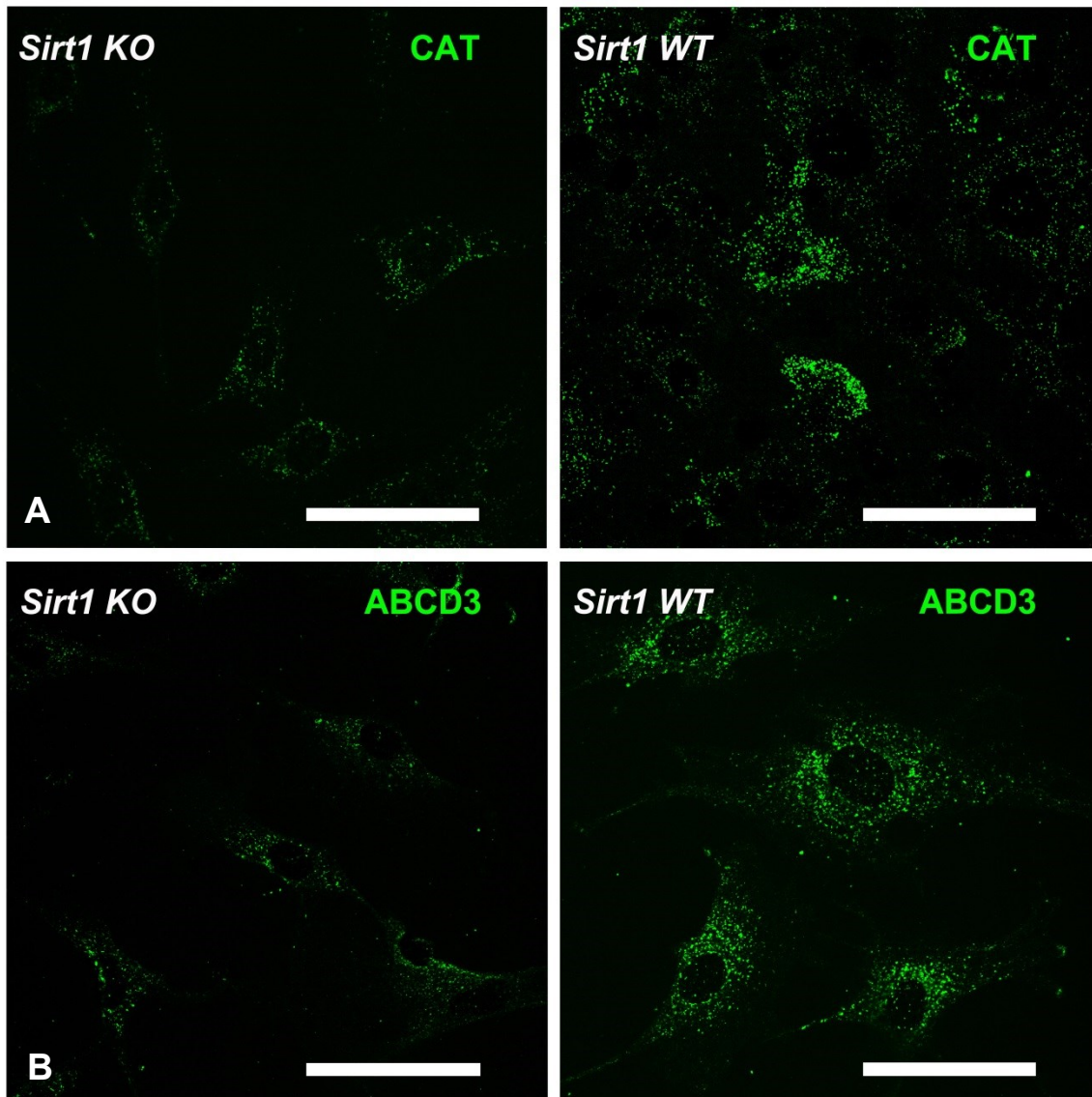
Figure.41. The abundance of catalase (CAT) and peroxisomal membrane transporters ABCD3 are decreased in *Sirt1* KO osteoblast compared to WT. Indirect IF staining was performed to detect catalase protein **(A)** and ABCD3 protein **(B)**.

As clearly visible catalase and ABCD3 are both decreased in *Sirt1* KO osteoblast. Bars represent 50 µm.

In summary, the peroxisome numbers and gene expression peroxisomal biogenesis protein as well as catalase and ABCD3 were significantly decreased due to a *Sirt1* KO in osteoblast.

4.3.5. Oxidative stress is dramatically increased in primary *Sirt1* KO osteoblast and in MC3T3-E1 cells with a stable *Sirt1* knockdown

Since the peroxisomal biogenesis and function are strongly attenuated in *Sirt1* KO osteoblast (see Section 4.3.4.), oxidative stress might be present in *Sirt1* KO cells and cause alterations of osteoblast differentiation. Therefore, some experiments were performed to determine a possible increase in oxidative stress.

H_2-DCFDA was used for FACS analysis to detect the total intracellular ROS level in *Sirt1* KO/WT osteoblast. The higher ROS level suggests that oxidative stress (see Figure.42.) is present in *Sirt1* KO osteoblast compared to WT osteoblast. The reason for the increased oxidative stress might be the lower the antioxidant capability in the cells by diminished peroxisomal abundance and functions (see Figure.39. and 41.).
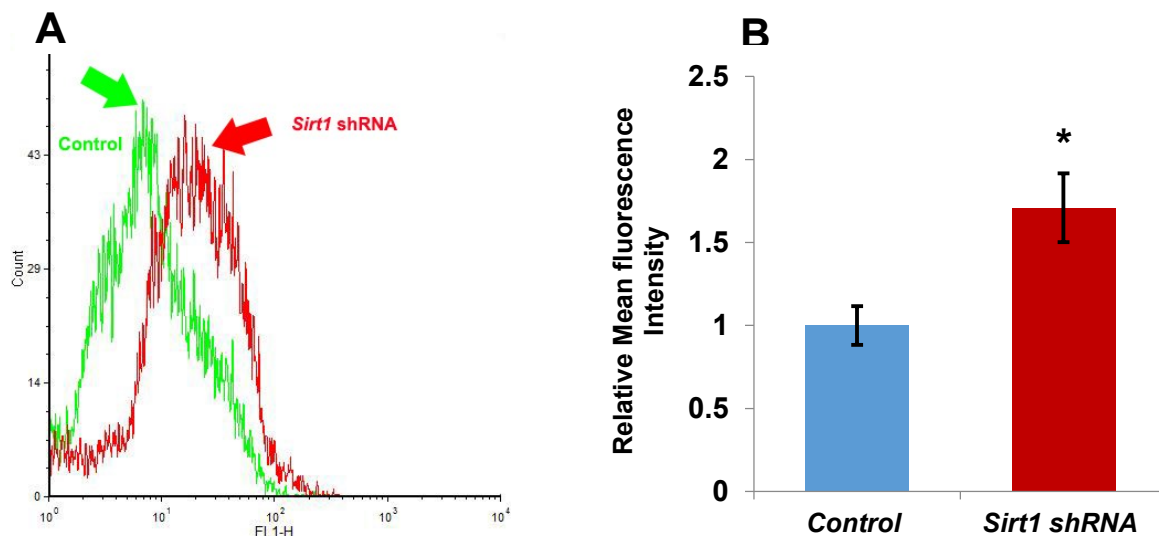
Figure.42. Global oxidative stress is increased in MC3T3-E1 cells with a *Sirt1* shRNA knockdown which was determined by H2-DCFDA staining of osteoblast

with FACS (A). The ROS level was about 70 % higher in the MC3T-E1 cells with the *Sirt1* knockdown compared to WT **(B)**.

4.3.6. *Sirt1* deletion results in an increased bone resorption via alteration of the RANKL/OPG system

The homeostasis of bone remodeling is maintained by the balance of bone generation and absorption by osteoblasts and osteoclasts. Interestingly, osteoclast differentiation can be regulated by osteoblast through RANKL/OPG system. To find out, how the osteoclast differentiation was altered in *Sirt1* KO mice, the expression levels of *Rankl* and *Opg* genes were determined in *Sirt1* KO/WT osteoblasts by qRT-PCR using primary osteoblasts and *Sirt1* shRNA knockdown in MC3T3-E1 cells (Figure.43.). The reduction of expression level of *Opg* and increase in *Rankl* in both cell types suggests that the osteoclast differentiation could be stimulated by osteoblast regulated RANKL/OPG system due to SIRT1 deletion.

A   **B**
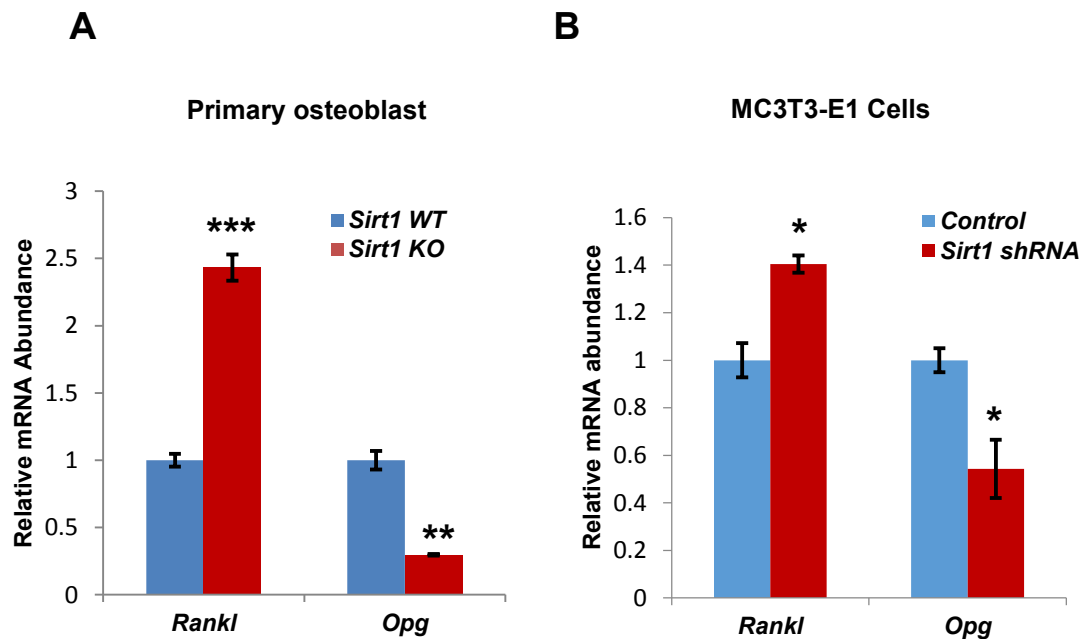
Figure.43. The balance of RANKL/OPG system is disturbed in *Sirt1* KO osteoblast characterized by the significantly reduced expression of *Opg* and increased

expression of *Rankl* compared to WT osteoblast. Total RNA of **A**: WT control and *Sirt1* KO osteoblast and **B**: *Sirt1* shRNA knockdown inMC3T3-E1 cells were analyzed for the gene expression level of *Rankl* and *Opg* by qRT-PCR.

4.3.7. Deletion of the *Sirt1* gene induces developmental defects, by induction of retinoic acid signaling in *Sirt1* KO mice

Our collaboration partner in which I was working for two laboratory rotations showed that the retinoic acid binding protein II (CRABPII) can be deacetylated by SIRT1. It is known from the literature that retinoid homeostasis is essential for the differentiation process and normal embryonic development. Wherefore, alteration in retinoic acid receptors β (RARβ) abundance and activity could exert strong influences on the differentiation process also on osteoblasts. Retinoid pathway activation could have an impact both on the expression of bone marker genes as well as on the peroxisome compartment. In line with this, we hypothesized that also the nuclear receptor mediating retinoic acid effect might be altered in the bone of the *Sirt1* KO mice. Therefore, the RARβ abundance was analyzed in bone of *Sirt1* KO/WT mice via IF staining (Figure.44.). The results show that the abundance of RARβ was strongly increased in the *Sirt1* KO bone cells, including osteoblast and chondrocyte, associated with the increasing nuclear accumulation of CRABPII caused by *Sirt1* gene deletion, suggesting that retinoic acid (RA) signaling actually has been enhanced in *Sirt1* KO bone cells compared to WT.
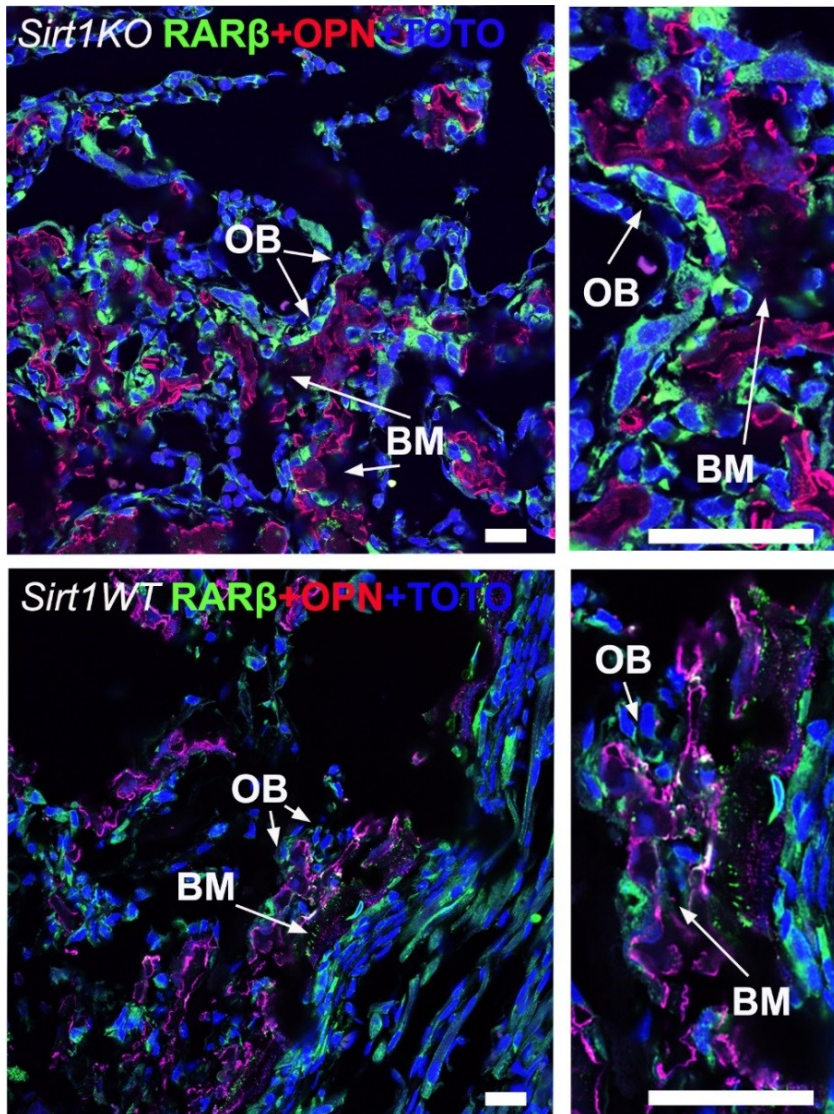
Figure.44. The loss of SIRT1 protein in bone of *Sirt1* KO mice increases cellular abundance of RARβ and OPN in osteoblast compared to WT. Double immunofluorescence staining of RARβ and OPN in the diaphysis of bone (femurs).The OPN staining (red fluorescence) depicts the differentiated osteoblast (indicated by the arrows). The RARβ staining (green fluorescence) displays a much stronger labeling in *Sirt1* KO tissue, which indicates that the RARβ abundance is higher in *Sirt1* KO osteoblast compared to WT. Bars represent 10 µm (published as Figure number 7 C in Tang et al, 2014).

As proven by RARβ staining, this retinoid receptor is strongly induced in the *Sirt1* KO osteoblast. RARβ activation might indeed explain the upregulation of bone markers and also of the PPARs and the other "peroxisome-related" gene expression (Figure.39.).

5. Discussion

Dysregulation of osteoblasts differentiation and their function has been reported in the literature as important factors contributing to a wide range of bone diseases, such as osteoporosis in adults or ossification defect and growth retardation in children(James, 2013; Marie and Kassem, 2011; Pino et al., 2012; Price et al., 1994). According to the report of the World Health Organization (Brussels, Belgium, May 2004), the osteoporosis caused more than 8.9 million fractures annually worldwide, of which more than 4.5 million occurred in America and Europe. Additionally, the dysregulation of RANKL/OPG system which results in the over-absorption of bone matrix by differentiated osteoclasts is also the main factor contributing to pathogenesis of osteoporosis (McCormick, 2007).

In this work, the deletion of two of the Peroxin genes, *Pex11β* and *Pex13*, caused a dysregulation of osteoblast differentiation. These two ZS mouse models with a strong metabolic defect were used to investigate how osteoblast differentiation is disturbed by peroxisomal dysfunction peroxin. Interestingly, either the phenotypes of new born pup skeletons or the progressing of osteoblast differentiation were remarkably similar in *Pex11β* (Qian, 2010a) (Figure.19.-20.) or *Pex13 KO* (Figure.26.-28.) mouse models. In Zellweger patients with peroxisome deficiency the growth retardation and craniofacial dysmorphism have been noted; however it was not known how these skeleton phenotype was induced. Therefore, the *Pex11β* KO and *Pex13* KO mouse model were used here to study the molecular pathogenesis of bone defect induced by peroxisomal deficiency. Indicated by gene expression level of osteoblast stage markers, the osteoblast differentiation process was strongly affected by peroxisomal biogenesis and function defect. In primary osteoblasts, the deletion of *Pex11β* and *Pex13* genes results in the decrease of SIRT1 (Figure.33.and 34.) and more interestingly, the expression level and the protein abundance of the most important peroxisome biogenesis genes and metabolic enzymes were significantly decreased by KO or knockdown *Sirt1* in osteoblast (Figure.39.-41.). We have found the deletion of SIRT1 enhances RA signaling (Tang et al., 2014)

and the RA has been found negatively regulate the osteoblast mineralization and osteoblastogenesis (Bi et al., 2013; Lind et al., 2013).

5.1. Attenuation of peroxisome biogenesis and peroxisomal functions in Zellweger Syndrome and *Sirt1* KO mouse model

5.1.1. The possible role of peroxisomes in osteoblast differentiation

In the literature there is still no information available on the abundance and enzyme composition of peroxisomes in different cell types of the skeleton. However, the importance of peroxisomes for the skeleton is well known due to abnormal skeletal deformations found in patients with peroxisomal disorders (Agamanolis and Novak, 1995; Braverman et al., 2002; Brosius and Gartner, 2002; Heymans et al., 1985). These observed skeletal defects suggest that normal peroxisomal function is essential for endochondral as well as intramembranous ossification process.

Therefore, the present study as well as our preliminary research aimed to find out the correlation between peroxisome function and ossification has been carried out in our lab. The strong phenotype of ossification defects were shown in ZS mice model, such as reduction of bone volume, mass and density, accompanying with a delay in the osteoblast differentiation and alteration in bone development regulation signaling, such as Wnt signaling(Qian, 2010a). Theoretically, as an important metabolic cell organelle, the peroxisome has the potential to influence the function of osteoblast. Since peroxisomes are involved in cholesterol and ether lipid synthesis, alteration due to peroxisomal problem might influence the physiological properties of cell membranes (Brown and London, 1998) and thus might facilitate the formation of phospholipid-rich matrix vesicles in hypertrophic chondrocytes and osteoblasts. Moreover, the peroxisomes may be involved in the synthesis of precursors of vitamin D and retinoids (Fransen et al., 1999) which are important for osteoblast maturation. The influence of peroxisomal metabolism on osteoblast mineralization also was pointed out by the fact that the number of peroxisomes increased during osteoblast differentiation and that the

peroxisomes are most abundant in the metabolically activate state, namely in the differentiating osteoblast, but less abundant in the stable status, namely in osteocyte (Qian, 2010a).

5.1.2. The *Pex13* gene deletion results in the global collapse of biogenesis and enzymatic functions

PEX13 is a metabolic peroxisomal integral membrane protein with an essential role in both PTS1 and PTS2 protein import. In the above section "Peroxisome Biogenesis" (see section 1.1.2.), it has been mentioned already that in a model of *Saccharomyces cerevisiae*, the cytoplasmic SH3 domain of PEX13 binds to PEX5, the PTS1 receptor. Deletion of *Pex13* results in a reduction of the level of PEX5 associated with the peroxisomal membrane at steady state and loss of both PTS1 and PTS2 protein import (Gould et al., 1996). In contrast, peroxisomal membrane proteins are still detectable in "ghost" like structures (Santos et al., 1988) forming spherical membranous structures. However, due to the matrix protein import deficiency, peroxisomal metabolic function is seriously disrupted within these osteoblast due to *Pex13* gene deletion. This has been proven by latest data obtained in our lab with *Pex13* KO osteoblast stained with immunofluorescence assay using primary *Pex13* KO osteoblast cells, which revealed the import defect of peroxisomal matrix protein, such as the antioxidant enzyme Catalase was mislocalized to the cytoplasm and the nucleus of osteoblasts. Moreover, in IF staining for PEX14, peroxisomal membrane "ghosts" are present, which are however less intensive by stained for the peroxisomal lipid transporter ABCD3.

In primary *Pex13* KO osteoblast, the gene expression levels of peroxisome biogenesis and peroxisomal enzymes were severely down-regulated (Figure.29.), possibly explaining the lower staining intensities for other peroxisomal matrix enzymes and membrane protein than catalase and ABCD3.

In comparison to *Pex11β* KO mice, in *Pex13* KO osteoblast the defects in the peroxisomal protein import and metabolic abnormalities have been found, exactly

like in ZS patients and ZS mouse models of *Pex2* and *Pex5* KO (Baes et al., 1997; Faust et al., 2001), which result in the accumulation of VLCFA in the liver, brain, and skin fibroblasts and severe reduction of the oxidation of branched-chain fatty acid in fibroblasts (Maxwell et al., 2003).

5.1.3. The peroxisomal biogenesis and peroxisomal metabolic function are diminished in *Sirt1* KO osteoblast cells

The obtained results in this thesis (Figure.39.-41.) indicate that also the deletion of the *Sirt1* gene diminishes peroxisomal biogenesis and peroxisomal metabolic functions. The expression levels of many peroxisomal biogenesis genes such as *Pex5, Pex11α, Pex11β, Pex11γ, Pex13, Pex14, Pex19*, peroxisomal antioxidant (*catalase*), and β-oxidation enzymes (*Acox1-3, Mfp1,2*), were decreased. Similarly a decreased number of peroxisomes as well as decreased protein of PEX13 and PEX14 levels were noted in *Sirt1* deficient osteoblasts (Figure.40.) and for the peroxisomal targeting sequence 1-containing proteins (data not shown) which were all reduced in individual peroxisomes of *Sirt1* KO osteoblast.

Peroxisome biogenesis and metabolism are under the control of intrinsic transcriptional pathways including the PPAR nuclear receptors and their co-activator PGC-1α. Previous studies have shown that SIRT1 modulates the activities of both PPARs and PGC-1α, either through direct deacetylation or via co-factor recruitment in response to different environmental cues (Li, 2013). To further dissect the molecular mechanism of peroxisome biogenesis deficiency in *Sirt1* KO osteoblasts, we examined the mRNA levels of PPARγ, the predominate form of PPARs in this cell type, and PGC-1α. Most interestingly, the expression levels of the *Pparγ* and its co-activator *Pgc-1α* were significantly decreased (see Figure.39.D). It has been known that the "switch" of adipogenesis or osteogenesis of MSC are regulated by the master regulator PPARγ via ROS/FoxO/PPARγ/β-catenin cascade under oxidative stress and lipid toxicity condition in osteoblast (Section 1.3.2.2.). These results suggest that the down-regulated Pparγ and co-factor Pgc-1α may contribute to the earlier differentiation

of *Sirt1* KO osteoblast under the increasing oxidative stress (Figure.42.). These observations, together with our previous data on peroxisomal deficient animals indicate that peroxisomal dysfunction in *Sirt1* KO mice might contribute to the alteration of osteoblast functions and ossification disturbance of these animals.

Furthermore, the latest literature suggested the PPARβ also might be the key regulator of bone turnover and the crosstalk between osteoblasts and osteoclasts. The osteoblast differentiation can be promoted by amplified Wnt-dependent and β-catenin-dependent signaling due to activation of PPARβ, in particular the activated PPARβ can increasing binding activity to PPRE where is also located within the promoter region of Wnt signaling co-activator LRP5 to promote its expression level (Scholtysek et al., 2013). Moreover, it has been found that the PPARα expression level was up regulated during the osteoblast differentiation process (Qian, 2010a). Therefore, the dysregulation of *Sirt1* KO osteoblasts also might be caused by a possible alteration of PPARβ and α and which might be studied in further experiments.

5.2. Skeletal ossification defect and osteoblast dysregulation of differentiation

5.2.1. Severe ossification defect and the skeletal deformation of Zellweger Syndrome and *Sirt1* KO mouse model

5.2.1.1. Strong phenotype of Zellweger Syndrome and ossification defect in *Pex11β* KO mice

The recognition of the *Pex11β* KO mouse as a ZS model was based on the fact that several pathological features were shared by *Pex11β* KO and *Pex5* (Baes et al., 1997; Baumgart et al., 2001) or *Pex2* (Faust and Hatten, 1997; Kovacs et al., 2004) mouse models, which reproduce virtually all of the hallmarks of the human disease, including neuronal migration defects, enhanced neuronal apoptosis within the neocortex, intrauterine growth defects retardation which cause a developmental delay, hypotonia, and neonatal lethality (Li et al., 2002b).

Even though the typical craniofacial dysmorphism of the ZS patient is not observed in these mouse models, a calvariae ossification delay was described (Faust and Hatten, 1997). The human disease RCPD is autosomal recessive disorder caused by the defects in PEX7 encoding the receptor for PTS2-targeted peroxisome matrix enzymes (Braverman et al., 1997; Steinberg et al., 2006). This disease is chartered be the strong phenotypes of skeletal, eye and brain abnormalities and the animal model of *Pex7* KO mice shows defect in ossification of distal bone elements of the limbs as well as parts of the skull and vertebrae, and abnormalities in lens fibers(Braverman et al., 2010; Brites et al., 2003).

5.2.1.2. The *Pex13* KO mice show growth and developmental abnormalities of Zellweger Syndrome but delayed ossification defect started later after birth compared to *Pex11β* KO mice

Previous quantitative morphometric analysis via fpvCT determination has been done in our laboratory on E19 *Pex13* KO mice revealed no significant differences in bone volume and bone mass between *Pex13 KO* mouse pups and WT (my preliminary experiments data not shown); In contrast, in E19 *Pex11β* KO pups, a decrease of total bone volume, bone mass and whole-body bone mineral density has been observed compared to WT (Qian, 2010a).

The lifespan of *Pex13 KO* pups was around 6-12 hours after birth which is slightly longer than that of *Pex11β* KO mouse pups that die meanwhile before birth. Therefore, to determine the possible ossification defect of *Pex13* KO mouse pups, the P0.5 *Pex13* KO/WT mouse pups were used for fpvCT determination and quantitative morphometric analysis. The results revealed that the bone volume of *Pex13* KO mouse pups was around 80% of that of littermates WT and HTZ pups at the same stage, suggesting a severe ossification defect due to *Pex13* gene deletion (Figure.26.). We observed , the severe skeletal deformation of *Pex13* KO mouse pups, in particular the reduced size of the skull and the long bones such as tibia and femur (Figure.26.), which might be the reason for the maintenance of a contracted "C" posture that appeared to

particularly affect the hind limbs in the newborn *Pex13* KO mouse pups (Figure.10.) (Maxwell et al., 2003).

5.2.1.3. Intrauterine growth retardation and developmental defects of *Sirt1* KO mouse pups

It has been believed that SIRT1 plays a critical role in development, which can be proven by deletion of the *Sirt1* gene which results in severe developmental defects, such as neonatal lethality, defective germ cell differentiation, developmental defects of the retina and heart and intrauterine growth retardation (Cheng et al., 2003; McBurney et al., 2003; Wang et al., 2008). For instance, only around 1% of *Sirt1* KO mice with a 129SvEv/FVB background can survive (Wang et al., 2008). By using a general *Sirt1* KO mouse in the C57BL/6 background we have found that the mineralization process of endochondral ossification was delayed in *Sirt1 KO* mice compared to WT littermates (Tang et al., 2014).

Additionally, even the molecular mechanism of the regulation of development and stem cells by SIRT1 are still not completely understood, the wide spread developmental defects of *Sirt1* KO mouse pups might be due to the multifunctionality and central role of the SIRT1 protein in regulation of the activity of a range of important transcription factors and transport proteins (Tang et al., 2014). It has been determined that SIRT1 also regulates skeletal myoblast differentiation (Fulco et al., 2008; Fulco et al., 2003),it influences spermatogenesis (Coussens et al., 2008) and modulates of neural and glial specification from neural precursors cells (Kang et al., 2009; Prozorovski et al., 2008).

In summary, either the Zellweger Syndrome or the *Sirt1* KO mouse model all showed the typical ossification defect and abnormal bone development, which can be summarized and compared as following Table.17.

Table.17. The comparison of ossification defect of Zellweger Syndrome and the _Sirt1_ KO mouse model

Ossification defect	Zellweger Syndrome Mice model		_Sirt1_ KO Mice
	Pex11β KO mice pups	_Pex13_ KO mice pups	
Time point of ossification defect can be observed	E18.5	P0.5	No obvious aeration observed till P0.5
How the ossification was impaired compared with WT control mouse.	Dramatically decreased bone mass, especially in calvaria, vertebrae and limbs (Qian, 2010a)	Small skull, shorter size of long bones eg. tibiae, ribs, femora	The mineralization very lightly decreased (Tang et al., 2011)

The comparison in Table.17. reveals the Zellweger Syndrome mice, the _Pex11β_ KO and _Pex13_ KO mice pups, have much stronger ossification defect phenotype than _Sirt1_ KO mice pups, therefore the attenuation of SIRT1 in _Pex11β_ KO and _Pex13_ KO osteoblast (Figure.33. and 34.) maybe not the dominant factors results in the ossification delay in Zellweger Syndrome mice. Additionally, since the ossification defect can be observed earlier in _Pex11β_ KO mice compared with _Pex13_ KO mice, the _Pex11β_ KO osteoblast functions might be more disturbed than the one of _Pex13_ KO osteoblast.

5.2.2. Interference of the osteoblast differentiation process in a different manner within Zellweger Syndrome and _Sirt1_ KO mouse models

It has afore been described (see Section 1.3.2.1.) that the differentiation of pre-osteoblasts into mature osteoblasts and osteocytes is a multi-stage process which involves coordinated induction of various markers (Table.3.). The differentiation of osteoblast is a critical requisite for ossification and bone production.

5.2.2.1. The role of osteoblast differentiation in ossification

Ossification can be classified as the intramembranous ossification and the endochondral ossification (Caetano-Lopes et al., 2007). Compared to the endochondral ossification, the intramembranous ossification is occurring without any participation of intermedia structure. The formations of the flat bones of the calvaria, the clavicle, some parts of the mandible, parts of facial bones and the cranial suture lines, are generated directly from the osteoblasts which differentiates from MSC.

Endochondral ossification is also called secondary ossification process and it is the essential ossification process for the long bone growth process. In contrast to intramembranous ossification, cartilage plays an essential role during endochondral ossification. Firstly, the chondrocytes which differentiate from MSCs form a cartilaginous model of the bone by their extracellular matrix. Secondly, proliferating cartilage will develop a hypertrophic cartilage. Thirdly, the apoptosis of hypertrophic chondrocytes and opening by chondroclast enable the invasion of blood vessels to transport the MSCs to the cavities which settle down on mineralized cartilage surface and finally differentiate into mature osteoblasts which deposit bone matrix (Brighton et al., 1973; Caplan, 1988).

Since the primary mineralization process of ossification is carried out by maturely differentiated osteoblast, the osteoblast differentiation is a critical step to determine the ossification process. The reason for the alteration of the osteoblast differentiation (Figure.19.,20.,28.and 37.) might be caused by the peroxisome biogenesis and functions as found in *Pex11β, Pex13* and *Sirt1* gene deleted mice (Figure.17.,18., 29. and 39.), and also contribute to the difference among defects in the ossification caused in these mice models.

5.2.2.2. Osteoblast differentiation was delayed in Zellweger Syndrome and promoted in *Sirt1* KO mice model

Primary osteoblasts were isolated from the neonatal mouse calvaria which is formed through the intramembranous ossification process. In the cell culture model it was described that, the MSCs directly condense and differentiate to osteoblast progenitors and further differentiate into pre-osteoblast and then into mature functional osteoblast for mineralization. Therefore the initial cell culture isolated from mouse calvaria contain a mixture of osteoblast progenitor cells which forward to differentiate to pre-osteoblast, differentiating pre-osteoblast and differentiated mature functional osteoblast (See Section 1.3.). Previous experiments in our lab have found that the middle stage osteoblast marker OPN and osteoblast maturation stage marker BGLAP were continuously increased throughout a 10 day period of osteoblast culturing (Qian, 2010a) which indicates a combination of osteoblast in different stages which were progressing in differentiation toward the mature stage. Therefore, the different portions of osteoblast in different stages could be screened by the expression level of osteoblast differentiation stage markers.

According to the expression level of osteoblast stage markers in *Pex11β* and *Pex13* KO osteoblast, the differentiation process is partially delayed in *Pex11β* KO osteoblasts (Figure.19.and 20.), whereas the osteoblast differentiation process is delayed in all stages of *Pex13* KO osteoblast differentiation (Figure.28.), wherefore the bone mineralization defect occurred in these ZS animal models (Figure.27.) (Qian, 2010a). Interestingly, even the osteoblast differentiation process is less delayed in *Pex11β KO* mice than *Pex13* KO mice; the ossification defect in *Pex11β* KO mice is more severe than in *Pex13* KO mice, as for the fact that the ossification defect of *Pex11β* KO mice was detected at E19 but only after day of P0.5 in *Pex13* KO mice.

In summary, the alteration of differentiation of osteoblasts isolated from Zellweger Syndrome mice and the *Sirt1* KO mouse can be summarized and compared as following Table.18.

Table.18.The comparison of osteoblast differentiation progress Zellweger Syndrome and the *Sirt1* KO mouse model

Osteoblast Differentiation Process		Early Stage	Middle Stage	Mature Stage
Osteoblasts isolated from Zellweger Syndrome Mice	***Pex11β* KO**	**Slightly increased**	**Delayed**	**Severely delayed**
	***Pex13* KO**	**Severely delayed**	**Severely delayed**	**Severely delayed**
***Sirt1* KO osteoblast**		**No significant alteration**	**Strongly increased expression of bone markers**	**No significant alteration**

Similar like the ossification phenotype (Table.17.), the differentiation process might be different in *Pex11β* KO and *Pex13* KO compared with Sirt1 KO osteoblast as indicated by expression level of bone markers. However, in the *Sirt1* KO osteoblast, the hyperexpression of middle stage osteoblast *Opn* and *Ibsp* (Figure.37.) might be result in the negative consequence to embryonic development of *Sirt1* KO mice. It has been known the OPN is a potent constraining factor on haemopoietic stem cells proliferation and overexpression of *Opn* is a feature of haemopoietic malignancies, such as multiple myeloma and chronic myeloid leukaemia (Haylock and Nilsson, 2006). In human body, the Bone sialoprotein is expressed in breast, lung, thyroid and prostate cancers and expression of bone sialoprotein by cancer cells could play a major role in the mineral deposition and in preferred bone homing of breast cancer cells (Ogata, 2008).

5.3. Signaling pathways of osteoblast differentiation regulation are already altered in *Pex11β, Pex13* and *Sirt1* KO mouse models

Critical roles of peroxisomes in the development of calcified tissues has been noted in previous researches in our lab, such as the peroxisome abundance increasing during differentiation of ameloblasts and odontoblasts and strong heterogeneity of peroxisomal enzyme content during differentiation of these dental cell types (Stelzig et al., 2013)

It has been discussed in a previous section (see Section 1.3.2.2.) that the precursors of various cell types of calcified tissue, such as osteoblasts, and osteocytes are differentiated from MSCs; whereas the MSCs can also differentiate to adipocytes. This "switch" of inverse relationship balancing between osteogenic and adipogenic lineage orientation is controlled by several signaling pathways which converge on various transcription factors, such as FoxO1, PPARγ and Runx2 (James, 2013; Teixeira et al., 2010). These key transcription factors can be realized as the master regulators of adipogenesis and osteogenesis by determining and sensing environmental alterations, which might be altered by the peroxisomal dysfunction due to oxidative stress and lipid toxicity.

5.3.1. Strong oxidative stress in *Pex11β, Pex13* and *Sirt1* KO osteoblast

Previous research has revealed that missing peroxisome proliferation capacity caused by *Pex11β* gene deletion resulted in strongly increased oxidative stress and lipid peroxidation, determined by the increase of lipid peroxidation product 4-hydroxynonenal (4-HNE) (Qian, 2010a). In my research, the TUNEL assay was used to detect apoptosis in *Pex11β* KO osteoblast cell culture: that might be caused by the possible severe oxidative stress; the results showed that the number of cells positively stained with the TUNEL assay was significantly higher in KO than in WT osteoblast culture (Figure.24.). Moreover, the TUNEL-positively stained osteoblasts showed also the typical alterations of nuclear morphology (shrinking, condensation, and fragmentation of chromatin) that are observed during apoptosis. It is universally accepted that the TUNEL staining cannot only

detect the apoptotic cells *in situ*, but also DNA damage associated with non-apoptotic events caused by exposure to toxic compounds or other stress (Ansari et al., 1993). Indeed, it has been found that oxidative stress induced DNA damage was also dramatically increased in osteoblast of *Pex11β* KO mouse calveria as shown by strong nuclear IF labelling with an antibody against 8-hydroxy-2'-deoxyguanosine (8-OHdG) (Qian, 2010a). Therefore, the osteoblast apoptosis may be induced by oxidative DNA damage in *Pex11β KO* osteoblast.

Also in *Pex13 KO* animal a strong oxidative response was stimulated by the oxidative stress in the bone (Figure.30.) and in osteoblasts culture (Figure.31.). Maybe one of the reasons why catalase is not degraded in the cytoplasm and even transported to the nucleus is to prevent osteoblasts against cell death. Catalase is one of the fastest enzymes to degrade H_2O_2 and has a very high capacity to remove this reactive oxygen species. Cytoplasmic and nuclear catalase is a typical feature of peroxisomal matrix protein import deficiencies, whereas most other peroxisomal enzymes are degraded in the cytoplasm. Interestingly, reduction of peroxisomal enzymes and transporters and biogenesis proteins were also present in the *Sirt1* KO osteoblast, and the ROS levels significantly increased in MC3T3-E1 cells with a *Sirt1* shRNA knockdown (Figure.42.).

5.3.2. Runx2 functional activity was attenuated in *Pex11β* and *Pex13* osteoblast cells

Runx2 is a member of the Runx family of transcription factors and the importance of this transcription factor for human and animal physiology can be determined by the human disease cleidocranial dysplasia due to *Runx2* gene deficiency (Mundlos et al., 1997; Otto et al., 1997; Ziros et al., 2008). This transcription factor is also essential for normal osteoblast differentiation, maturation and homeostasis (Ziros et al., 2008).The study on the functions of Runx2 started from the capability of RUNX2 to induce the differentiation of multipotent MCS into immature osteoblasts and guiding the immature bone formation (O'Donnell and Meyers, 1985). In particular the overexpression of *Runx2* in MSC cell lines leads

to an up-regulation of osteoblast specific genes (Ducy et al., 1997). Interestingly, in later research it has been found that, RUNX2 actually plays "dual-roles" in the different stages of the osteoblast differentiation process. It enhances osteoblast differentiation at an early stage when it has a high level of expression and inhibits osteoblast differentiation at a late stage when its expression level is down regulated (Komori, 2003). Therefore, the entire osteoblast differentiation process consist of two periods: differentiation from MSCs to precursor osteoblasts is regulated by RUNX2 and from *Runx2*-expressing precursors into mature and functional osteoblasts is regulated by Osterix (Sinha and Zhou, 2013).

Being an essential transcription factor for osteoblast differentiation, the DNA binding capability is critical for the proper function of RUNX2. Interestingly, the *Runx2* gene expression and functions can be partially autoregulated by binding its own promoter during bone formation (Drissi et al., 2000). In *Pex11β* and *Pex13 KO* osteoblast, both the gene expression of Runx2 and Osterix were strongly down regulated (Figure.19.and 28.), whereas there was no change in *Sirt1* KO osteoblast compared to WT (Figure.37.). This reveals that the activation of bone-specific genes were severely repressed in ZS mice compared to *Sirt1* KO mice.

The results from the luciferase transcriptional assay with plasmids containing RUNX2 DNA binding sequences show the dramatically down-regulated RUNX2 DNA binding capability in *Pex11β* shRNA knockdown MC3T3-E1 cells (Figure.23.) and primary *Pex13* KO osteoblasts (Figure.32.) compared to WT. It has been known that RUNX2 regulates Osterix expression at an early stage of osteoblast differentiation and Osterix is required for the major signaling pathways fibroblast growth factor (FGF), Wnt, and Indian hedgehog (IHH) signaling pathways during skeletal development (Komori, 2011). The latest research found the RUNX2 DNA binding can be repressed by oxidative stress (ROS) and compensated by antioxidants in endothelial cells to regulate the further differentiation process of these cells (Mochin et al., 2014). Therefore, it can be assumed the decreased RUNX2 DNA binding capability may be caused by the

increasing oxidative stress due to peroxisomal dysfunction in *Pex11β* shRNA knockdown MC3T3-E1 cells and *Pex13 KO* osteoblasts.

In addition to its role in osteoblast differentiation, RUNX2 seems to control the cell cycle. Indeed, the severe reduction of the gene expression and protein abundance of RUNX2 (Qian, 2010a) may contribute to the remarkable alteration of the cell cycle of *Pex11β* KO osteoblast compared to WT (Figure.25.). It has been reported that RUNX2 can play ambivalent roles in tumorigenesis, in particular it initiates the proliferative phase of cell differentiation in an oncogenic manner, whereas it promotes the arrest of the cells into the post-mitotic state anti-oncogenically (Thomas and Kansara, 2006). It has been found that in osteosarcoma the DNA copies and expression of RUNX2 were strongly up-regulated. Therefore RUNX2 may have both tumor suppressive and tumor promoting roles in bone morphogenesis (Martin et al., 2011).

5.3.3. The function of PPAR, PPRE DNA binding activity, was increased in *Pex11β* KO osteoblast

PPARs act as metabolic sensors and central regulators of fat and glucose homeostasis (Ammerschlaeger et al., 2004; Duclos et al., 1997; Goll et al., 1999; Osumi et al., 1990). PPARs of all subtypes form heterodimers with RXRs and bind to consensus peroxisome proliferator response elements (PPRE), composed of two core motifs separated by a single base pair (DR1 element: 5'-AGGTCA-N-AGGTCA-3') (Michalik et al., 2006). PPRE-driven luciferase gene report gene assay is an efficient tool for the evaluation of potential PPAR agonists (Tsai et al., 2014). Indeed also in this study an increase of PPRE activity in *Pex11β* KO osteoblast (Figure.22.) was noted possibly caused by increased oxidative stress and the accumulation of oxidized fatty acid as ligands for PPARγ activity. Interestingly, PPARγ is a major catabolic regulator of bone mass in mice and humans. It has been shown that stimulation of PPARγ inhibits osteoblast maturation and can transdifferentiate mature osteoblasts into adipocytes (Lecka-Czernik et al., 2002; Nuttall et al., 1998). Indeed, in *Pex11β* or *Pex13* KO animals

inhibition of osteoblast maturation and a reduced bone mass were found. Under normal conditions in WT cells, PPARγ is suppressed during osteoblastogenesis (Kang et al., 2007) and the PPARγ knockdown enhances osteogenesis (Akune et al., 2004; Yamashita et al., 2006). In contrast an increase in PPARγ is accompanied by a decrease in canonical wnt signaling and the translocation of RUNX2 into the cytoplasm, leading to less osteoblast differentiation and decreased ossification (Tanaka et al., 2012). This knowledge from the literature fully supports the results of this thesis that peroxisome deficiency leads to PPARγ overactivation and in consequence to the observed ossification defect in our *Pex11β* or *Pex13* KO animal model.

5.3.4. The FoxOs protect osteoblast against oxidative stress with transcriptional function

The FOXO forkhead transcription factors are involved in metabolism control, cell survival, cellular proliferation, DNA damage repair response, and stress resistance. Their transcriptional activity is regulated through a number of posttranslational modifications, including phosphorylation, acetylation and ubiquitination (Kousteni, 2011b; Obsil and Obsilova, 2011). In principle, the protein stability and transcriptional activity of FoxOs can be activated by oxidative stress, and this will initiate an anti-oxidative defense response. Thus, FoxOs transcription factors can protect osteoblasts against oxidative stress to maintain the bone mass homeostasis by activating genes regulating ROS scavenge and apoptosis (Ambrogini et al., 2010). The increased apoptosis (Figure.24.) and strong alteration of cell cycle (Figure.25.) in *Pex11β* KO osteoblast may be contributed by down-regulated transcriptional activity of FoxOs, indicated by the decrease of FoxOs DNA binding capability (Figure.21.) due to *Pex11β* gene deletion.

Beside the DNA binding, also nuclear translocation is essential for the transcriptional function of FoxOs, which are both regulated by a two-tiered mechanism of deacetylation and phosphorylation (Kousteni, 2011b). It has been found that FoxOs can be acetylated by p300 and nuclear hormone receptor

coactivators CREB-binding protein (CBP) (acetyltransferase) under conditions of cellular stress and also can be deacetylated by expression of sirtuins in the nucleus (Sandri et al., 2004).

Especially the most important functional member of the FoxO family, FoxO1 can not only maintain bone homeostasis with promoting osteoblast proliferation by regulating protein synthesis and maintain redox balance (Rached et al., 2010), but also regulates glucose metabolism via the skeleton with transcriptional function in osteoblast when the skeleton functions as an endocrine organ (Kousteni, 2011a). Significantly increased levels of ROS and lipid peroxidation products as well as an activation of the stress-evoked p53-dependent signaling cascade have been found in the bones of FoxO1 KO mice. On this basis, the FoxO1 function can be identified as a crucial regulator of osteoblast physiology and it provides a direct mechanistic link between oxidative stress in osteoblast and control of bone mass (Ambrogini et al., 2010; Rached et al., 2010). The ossification defects in *Pex11β* KO mouse are partially caused by the reduction of the FoxO1 protein (Qian, 2010a) and the decreased FoxO DNA binding capability due to oxidative stress in *Pex11β* KO osteoblasts.

5.4. The regulation of SIRT1 on osteoblast and osteoclast differentiation

5.4.1. The transcriptional functions of PPARγ and FoxOs and RUNX2 are related with SIRT1 interaction and deacetylation

It has been found that many important transcription factors, in particular PPARs (α and γ), PGC-1α and FoxOs interact and be deacetylated by SIRT1 to promote metabolic responses to cellular stimulation, such as oxidative stress and fatty acid oxidation(Haigis and Sinclair, 2010). Further, PPARγ can directly interact with SIRT1 and its DNA binding and transcriptional function are in part related to SIRT1 deacetylation activity (Han et al., 2010). The latest literature suggests that the Sirt1/Runx2 association and deacetylation of Runx2 may partially influence the transcriptional function of RUNX2 and contribute to the regulation of differentiation of MSCs and pre-osteoblast to osteoblasts (Shakibaei et al., 2012).

Most importantly, the SIRT1 protein is contradictorily translocated into the nuclear region in *Pex11β* and *Pex13* KO osteoblast. In particular the nuclear abundance of SIRT1 was massively reduced in *Pex11* KO osteoblast (Figure.33.). In contrast it was very concentrated in *Pex13* KO osteoblast compared to WT. However, this difference suggests that SIRT1 functions were severely altered in *Pex11β* and *Pex13* KO osteoblast; we cannot conclude a different outcome in *Pex11β* and *Pex13* KO osteoblast, because SIRT1 actually regulates the transcriptional capability of PPARs, FoxOs and Runx2 via deacetylation. Further investigations on how PPARs, FoxOs and RUNX2 are regulated by SIRT1 with the deacetylation of these transcription factors should be performed in *Pex11β* and *Pex13* KO osteoblast.

5.4.2. The Regulation of retinoic acid signaling by SIRT1 deacetylation

It has been known that the retinoid homeostasis is critical for normal embryonic development; in particular both the deficiency and excess of these compounds are associated with congenital malformations (Tang et al., 2014). The retinoic acid binding protein II (CRABPII) can act as a retinoic acid (RA) carrier which can transport RA from the cytosol into the nucleus upon RA binding to activate the nuclear RA receptors (Delva et al., 1999; Dong et al., 1999; Sessler and Noy, 2005). Moreover it has been determined that the cellular CRABPII can be deacetylased by SIRT1 and that the loss of SIRT1 increases the nuclear accumulation of CRABPII (Tang et al., 2014).

As a key regulatory factor, Sirt1 mediates the pleiotropic effects of RA and therefore the RA binding to retinoic acid receptors β (RARβ) can be altered by a Sirt1 gene deletion which in turn could induce a nuclear accumulation of CRABPII.

5.4.3. The osteoclast differentiation can be encouraged by osteoblast cell SIRT1 protein deletion via the RANKL /OPG system

Previous studies have shown that in response to bone-resorbing factors, osteoblasts release RANKL to bind RANK on the surface of osteoclasts,

promoting the differentiation of osteoclasts through activation of NFATc1, a master regulator of osteoclastogenesis (Khosla, 2001; Nakashima and Takayanagi, 2011). Osteoblasts also produce OPG, a soluble decoy receptor of RANKL, for the competition of RANKL with RANK, and thereby limiting osteoclast formation.

Indeed, a significant interference with this system was noted in *Sirt1* KO cells, exhibiting higher *Rankl* and lower *Opg* mRNA levels compared to WT cells. This suggests that RANKL can promote osteoclast precursor cells to further differentiate to functional osteoclasts, whereas OPG can bind to RANKL to diminish this promoting effect. Therefore, the ratio of intercellular RANKL/OPG secreted by *Sirt1* KO osteoblast may also increase, which may possibly result in an increase of osteoclasts differentiation promoting effects in *Sirt1* KO mice compared to WT. For further confirmation, an ELISA test should be applied to detect intercellular soluble RANKL/OPG protein concentration in *Sirt1* KO/WT mice.
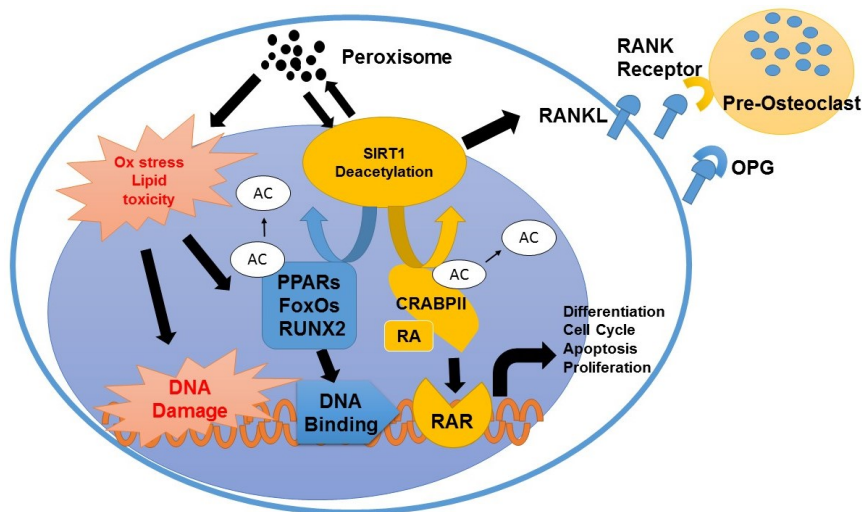
6. Summary

Peroxisomes are cell organelles that play critical roles from yeasts to humans during development, differentiation and morphogenesis and host a wide range of essential metabolic pathways such as lipid metabolism and the free radical detoxification. The importance of normal peroxisomal function and signaling in bone development is demonstrated by patients with Zellweger syndrome (ZS) and ZS mouse models. Zellweger syndrome is a human disorder caused by mutations in peroxisomal biogenesis genes. Patients exhibit typical skeletal deformations in addition to other developmental defects. Similarly, SIRT1, a highly conserved NAD^+-dependent protein deacetylase, regulates lipid and antioxidative metabolism as well as proliferation pathways to extend mammalian lifespan, through deacetylation of histones and central transcription factors and cofactors, such as PPARs, FoxOs and RUNX2.

By using the *Pex11* and *Pex13* KO animal models with a Zellweger phenotype including strong ossification defects and skeletal deformation, we found that the differentiation and maturation processes in primary osteoblasts isolated from these animals were dramatically delayed when peroxisome biogenesis and peroxisomal enzymatic function were dysfunctional. Furthermore in osteoblasts of these ZS mouse osteoblasts, cell apoptosis and cell cycle were severely altered as well as the DNA binding capability of PPARs, FoxOs and RUNX2 together with increasing cellular oxidative stress and lipid toxicity.

Interestingly, disturbances within the process of ossification and osteoblast differentiation were observed also in the *Sirt1* KO mouse model. Moreover, the peroxisome biogenesis and their enzymatic functions were significantly reduced and oxidative stress was increased. Interestingly we could show that SIRT1 also maintains homeostatic RA signaling by regulating the subcellular localization of CRABPII through its deacetylation activity. Therefore, the nuclear accumulation of the hyper-acetylated CRABPII and elevated RA signaling were induced by SIRT1 deficiency, which resulted in the accelerating differentiation of

mesenchymal stem cells (MSCs) and developmental defects in *Sirt1* KO mice. Whether the deacetylation function of SIRT1 may have been altered in *Pex11* and *Pex13* KO osteoblast due to the strong downregulation of the SIRT1 abundance and nuclear translocation has to be investigated in future. Additionally, the capability to enhance osteoclastogenesis was increased in *Sirt1* KO osteoblast via an unbalanced RANKL/OPG system.

Taken my results together and in respect to our previous data and the latest literature, the functions of peroxisomes in these cell types are summarized in Figure.45. The peroxisome contributes to the maintenance of the homeostasis of lipid metabolism and cellular redox stress. Peroxin gene deletion induced peroxisomal dysfunction which results in increased cellular oxidative stress, lipid toxicity and possible alterations in the deacetylation state of SIRT1. The activity of the transcription factors PPARs, FoxOs and RUNX2 induced by oxidative stress and lipid accumulation might be altered by SIRT1 deacetylation, as well as the RA signaling and this interference may in part contribute to the severe changes of differentiation, cell cycle, apoptosis and proliferation process observed in osteoblast and ossification disturbance of ZS mice.

Figure.45. Schematic illustration of the possible mechanism of peroxisome regulation on osteoblast differentiation via the SIRT1 deacetylation activity. Ox: oxidative stress; AC: acetylation.
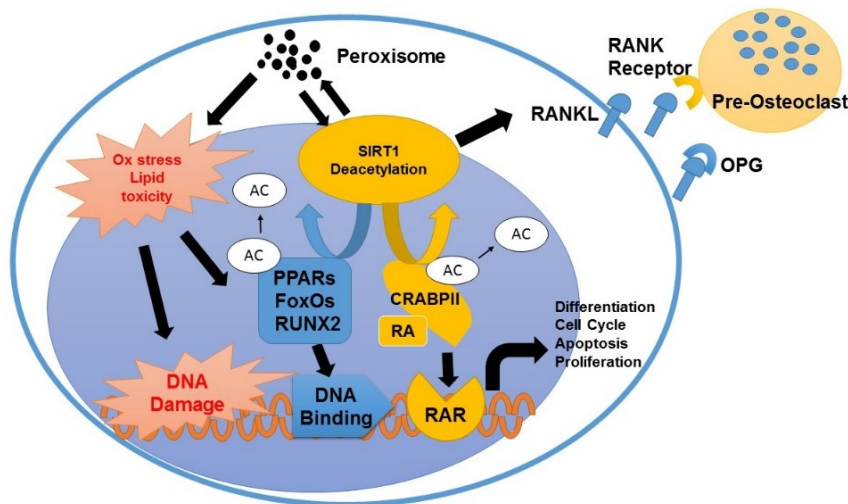
7. Zusammenfassung

Peroxisomen sind Zellorganellen, die von Hefen bis hin zum Menschen an einem breiten Spektrum wichtiger Stoffwechselwege beteiligt sind. Außerdem spielen sie eine wichtige Rolle im Lipidaufbau, beim Abbau freier Radikale, sowie in der Entwicklung, Differenzierung und Morphogenese. Das Zellweger Syndrom (ZS) sowie ZS-Mausmodelle belegen die Wichtigkeit einer normalen peroxisomalen Funktion während der Knochenentwicklung. Diese humane Erkrankung ist durch Mutationen von Peroxin-Genen mit Verlust der peroxisomalen Funktion verursacht, und ist durch typische Skelettfehlbildungen und weitere Entwicklungsdefekte gekennzeichnet. Die hochkonservierte, NAD^+-abhängige Proteindeacetylase SIRT1 reguliert den Lipidaufbau, den antioxidativen Stoffwechsel, sowie die Proliferation. SIRT1 ist einerseits an der Verlängerung der Lebensdauer von Säugern beteiligt und beeinflusst andererseits Erkrankungen, die mit dem Stoffwechsel und dem Altern zusammenhängen. Die Funktionsweise von SIRT1 beruht auf der Deacetylierung von Histonen und Transkriptionsfaktoren und deren Co-Faktoren wie z.B. PPARs, FoxOs und RUNX2.

Mit Hilfe von *Pex11*- bzw. *Pex13*-KO-Mäusen (ZS-Mausmodelle), die ZS-typische Phänotypen aufweisen, stellten wir fest, dass die Differenzierung und Reifung von primären Osteoblasten (OB) aus diesen ZS-Mäusen stark verzögert waren, sobald die Peroxisomentwicklung und die enzymatischen Funktionen zusammenbrachen. Ferner hält SIRT1 die RA-Homöostase mittels der Acetylierungs-Aktivität, die für die Regulierung der subzellulären Lokalisierung von CRABPII verantwortlich ist, aufrecht. Eine SIRT1-Defizienz induzierte die nukleäre Akkumulation des hyperacetylierten CRABPII und erhöhte die RA-Signalkaskade. Dies bewirkte eine beschleunigte Differenzierung der mesenchymalen Stammzellen (MSC) und führte zu Entwicklungsstörungen in *Sirt1*-KO-Mäusen. Ob die in *Pex11*- und *Pex13*-KO-OB gefundene verminderte SIRT1-Expression und SIRT1-Translokation in den Nucleus tatsächlich zu einer Redukion der Deacetlyierung von SIRT1-Substraten führt, müssen zukünftige

Experimente zeigen. Außerdem kam es durch das unausgeglichene RANKL/OPG-System zu einer erhöhten Osteklastenentwicklung in *Sirt1*-KO-OB.

Aus all meinen Ergebnissen und in Anbetracht der vorangegangenen Daten sowie der neuesten Literatur kann folgendes Modell (s. Abb. 45) für die Rolle der Peroxisomen während der OB-Differenzierung erstellt werden: Peroxisomen tragen zur Aufrechterhaltung der Homöostase des Lipidmetabolismus sowie des zellulären Redox-Stresses bei. Die Peroxisomendysfunktion, die durch die Deletion der Peroxingene *Pex11β* und *Pex13* induziert wird, löst erhöhten zellulären oxidativen Stress, Lipidtoxizität und mögliche Änderungen der Deacetylierungsfähigkeit von SIRT1 aus. Die Aktivitäten der Transkriptionsfaktoren PPAR, FoxO und RUNX2 werden wiederum durch oxidativen Stress und Lipidakkumulation induziert. Diese Induktion wird durch die Deacetylierung der oben genannten Transkriptionfaktoren mittels SIRT1 und der RA-Signalkaskade beeinflusst. Folglich könnte diese Beeinflussung zum Teil zu den gravierenden Veränderungen in der Differenzierung, der Apoptose, dem Zellzyklus und der Proliferation in OB, sowie während der Ossifikation in ZS-Mäusen beitragen.

Abbildung.45. Schematische Darstellung des angenommenen Mechanismus der Regulation der OB-Differenzierung durch Peroxisomen über die Deacetylierungsaktivität von SIRT1. Ox: oxidativer Stress; AC: Acetylierung.

8. References

Agamanolis, D.P., and Novak, R.W. (1995). Rhizomelic chondrodysplasia punctata: report of a case with review of the literature and correlation with other peroxisomal disorders. Pediatric pathology & laboratory medicine : journal of the Society for Pediatric Pathology, affiliated with the International Paediatric Pathology Association *15*, 503-513.

Akune, T., Ohba, S., Kamekura, S., Yamaguchi, M., Chung, U.I., Kubota, N., Terauchi, Y., Harada, Y., Azuma, Y., Nakamura, K.*, et al.* (2004). PPARgamma insufficiency enhances osteogenesis through osteoblast formation from bone marrow progenitors. The Journal of clinical investigation *113*, 846-855.

Albertini, M., Rehling, P., Erdmann, R., Girzalsky, W., Kiel, J.A., Veenhuis, M., and Kunau, W.H. (1997). Pex14p, a peroxisomal membrane protein binding both receptors of the two PTS-dependent import pathways. Cell *89*, 83-92.

Almeida, M., Ambrogini, E., Han, L., Manolagas, S.C., and Jilka, R.L. (2009). Increased lipid oxidation causes oxidative stress, increased peroxisome proliferator-activated receptor-gamma expression, and diminished pro-osteogenic Wnt signaling in the skeleton. The Journal of biological chemistry *284*, 27438-27448.

Alvares, K., Widrow, R.J., Abu-Jawdeh, G.M., Schmidt, J.V., Yeldandi, A.V., Rao, M.S., and Reddy, J.K. (1992). Rat urate oxidase produced by recombinant baculovirus expression: formation of peroxisome crystalloid core-like structures. Proceedings of the National Academy of Sciences of the United States of America *89*, 4908-4912.

Ambrogini, E., Almeida, M., Martin-Millan, M., Paik, J.H., Depinho, R.A., Han, L., Goellner, J., Weinstein, R.S., Jilka, R.L., O'Brien, C.A.*, et al.* (2010). FoxO-mediated defense against oxidative stress in osteoblasts is indispensable for skeletal homeostasis in mice. Cell metabolism *11*, 136-146.

Ammerschlaeger, M., Beigel, J., Klein, K.U., and Mueller, S.O. (2004). Characterization of the species-specificity of peroxisome proliferators in rat and human hepatocytes. Toxicological sciences : an official journal of the Society of Toxicology *78*, 229-240.

Angermüller, S., Leupold, C., Volkl, A., and Fahimi, H.D. (1986). Electron microscopic cytochemical localization of alpha-hydroxyacid oxidase in rat liver. Association with the crystalline core and matrix of peroxisomes. Histochemistry *85*, 403-409.

Ansari, B., Coates, P.J., Greenstein, B.D., and Hall, P.A. (1993). In situ end-labelling detects DNA strand breaks in apoptosis and other physiological and pathological states. The Journal of pathology *170*, 1-8.

Anthonio, E.A., Brees, C., Baumgart-Vogt, E., Hongu, T., Huybrechts, S.J., Van Dijck, P., Mannaerts, G.P., Kanaho, Y., Van Veldhoven, P.P., and Fransen, M. (2009). Small G proteins in peroxisome biogenesis: the potential involvement of ADP-ribosylation factor 6. BMC cell biology *10*, 58.

Antonenkov, V.D., Grunau, S., Ohlmeier, S., and Hiltunen, J.K. (2010). Peroxisomes are oxidative organelles. Antioxidants & redox signaling *13*, 525-537.

Antonenkov, V.D., Van Veldhoven, P.P., Waelkens, E., and Mannaerts, G.P. (1997). Substrate specificities of 3-oxoacyl-CoA thiolase A and sterol carrier protein 2/3-oxoacyl-CoA thiolase purified from normal rat liver peroxisomes. Sterol carrier protein 2/3-

oxoacyl-CoA thiolase is involved in the metabolism of 2-methyl-branched fatty acids and bile acid intermediates. The Journal of biological chemistry *272*, 26023-26031.

Baes, M., Gressens, P., Baumgart, E., Carmeliet, P., Casteels, M., Fransen, M., Evrard, P., Fahimi, D., Declercq, P.E., Collen, D.*, et al.* (1997). A mouse model for Zellweger syndrome. Nature genetics *17*, 49-57.

Baumgart, E. (1997). Application of in situ hybridization, cytochemical and immunocytochemical techniques for the investigation of peroxisomes. A review including novel data. Robert Feulgen Prize Lecture 1997. Histochemistry and cell biology *108*, 185-210.

Baumgart, E., Vanhooren, J.C., Fransen, M., Marynen, P., Puype, M., Vandekerckhove, J., Leunissen, J.A., Fahimi, H.D., Mannaerts, G.P., and van Veldhoven, P.P. (1996a). Molecular characterization of the human peroxisomal branched-chain acyl-CoA oxidase: cDNA cloning, chromosomal assignment, tissue distribution, and evidence for the absence of the protein in Zellweger syndrome. Proceedings of the National Academy of Sciences of the United States of America *93*, 13748-13753.

Baumgart, E., Vanhooren, J.C., Fransen, M., Van Leuven, F., Fahimi, H.D., Van Veldhoven, P.P., and Mannaerts, G.P. (1996b). Molecular cloning and further characterization of rat peroxisomal trihydroxycoprostanoyl-CoA oxidase. The Biochemical journal *320 (Pt 1)*, 115-121.

Baumgart, E., Vanhorebeek, I., Grabenbauer, M., Borgers, M., Declercq, P.E., Fahimi, H.D., and Baes, M. (2001). Mitochondrial alterations caused by defective peroxisomal biogenesis in a mouse model for Zellweger syndrome (PEX5 knockout mouse). The American journal of pathology *159*, 1477-1494.

Bi, W., Gu, Z., Zheng, Y., Zhang, X., Guo, J., and Wu, G. (2013). Heterodimeric BMP-2/7 antagonizes the inhibition of all-trans retinoic acid and promotes the osteoblastogenesis. PloS one *8*, e78198.

Biardi, L., Sreedhar, A., Zokaei, A., Vartak, N.B., Bozeat, R.L., Shackelford, J.E., Keller, G.A., and Krisans, S.K. (1994). Mevalonate kinase is predominantly localized in peroxisomes and is defective in patients with peroxisome deficiency disorders. The Journal of biological chemistry *269*, 1197-1205.

Bodine, P.V. (2008). Wnt signaling control of bone cell apoptosis. Cell research *18*, 248-253.

Boyce, B.F., Rosenberg, E., de Papp, A.E., and Duong le, T. (2012). The osteoclast, bone remodelling and treatment of metabolic bone disease. Eur J Clin Invest *42*, 1332-1341.

Boyle, W.J., Simonet, W.S., and Lacey, D.L. (2003). Osteoclast differentiation and activation. Nature *423*, 337-342.

Bradford, M.M. (1976). A rapid and sensitive method for the quantitation of microgram quantities of protein utilizing the principle of protein-dye binding. Analytical biochemistry *72*, 248-254.

Braverman, N., Chen, L., Lin, P., Obie, C., Steel, G., Douglas, P., Chakraborty, P.K., Clarke, J.T., Boneh, A., Moser, A.*, et al.* (2002). Mutation analysis of PEX7 in 60 probands with rhizomelic chondrodysplasia punctata and functional correlations of genotype with phenotype. Human mutation *20*, 284-297.

Braverman, N., Steel, G., Obie, C., Moser, A., Moser, H., Gould, S.J., and Valle, D. (1997). Human PEX7 encodes the peroxisomal PTS2 receptor and is responsible for rhizomelic chondrodysplasia punctata. Nature genetics *15*, 369-376.

Braverman, N., Zhang, R., Chen, L., Nimmo, G., Scheper, S., Tran, T., Chaudhury, R., Moser, A., and Steinberg, S. (2010). A Pex7 hypomorphic mouse model for plasmalogen deficiency affecting the lens and skeleton. Mol Genet Metab *99*, 408-416.

Brighton, C.T., Sugioka, Y., and Hunt, R.M. (1973). Cytoplasmic structures of epiphyseal plate chondrocytes. Quantitative evaluation using electron micrographs of rat costochondral junctions with special reference to the fate of hypertrophic cells. J Bone Joint Surg Am *55*, 771-784.

Brites, P., Motley, A.M., Gressens, P., Mooyer, P.A., Ploegaert, I., Everts, V., Evrard, P., Carmeliet, P., Dewerchin, M., Schoonjans, L.*, et al.* (2003). Impaired neuronal migration and endochondral ossification in Pex7 knockout mice: a model for rhizomelic chondrodysplasia punctata. Human molecular genetics *12*, 2255-2267.

Brites, P., Waterham, H.R., and Wanders, R.J. (2004). Functions and biosynthesis of plasmalogens in health and disease. Biochimica et biophysica acta *1636*, 219-231.

Brosius, U., and Gartner, J. (2002). Cellular and molecular aspects of Zellweger syndrome and other peroxisome biogenesis disorders. Cellular and molecular life sciences : CMLS *59*, 1058-1069.

Brown, D.A., and London, E. (1998). Functions of lipid rafts in biological membranes. Annual review of cell and developmental biology *14*, 111-136.

Caetano-Lopes, J., Canhao, H., and Fonseca, J.E. (2007). Osteoblasts and bone formation. Acta Reumatol Port *32*, 103-110.

Caplan, A.I. (1988). Bone development. Ciba Found Symp *136*, 3-21.

Cheng, H.L., Mostoslavsky, R., Saito, S., Manis, J.P., Gu, Y., Patel, P., Bronson, R., Appella, E., Alt, F.W., and Chua, K.F. (2003). Developmental defects and p53 hyperacetylation in Sir2 homolog (SIRT1)-deficient mice. Proc Natl Acad Sci U S A.

Cohen-Kfir, E., Artsi, H., Levin, A., Abramowitz, E., Bajayo, A., Gurt, I., Zhong, L., D'Urso, A., Toiber, D., Mostoslavsky, R.*, et al.* (2011). Sirt1 is a regulator of bone mass and a repressor of Sost encoding for sclerostin, a bone formation inhibitor. Endocrinology *152*, 4514-4524.

Cooper, T.G., and Beevers, H. (1969). Beta oxidation in glyoxysomes from castor bean endosperm. The Journal of biological chemistry *244*, 3514-3520.

Coussens, M., Maresh, J.G., Yanagimachi, R., Maeda, G., and Allsopp, R. (2008). Sirt1 deficiency attenuates spermatogenesis and germ cell function. PLoS One *3*, e1571.

Dammai, V., and Subramani, S. (2001). The human peroxisomal targeting signal receptor, Pex5p, is translocated into the peroxisomal matrix and recycled to the cytosol. Cell *105*, 187-196.

Danino, D., and Hinshaw, J.E. (2001). Dynamin family of mechanoenzymes. Current opinion in cell biology *13*, 454-460.

Delva, L., Bastie, J.N., Rochette-Egly, C., Kraiba, R., Balitrand, N., Despouy, G., Chambon, P., and Chomienne, C. (1999). Physical and functional interactions between cellular retinoic acid binding protein II and the retinoic acid-dependent nuclear complex. Mol Cell Biol *19*, 7158-7167.

Diestelkotter, P., and Just, W.W. (1993). In vitro insertion of the 22-kD peroxisomal membrane protein into isolated rat liver peroxisomes. The Journal of cell biology *123*, 1717-1725.

Dieuaide-Noubhani, M., Asselberghs, S., Mannaerts, G.P., and Van Veldhoven, P.P. (1997). Evidence that multifunctional protein 2, and not multifunctional protein 1, is involved in the peroxisomal beta-oxidation of pristanic acid. The Biochemical journal *325 (Pt 2)*, 367-373.

Dieuaide-Noubhani, M., Novikov, D., Baumgart, E., Vanhooren, J.C., Fransen, M., Goethals, M., Vandekerckhove, J., Van Veldhoven, P.P., and Mannaerts, G.P. (1996). Further characterization of the peroxisomal 3-hydroxyacyl-CoA dehydrogenases from rat liver. Relationship between the different dehydrogenases and evidence that fatty acids and the C27 bile acids di- and tri-hydroxycoprostanic acids are metabolized by separate multifunctional proteins. European journal of biochemistry / FEBS *240*, 660-666.

Distel, B., Erdmann, R., Gould, S.J., Blobel, G., Crane, D.I., Cregg, J.M., Dodt, G., Fujiki, Y., Goodman, J.M., Just, W.W.*, et al.* (1996). A unified nomenclature for peroxisome biogenesis factors. The Journal of cell biology *135*, 1-3.

Dong, D., Ruuska, S.E., Levinthal, D.J., and Noy, N. (1999). Distinct roles for cellular retinoic acid-binding proteins I and II in regulating signaling by retinoic acid. J Biol Chem *274*, 23695-23698.

Drissi, H., Luc, Q., Shakoori, R., Chuva De Sousa Lopes, S., Choi, J.Y., Terry, A., Hu, M., Jones, S., Neil, J.C., Lian, J.B.*, et al.* (2000). Transcriptional autoregulation of the bone related CBFA1/RUNX2 gene. Journal of cellular physiology *184*, 341-350.

Duclos, S., Bride, J., Ramirez, L.C., and Bournot, P. (1997). Peroxisome proliferation and beta-oxidation in Fao and MH1C1 rat hepatoma cells, HepG2 human hepatoblastoma cells and cultured human hepatocytes: effect of ciprofibrate. European journal of cell biology *72*, 314-323.

Ducy, P., Zhang, R., Geoffroy, V., Ridall, A.L., and Karsenty, G. (1997). Osf2/Cbfa1: a transcriptional activator of osteoblast differentiation. Cell *89*, 747-754.

Eckert, J.H., and Erdmann, R. (2003). Peroxisome biogenesis. Reviews of physiology, biochemistry and pharmacology *147*, 75-121.

En-Nosse, M., Hartmann, S., Trinkaus, K., Alt, V., Stigler, B., Heiss, C., Kilian, O., Schnettler, R., and Lips, K.S. (2009). Expression of non-neuronal cholinergic system in osteoblast-like cells and its involvement in osteogenesis. Cell and tissue research *338*, 203-215.

Erdmann, R., and Blobel, G. (1995). Giant peroxisomes in oleic acid-induced Saccharomyces cerevisiae lacking the peroxisomal membrane protein Pmp27p. The Journal of cell biology *128*, 509-523.

Ewa, S. (2011). Acceleration of New Biomarkers Development and Discovery in Synergistic Diagnostics of Coronary Artery Disease.

Faust, P.L., and Hatten, M.E. (1997). Targeted deletion of the PEX2 peroxisome assembly gene in mice provides a model for Zellweger syndrome, a human neuronal migration disorder. The Journal of cell biology *139*, 1293-1305.

Faust, P.L., Su, H.M., Moser, A., and Moser, H.W. (2001). The peroxisome deficient PEX2 Zellweger mouse: pathologic and biochemical correlates of lipid dysfunction. Journal of molecular neuroscience : MN *16*, 289-297; discussion 317-221.

Fransen, M., Brees, C., Ghys, K., Amery, L., Mannaerts, G.P., Ladant, D., and Van Veldhoven, P.P. (2002). Analysis of mammalian peroxin interactions using a non-transcription-based bacterial two-hybrid assay. Molecular & cellular proteomics : MCP *1*, 243-252.

Fransen, M., Nordgren, M., Wang, B., and Apanasets, O. (2012). Role of peroxisomes in ROS/RNS-metabolism: implications for human disease. Biochimica et biophysica acta *1822*, 1363-1373.

Fransen, M., Van Veldhoven, P.P., and Subramani, S. (1999). Identification of peroxisomal proteins by using M13 phage protein VI phage display: molecular evidence that mammalian peroxisomes contain a 2,4-dienoyl-CoA reductase. The Biochemical journal *340 (Pt 2)*, 561-568.

Fulco, M., Cen, Y., Zhao, P., Hoffman, E.P., McBurney, M.W., Sauve, A.A., and Sartorelli, V. (2008). Glucose restriction inhibits skeletal myoblast differentiation by activating SIRT1 through AMPK-mediated regulation of Nampt. Dev Cell *14*, 661-673.

Fulco, M., Schiltz, R.L., Iezzi, S., King, M.T., Zhao, P., Kashiwaya, Y., Hoffman, E., Veech, R.L., and Sartorelli, V. (2003). Sir2 regulates skeletal muscle differentiation as a potential sensor of the redox state. Mol Cell *12*, 51-62.

Geary, D.F., Fennell, R.S., Braylan, R.C., Iravani, A., Garin, E.H., and Richard, G.A. (1982). Hyperparathyroidism and anemia in chronic renal failure. European journal of pediatrics *139*, 296-298.

Ghaedi, K., Tamura, S., Okumoto, K., Matsuzono, Y., and Fujiki, Y. (2000). The peroxin pex3p initiates membrane assembly in peroxisome biogenesis. Molecular biology of the cell *11*, 2085-2102.

Ghys, K., Fransen, M., Mannaerts, G.P., and Van Veldhoven, P.P. (2002). Functional studies on human Pex7p: subcellular localization and interaction with proteins containing a peroxisome-targeting signal type 2 and other peroxins. The Biochemical journal *365*, 41-50.

Girzalsky, W., Platta, H.W., and Erdmann, R. (2009). Protein transport across the peroxisomal membrane. Biological chemistry *390*, 745-751.

Girzalsky, W., Rehling, P., Stein, K., Kipper, J., Blank, L., Kunau, W.H., and Erdmann, R. (1999). Involvement of Pex13p in Pex14p localization and peroxisomal targeting signal 2-dependent protein import into peroxisomes. The Journal of cell biology *144*, 1151-1162.

Glass, D.A., 2nd, and Karsenty, G. (2006a). Canonical Wnt signaling in osteoblasts is required for osteoclast differentiation. Annals of the New York Academy of Sciences *1068*, 117-130.

Glass, D.A., 2nd, and Karsenty, G. (2006b). Molecular bases of the regulation of bone remodeling by the canonical Wnt signaling pathway. Current topics in developmental biology *73*, 43-84.

Goll, V., Alexandre, E., Viollon-Abadie, C., Nicod, L., Jaeck, D., and Richert, L. (1999). Comparison of the effects of various peroxisome proliferators on peroxisomal enzyme

activities, DNA synthesis, and apoptosis in rat and human hepatocyte cultures. Toxicology and applied pharmacology *160*, 21-32.

Gould, S.J., Kalish, J.E., Morrell, J.C., Bjorkman, J., Urquhart, A.J., and Crane, D.I. (1996). Pex13p is an SH3 protein of the peroxisome membrane and a docking factor for the predominantly cytoplasmic PTs1 receptor. The Journal of cell biology *135*, 85-95.

Gould, S.J., Keller, G.A., Hosken, N., Wilkinson, J., and Subramani, S. (1989). A conserved tripeptide sorts proteins to peroxisomes. The Journal of cell biology *108*, 1657-1664.

Gould, S.J., and Valle, D. (2000). Peroxisome biogenesis disorders: genetics and cell biology. Trends in genetics : TIG *16*, 340-345.

Gregory, C.A., Gunn, W.G., Peister, A., and Prockop, D.J. (2004). An Alizarin red-based assay of mineralization by adherent cells in culture: comparison with cetylpyridinium chloride extraction. Analytical biochemistry *329*, 77-84.

Guarente, L. (2011). Sirtuins, aging, and metabolism. Cold Spring Harbor symposia on quantitative biology *76*, 81-90.

Haigis, M.C., and Sinclair, D.A. (2010). Mammalian sirtuins: biological insights and disease relevance. Annual review of pathology *5*, 253-295.

Han, L., Zhou, R., Niu, J., McNutt, M.A., Wang, P., and Tong, T. (2010). SIRT1 is regulated by a PPAR{gamma}-SIRT1 negative feedback loop associated with senescence. Nucleic acids research *38*, 7458-7471.

Harada, S., and Rodan, G.A. (2003). Control of osteoblast function and regulation of bone mass. Nature *423*, 349-355.

Harty-Golder, B., and Braylan, R.C. (1982). Lymphomas and their expression in peripheral blood. The American journal of medical technology *48*, 685-688.

Haylock, D.N., and Nilsson, S.K. (2006). Osteopontin: a bridge between bone and blood. British journal of haematology *134*, 467-474.

He, T.C., Chan, T.A., Vogelstein, B., and Kinzler, K.W. (1999). PPARdelta is an APC-regulated target of nonsteroidal anti-inflammatory drugs. Cell *99*, 335-345.

Herranz, D., Munoz-Martin, M., Canamero, M., Mulero, F., Martinez-Pastor, B., Fernandez-Capetillo, O., and Serrano, M. (2010). Sirt1 improves healthy ageing and protects from metabolic syndrome-associated cancer. Nature communications *1*, 3.

Hettema, E.H., Erdmann, R., van der Klei, I., and Veenhuis, M. (2014). Evolving models for peroxisome biogenesis. Current opinion in cell biology *29*, 25-30.

Heymans, H.S., Oorthuys, J.W., Nelck, G., Wanders, R.J., and Schutgens, R.B. (1985). Rhizomelic chondrodysplasia punctata: another peroxisomal disorder. The New England journal of medicine *313*, 187-188.

Hijikata, M., Wen, J.K., Osumi, T., and Hashimoto, T. (1990). Rat peroxisomal 3-ketoacyl-CoA thiolase gene. Occurrence of two closely related but differentially regulated genes. The Journal of biological chemistry *265*, 4600-4606.

Hoepfner, D., van den Berg, M., Philippsen, P., Tabak, H.F., and Hettema, E.H. (2001). A role for Vps1p, actin, and the Myo2p motor in peroxisome abundance and inheritance in Saccharomyces cerevisiae. The Journal of cell biology *155*, 979-990.

Honsho, M., Tamura, S., Shimozawa, N., Suzuki, Y., Kondo, N., and Fujiki, Y. (1998). Mutation in PEX16 is causal in the peroxisome-deficient Zellweger syndrome of complementation group D. American journal of human genetics *63*, 1622-1630.

Imai, S., Armstrong, C.M., Kaeberlein, M., and Guarente, L. (2000). Transcriptional silencing and longevity protein Sir2 is an NAD-dependent histone deacetylase. Nature *403*, 795-800.

Imanaka, T., Takano, T., Osumi, T., and Hashimoto, T. (1996). Sorting of the 70-kDa peroxisomal membrane protein into rat liver peroxisomes in vitro. Annals of the New York Academy of Sciences *804*, 663-665.

James, A.W. (2013). Review of Signaling Pathways Governing MSC Osteogenic and Adipogenic Differentiation. Scientifica *2013*, 684736.

Jedd, G., and Chua, N.H. (2000). A new self-assembled peroxisomal vesicle required for efficient resealing of the plasma membrane. Nature cell biology *2*, 226-231.

Kang, M.R., Lee, S.W., Um, E., Kang, H.T., Hwang, E.S., Kim, E.J., and Um, S.J. (2009). Reciprocal roles of SIRT1 and SKIP in the regulation of RAR activity: implication in the retinoic acid-induced neuronal differentiation of P19 cells. Nucleic Acids Res *38*, 822-831.

Kang, S., Bennett, C.N., Gerin, I., Rapp, L.A., Hankenson, K.D., and Macdougald, O.A. (2007). Wnt signaling stimulates osteoblastogenesis of mesenchymal precursors by suppressing CCAAT/enhancer-binding protein alpha and peroxisome proliferator-activated receptor gamma. The Journal of biological chemistry *282*, 14515-14524.

Karnati, S., and Baumgart-Vogt, E. (2008). Peroxisomes in mouse and human lung: their involvement in pulmonary lipid metabolism. Histochemistry and cell biology *130*, 719-740.

Karnati, S., Luers, G., Pfreimer, S., and Baumgart-Vogt, E. (2013). Mammalian SOD2 is exclusively located in mitochondria and not present in peroxisomes. Histochemistry and cell biology *140*, 105-117.

Khosla, S. (2001). Minireview: the OPG/RANKL/RANK system. Endocrinology *142*, 5050-5055.

Koch, A., Schneider, G., Luers, G.H., and Schrader, M. (2004). Peroxisome elongation and constriction but not fission can occur independently of dynamin-like protein 1. Journal of cell science *117*, 3995-4006.

Koch, A., Thiemann, M., Grabenbauer, M., Yoon, Y., McNiven, M.A., and Schrader, M. (2003). Dynamin-like protein 1 is involved in peroxisomal fission. The Journal of biological chemistry *278*, 8597-8605.

Komori, T. (2002). Runx2, a multifunctional transcription factor in skeletal development. Journal of cellular biochemistry *87*, 1-8.

Komori, T. (2003). Requisite roles of Runx2 and Cbfb in skeletal development. Journal of bone and mineral metabolism *21*, 193-197.

Komori, T. (2008). Regulation of bone development and maintenance by Runx2. Frontiers in bioscience : a journal and virtual library *13*, 898-903.

Komori, T. (2011). Signaling networks in RUNX2-dependent bone development. Journal of cellular biochemistry *112*, 750-755.

Kousteni, S. (2011a). FoxO1: a molecule for all seasons. Journal of bone and mineral research : the official journal of the American Society for Bone and Mineral Research *26*, 912-917.

Kousteni, S. (2011b). FoxOs: Unifying links between oxidative stress and skeletal homeostasis. Current osteoporosis reports *9*, 60-66.

Kovacs, W.J., Olivier, L.M., and Krisans, S.K. (2002). Central role of peroxisomes in isoprenoid biosynthesis. Prog Lipid Res *41*, 369-391.

Kovacs, W.J., Shackelford, J.E., Tape, K.N., Richards, M.J., Faust, P.L., Fliesler, S.J., and Krisans, S.K. (2004). Disturbed cholesterol homeostasis in a peroxisome-deficient PEX2 knockout mouse model. Mol Cell Biol *24*, 1-13.

Kovacs, W.J., Tape, K.N., Shackelford, J.E., Duan, X., Kasumov, T., Kelleher, J.K., Brunengraber, H., and Krisans, S.K. (2007). Localization of the pre-squalene segment of the isoprenoid biosynthetic pathway in mammalian peroxisomes. Histochemistry and cell biology *127*, 273-290.

Kozlov, M.M. (1999). Dynamin: possible mechanism of "Pinchase" action. Biophysical journal *77*, 604-616.

Krisans, S.K. (1992). The role of peroxisomes in cholesterol metabolism. American journal of respiratory cell and molecular biology *7*, 358-364.

Krisans, S.K., Ericsson, J., Edwards, P.A., and Keller, G.A. (1994). Farnesyl-diphosphate synthase is localized in peroxisomes. The Journal of biological chemistry *269*, 14165-14169.

Lanyon, L.E. (1992). The success and failure of the adaptive response to functional load-bearing in averting bone fracture. Bone *13 Suppl 2*, S17-21.

Lazarow, P.B., and De Duve, C. (1976). A fatty acyl-CoA oxidizing system in rat liver peroxisomes; enhancement by clofibrate, a hypolipidemic drug. Proceedings of the National Academy of Sciences of the United States of America *73*, 2043-2046.

Lazarow, P.B., and Fujiki, Y. (1985). Biogenesis of peroxisomes. Annual review of cell biology *1*, 489-530.

Lecka-Czernik, B., Moerman, E.J., Grant, D.F., Lehmann, J.M., Manolagas, S.C., and Jilka, R.L. (2002). Divergent effects of selective peroxisome proliferator-activated receptor-gamma 2 ligands on adipocyte versus osteoblast differentiation. Endocrinology *143*, 2376-2384.

Li, X. (2013). SIRT1 and energy metabolism. Acta biochimica et biophysica Sinica *45*, 51-60.

Li, X., Baumgart, E., Dong, G.X., Morrell, J.C., Jimenez-Sanchez, G., Valle, D., Smith, K.D., and Gould, S.J. (2002a). PEX11α Is Required for Peroxisome Proliferation in Response to 4-Phenylbutyrate but Is Dispensable for Peroxisome Proliferator-Activated Receptor Alpha-Mediated Peroxisome Proliferation. Molecular and Cellular Biology *22*, 8226-8240.

Li, X., Baumgart, E., Morrell, J.C., Jimenez-Sanchez, G., Valle, D., and Gould, S.J. (2002b). PEX11β deficiency is lethal and impairs neuronal migration but does not abrogate peroxisome function. Mol Cell Biol *22*, 4358-4365.

Li, X., and Gould, S.J. (2002). PEX11 promotes peroxisome division independently of peroxisome metabolism. The Journal of cell biology *156*, 643-651.

Li, X., and Gould, S.J. (2003). The dynamin-like GTPase DLP1 is essential for peroxisome division and is recruited to peroxisomes in part by PEX11. The Journal of biological chemistry *278*, 17012-17020.

Li, X., and Kazgan, N. (2011). Mammalian sirtuins and energy metabolism. International journal of biological sciences *7*, 575-587.

Lian, J.B., Javed, A., Zaidi, S.K., Lengner, C., Montecino, M., van Wijnen, A.J., Stein, J.L., and Stein, G.S. (2004). Regulatory controls for osteoblast growth and differentiation: role of Runx/Cbfa/AML factors. Critical reviews in eukaryotic gene expression *14*, 1-41.

Lind, T., Sundqvist, A., Hu, L., Pejler, G., Andersson, G., Jacobson, A., and Melhus, H. (2013). Vitamin a is a negative regulator of osteoblast mineralization. PloS one *8*, e82388.

Ling, L., Nurcombe, V., and Cool, S.M. (2009). Wnt signaling controls the fate of mesenchymal stem cells. Gene *433*, 1-7.

Loughran, P.A., Stolz, D.B., Vodovotz, Y., Watkins, S.C., Simmons, R.L., and Billiar, T.R. (2005). Monomeric inducible nitric oxide synthase localizes to peroxisomes in hepatocytes. Proceedings of the National Academy of Sciences of the United States of America *102*, 13837-13842.

Marie, P.J., and Kassem, M. (2011). Osteoblasts in osteoporosis: past, emerging, and future anabolic targets. European journal of endocrinology / European Federation of Endocrine Societies *165*, 1-10.

Marshall, P.A., Krimkevich, Y.I., Lark, R.H., Dyer, J.M., Veenhuis, M., and Goodman, J.M. (1995). Pmp27 promotes peroxisomal proliferation. The Journal of cell biology *129*, 345-355.

Martin, J.W., Zielenska, M., Stein, G.S., van Wijnen, A.J., and Squire, J.A. (2011). The Role of RUNX2 in Osteosarcoma Oncogenesis. Sarcoma *2011*, 282745.

Matsuzono, Y., Kinoshita, N., Tamura, S., Shimozawa, N., Hamasaki, M., Ghaedi, K., Wanders, R.J., Suzuki, Y., Kondo, N., and Fujiki, Y. (1999). Human PEX19: cDNA cloning by functional complementation, mutation analysis in a patient with Zellweger syndrome, and potential role in peroxisomal membrane assembly. Proceedings of the National Academy of Sciences of the United States of America *96*, 2116-2121.

Maxwell, M., Bjorkman, J., Nguyen, T., Sharp, P., Finnie, J., Paterson, C., Tonks, I., Paton, B.C., Kay, G.F., and Crane, D.I. (2003). Pex13 Inactivation in the Mouse Disrupts Peroxisome Biogenesis and Leads to a Zellweger Syndrome Phenotype. Molecular and Cellular Biology *23*, 5947-5957.

McBurney, M.W., Yang, X., Jardine, K., Hixon, M., Boekelheide, K., Webb, J.R., Lansdorp, P.M., and Lemieux, M. (2003). The mammalian SIR2alpha protein has a role in embryogenesis and gametogenesis. Mol Cell Biol *23*, 38-54.

McCormick, R.K. (2007). Osteoporosis: integrating biomarkers and other diagnostic correlates into the management of bone fragility. Alternative medicine review : a journal of clinical therapeutic *12*, 113-145.

McNew, J.A., and Goodman, J.M. (1994). An oligomeric protein is imported into peroxisomes in vivo. The Journal of cell biology *127*, 1245-1257.

McNiven, M.A. (1998). Dynamin: a molecular motor with pinchase action. Cell *94*, 151-154.

Michalik, L., Auwerx, J., Berger, J.P., Chatterjee, V.K., Glass, C.K., Gonzalez, F.J., Grimaldi, P.A., Kadowaki, T., Lazar, M.A., O'Rahilly, S*., et al.* (2006). International Union of Pharmacology. LXI. Peroxisome proliferator-activated receptors. Pharmacological reviews *58*, 726-741.

Mochin, M.T., Underwood, K.F., Cooper, B., McLenithan, J.C., Pierce, A.D., Nalvarte, C., Arbiser, J., Karlsson, A.I., Moise, A.R., Moskovitz, J*., et al.* (2014). Hyperglycemia and redox status regulate RUNX2 DNA-binding and an angiogenic phenotype in endothelial cells. Microvascular research *97C*, 55-64.

Motley, A.M., Hettema, E.H., Hogenhout, E.M., Brites, P., ten Asbroek, A.L., Wijburg, F.A., Baas, F., Heijmans, H.S., Tabak, H.F., Wanders, R.J*., et al.* (1997). Rhizomelic chondrodysplasia punctata is a peroxisomal protein targeting disease caused by a non-functional PTS2 receptor. Nature genetics *15*, 377-380.

Mukai, S., Ghaedi, K., and Fujiki, Y. (2002). Intracellular localization, function, and dysfunction of the peroxisome-targeting signal type 2 receptor, Pex7p, in mammalian cells. The Journal of biological chemistry *277*, 9548-9561.

Mundlos, S., Otto, F., Mundlos, C., Mulliken, J.B., Aylsworth, A.S., Albright, S., Lindhout, D., Cole, W.G., Henn, W., Knoll, J.H*., et al.* (1997). Mutations involving the transcription factor CBFA1 cause cleidocranial dysplasia. Cell *89*, 773-779.

Naidu, S., Vijayan, V., Santoso, S., Kietzmann, T., and Immenschuh, S. (2009). Inhibition and genetic deficiency of p38 MAPK up-regulates heme oxygenase-1 gene expression via Nrf2. Journal of immunology *182*, 7048-7057.

Nakashima, T., and Takayanagi, H. (2011). New regulation mechanisms of osteoclast differentiation. Annals of the New York Academy of Sciences *1240*, E13-18.

Nenicu, A., Luers, G.H., Kovacs, W., David, M., Zimmer, A., Bergmann, M., and Baumgart-Vogt, E. (2007). Peroxisomes in human and mouse testis: differential expression of peroxisomal proteins in germ cells and distinct somatic cell types of the testis. Biology of reproduction *77*, 1060-1072.

Noguchi, T., and Fujiwara, S. (1988). Identification of mammalian aminotransferases utilizing glyoxylate or pyruvate as amino acceptor. Peroxisomal and mitochondrial asparagine aminotransferase. The Journal of biological chemistry *263*, 182-186.

Nuttall, M.E., Patton, A.J., Olivera, D.L., Nadeau, D.P., and Gowen, M. (1998). Human trabecular bone cells are able to express both osteoblastic and adipocytic phenotype: implications for osteopenic disorders. Journal of bone and mineral research : the official journal of the American Society for Bone and Mineral Research *13*, 371-382.

O'Donnell, D., and Meyers, A.M. (1985). Hypophosphataemic osteomalacia misdiagnosed as metastatic carcinoma. A case report. South African medical journal = Suid-Afrikaanse tydskrif vir geneeskunde *67*, 934-935.

Obert, M., Ahlemeyer, B., Baumgart-Vogt, E., and Traupe, H. (2005). Flat-panel volumetric computed tomography: a new method for visualizing fine bone detail in living mice. Journal of computer assisted tomography *29*, 560-565.

Obsil, T., and Obsilova, V. (2011). Structural basis for DNA recognition by FOXO proteins. Biochimica et biophysica acta *1813*, 1946-1953.

Ogata, Y. (2008). Bone sialoprotein and its transcriptional regulatory mechanism. Journal of periodontal research *43*, 127-135.

Oshino, N., Chance, B., Sies, H., and Bucher, T. (1973). The role of H 2 O 2 generation in perfused rat liver and the reaction of catalase compound I and hydrogen donors. Arch Biochem Biophys *154*, 117-131.

Osumi, T., Yokota, S., and Hashimoto, T. (1990). Proliferation of peroxisomes and induction of peroxisomal beta-oxidation enzymes in rat hepatoma H4IIEC3 by ciprofibrate. Journal of biochemistry *108*, 614-621.

Otto, F., Thornell, A.P., Crompton, T., Denzel, A., Gilmour, K.C., Rosewell, I.R., Stamp, G.W., Beddington, R.S., Mundlos, S., Olsen, B.R*., et al.* (1997). Cbfa1, a candidate gene for cleidocranial dysplasia syndrome, is essential for osteoblast differentiation and bone development. Cell *89*, 765-771.

Passreiter, M., Anton, M., Lay, D., Frank, R., Harter, C., Wieland, F.T., Gorgas, K., and Just, W.W. (1998). Peroxisome biogenesis: involvement of ARF and coatomer. The Journal of cell biology *141*, 373-383.

Pause, B., Saffrich, R., Hunziker, A., Ansorge, W., and Just, W.W. (2000). Targeting of the 22 kDa integral peroxisomal membrane protein. FEBS letters *471*, 23-28.

Pino, A.M., Rosen, C.J., and Rodriguez, J.P. (2012). In osteoporosis, differentiation of mesenchymal stem cells (MSCs) improves bone marrow adipogenesis. Biological research *45*, 279-287.

Pires, J.R., Hong, X., Brockmann, C., Volkmer-Engert, R., Schneider-Mergener, J., Oschkinat, H., and Erdmann, R. (2003). The ScPex13p SH3 domain exposes two distinct binding sites for Pex5p and Pex14p. Journal of molecular biology *326*, 1427-1435.

Price, J.S., Oyajobi, B.O., and Russell, R.G. (1994). The cell biology of bone growth. European journal of clinical nutrition *48 Suppl 1*, S131-149.

Prozorovski, T., Schulze-Topphoff, U., Glumm, R., Baumgart, J., Schroter, F., Ninnemann, O., Siegert, E., Bendix, I., Brustle, O., Nitsch, R*., et al.* (2008). Sirt1 contributes critically to the redox-dependent fate of neural progenitors. Nat Cell Biol *10*, 385-394.

Purdue, P.E., Skoneczny, M., Yang, X., Zhang, J.W., and Lazarow, P.B. (1999). Rhizomelic chondrodysplasia punctata, a peroxisomal biogenesis disorder caused by defects in Pex7p, a peroxisomal protein import receptor: a minireview. Neurochemical research *24*, 581-586.

Purdue, P.E., Zhang, J.W., Skoneczny, M., and Lazarow, P.B. (1997). Rhizomelic chondrodysplasia punctata is caused by deficiency of human PEX7, a homologue of the yeast PTS2 receptor. Nature genetics *15*, 381-384.

Purushotham, A., Xu, Q., and Li, X. (2012). Systemic SIRT1 insufficiency results in disruption of energy homeostasis and steroid hormone metabolism upon high-fat-diet feeding. FASEB J *26*, 656-667.

Qian, G. (2010a). Role of peroxisomes in physiology and pathology of ossification and bone metabolism. In Faculties of Veterinary Medicine and Medicine of the Justus Liebig University Giessen Germany (Giessen Germany: Justus Liebig University Giessen Germany).

Qian, G., Ahlemeyer, B., Obert, M., Traupe, H., Baumgart-Vogt, E. (2010b). Impaired ossification due to peroxisomal deficiency Studies with PEX11beta knockout mice. Bone *44*, s294.

Rached, M.T., Kode, A., Xu, L., Yoshikawa, Y., Paik, J.H., Depinho, R.A., and Kousteni, S. (2010). FoxO1 is a positive regulator of bone formation by favoring protein synthesis and resistance to oxidative stress in osteoblasts. Cell metabolism *11*, 147-160.

Rachubinski, R.A., and Subramani, S. (1995). How proteins penetrate peroxisomes. Cell *83*, 525-528.

Rehling, P., Marzioch, M., Niesen, F., Wittke, E., Veenhuis, M., and Kunau, W.H. (1996). The import receptor for the peroxisomal targeting signal 2 (PTS2) in Saccharomyces cerevisiae is encoded by the PAS7 gene. The EMBO journal *15*, 2901-2913.

Rodda, S.J., and McMahon, A.P. (2006). Distinct roles for Hedgehog and canonical Wnt signaling in specification, differentiation and maintenance of osteoblast progenitors. Development *133*, 3231-3244.

Ryall, J.G. (2012). The role of sirtuins in the regulation of metabolic homeostasis in skeletal muscle. Current opinion in clinical nutrition and metabolic care *15*, 561-566.

Sacksteder, K.A., Jones, J.M., South, S.T., Li, X., Liu, Y., and Gould, S.J. (2000). PEX19 binds multiple peroxisomal membrane proteins, is predominantly cytoplasmic, and is required for peroxisome membrane synthesis. The Journal of cell biology *148*, 931-944.

Sanchez, A.M., Candau, R.B., and Bernardi, H. (2014). FoxO transcription factors: their roles in the maintenance of skeletal muscle homeostasis. Cellular and molecular life sciences : CMLS *71*, 1657-1671.

Sandri, M., Sandri, C., Gilbert, A., Skurk, C., Calabria, E., Picard, A., Walsh, K., Schiaffino, S., Lecker, S.H., and Goldberg, A.L. (2004). Foxo transcription factors induce the atrophy-related ubiquitin ligase atrogin-1 and cause skeletal muscle atrophy. Cell *117*, 399-412.

Sang, T., Cao, Q., Wang, Y., Liu, F., and Chen, S. (2014). Overexpression or silencing of FOXO3a affects proliferation of endothelial progenitor cells and expression of cell cycle regulatory proteins. PloS one *9*, e101703.

Santos, M.J., Imanaka, T., Shio, H., Small, G.M., and Lazarow, P.B. (1988). Peroxisomal membrane ghosts in Zellweger syndrome--aberrant organelle assembly. Science *239*, 1536-1538.

Scholtysek, C., Katzenbeisser, J., Fu, H., Uderhardt, S., Ipseiz, N., Stoll, C., Zaiss, M.M., Stock, M., Donhauser, L., Bohm, C.*, et al.* (2013). PPARbeta/delta governs Wnt signaling and bone turnover. Nature medicine *19*, 608-613.

Schrader, M., Bonekamp, N.A., and Islinger, M. (2012). Fission and proliferation of peroxisomes. Biochimica et biophysica acta *1822*, 1343-1357.

Schrader, M., Reuber, B.E., Morrell, J.C., Jimenez-Sanchez, G., Obie, C., Stroh, T.A., Valle, D., Schroer, T.A., and Gould, S.J. (1998). Expression of PEX11beta mediates peroxisome proliferation in the absence of extracellular stimuli. The Journal of biological chemistry *273*, 29607-29614.

Schug, T.T., Xu, Q., Gao, H., Peres-da-Silva, A., Draper, D.W., Fessler, M.B., Purushotham, A., and Li, X. (2010). Myeloid deletion of SIRT1 induces inflammatory signaling in response to environmental stress. Mol Cell Biol.

Seedorf, U., Brysch, P., Engel, T., Schrage, K., and Assmann, G. (1994). Sterol carrier protein X is peroxisomal 3-oxoacyl coenzyme A thiolase with intrinsic sterol carrier and lipid transfer activity. The Journal of biological chemistry *269*, 21277-21283.

Sessler, R.J., and Noy, N. (2005). A ligand-activated nuclear localization signal in cellular retinoic acid binding protein-II. Mol Cell *18*, 343-353.

Shakibaei, M., Shayan, P., Busch, F., Aldinger, C., Buhrmann, C., Lueders, C., and Mobasheri, A. (2012). Resveratrol mediated modulation of Sirt-1/Runx2 promotes osteogenic differentiation of mesenchymal stem cells: potential role of Runx2 deacetylation. PloS one *7*, e35712.

Shimozawa, N. (2007). Molecular and clinical aspects of peroxisomal diseases. Journal of inherited metabolic disease *30*, 193-197.

Shimozawa, N., Suzuki, Y., Zhang, Z., Imamura, A., Ghaedi, K., Fujiki, Y., and Kondo, N. (2000). Identification of PEX3 as the gene mutated in a Zellweger syndrome patient lacking peroxisomal remnant structures. Human molecular genetics *9*, 1995-1999.

Shulman, A.I., and Mangelsdorf, D.J. (2005). Retinoid x receptor heterodimers in the metabolic syndrome. The New England journal of medicine *353*, 604-615.

Simic, P., Zainabadi, K., Bell, E., Sykes, D.B., Saez, B., Lotinun, S., Baron, R., Scadden, D., Schipani, E., and Guarente, L. (2013). SIRT1 regulates differentiation of mesenchymal stem cells by deacetylating beta-catenin. EMBO molecular medicine *5*, 430-440.

Singh, A.K., Dobashi, K., Gupta, M.P., Asayama, K., Singh, I., and Orak, J.K. (1999). Manganese superoxide dismutase in rat liver peroxisomes: biochemical and immunochemical evidence. Molecular and cellular biochemistry *197*, 7-12.

Singh, H., Usher, S., and Poulos, A. (1989). Dihydroxyacetone phosphate acyltransferase and alkyldihydroxyacetone phosphate synthase activities in rat liver subcellular fractions and human skin fibroblasts. Arch Biochem Biophys *268*, 676-686.

Sinha, K.M., and Zhou, X. (2013). Genetic and molecular control of osterix in skeletal formation. Journal of cellular biochemistry *114*, 975-984.

Smith, J.J., and Aitchison, J.D. (2009). Regulation of peroxisome dynamics. Current opinion in cell biology *21*, 119-126.

South, S.T., and Gould, S.J. (1999). Peroxisome synthesis in the absence of preexisting peroxisomes. The Journal of cell biology *144*, 255-266.

Stein, K., Schell-Steven, A., Erdmann, R., and Rottensteiner, H. (2002). Interactions of Pex7p and Pex18p/Pex21p with the peroxisomal docking machinery: implications for the first steps in PTS2 protein import. Mol Cell Biol *22*, 6056-6069.

Steinberg, S.J., Dodt, G., Raymond, G.V., Braverman, N.E., Moser, A.B., and Moser, H.W. (2006). Peroxisome biogenesis disorders. Biochimica et biophysica acta *1763*, 1733-1748.

Stelzig, I., Karnati, S., Valerius, K.P., and Baumgart-Vogt, E. (2013). Peroxisomes in dental tissues of the mouse. Histochemistry and cell biology *140*, 443-462.

Stephens, A.S., Stephens, S.R., and Morrison, N.A. (2011). Internal control genes for quantitative RT-PCR expression analysis in mouse osteoblasts, osteoclasts and macrophages. BMC research notes *4*, 410.

Subramani, S. (1993). Protein import into peroxisomes and biogenesis of the organelle. Annual review of cell biology *9*, 445-478.

Suda, T., Takahashi, N., and Martin, T.J. (1992). Modulation of osteoclast differentiation. Endocrine reviews *13*, 66-80.

Sudo, H., Kodama, H.A., Amagai, Y., Yamamoto, S., and Kasai, S. (1983). In vitro differentiation and calcification in a new clonal osteogenic cell line derived from newborn mouse calvaria. The Journal of cell biology *96*, 191-198.

Swinkels, B.W., Gould, S.J., Bodnar, A.G., Rachubinski, R.A., and Subramani, S. (1991). A novel, cleavable peroxisomal targeting signal at the amino-terminus of the rat 3-ketoacyl-CoA thiolase. The EMBO journal *10*, 3255-3262.

Tanaka, K., Inoue, Y., Hendy, G.N., Canaff, L., Katagiri, T., Kitazawa, R., Komori, T., Sugimoto, T., Seino, S., and Kaji, H. (2012). Interaction of Tmem119 and the bone morphogenetic protein pathway in the commitment of myoblastic into osteoblastic cells. Bone *51*, 158-167.

Tang, M.M., Zhu, Q.E., Fan, W.Z., Zhang, S.L., Li, D.Z., Liu, L.Z., Chen, M., Zhang, M., Zhou, J., and Wei, C.J. (2011). Intra-arterial targeted islet-specific expression of Sirt1 protects beta cells from streptozotocin-induced apoptosis in mice. Molecular therapy : the journal of the American Society of Gene Therapy *19*, 60-66.

Tang, S., Huang, G., Fan, W., Chen, Y., Ward, J.M., Xu, X., Xu, Q., Kang, A., McBurney, M.W., Fargo, D.C.*, et al.* (2014). SIRT1-Mediated Deacetylation of CRABPII Regulates Cellular Retinoic Acid Signaling and Modulates Embryonic Stem Cell Differentiation. Molecular cell.

Teixeira, C.C., Liu, Y., Thant, L.M., Pang, J., Palmer, G., and Alikhani, M. (2010). Foxo1, a novel regulator of osteoblast differentiation and skeletogenesis. The Journal of biological chemistry *285*, 31055-31065.

Thomas, D., and Kansara, M. (2006). Epigenetic modifications in osteogenic differentiation and transformation. Journal of cellular biochemistry *98*, 757-769.

Tsai, F.Y., Cheng, Y.T., and Tsou, T.C. (2014). A recombinant PPRE-driven luciferase bioassay for identification of potential PPAR agonists. Vitamins and hormones *94*, 427-435.

van der Zand, A., Braakman, I., Geuze, H.J., and Tabak, H.F. (2006). The return of the peroxisome. Journal of cell science *119*, 989-994.

Van Veldhoven, P.P. Biochemistry and genetics of inherited disorders of peroxisomal fatty acid metabolism. J Lipid Res.

Vanhooren, J.C., Marynen, P., Mannaerts, G.P., and Van Veldhoven, P.P. (1997). Evidence for the existence of a pristanoyl-CoA oxidase gene in man. The Biochemical journal *325 (Pt 3)*, 593-599.

Vijayan, V., Baumgart-Vogt, E., Naidu, S., Qian, G., and Immenschuh, S. (2011). Bruton's tyrosine kinase is required for TLR-dependent heme oxygenase-1 gene activation via Nrf2 in macrophages. Journal of immunology *187*, 817-827.

Visser, W.F., van Roermund, C.W., Ijlst, L., Waterham, H.R., and Wanders, R.J. (2007). Metabolite transport across the peroxisomal membrane. The Biochemical journal *401*, 365-375.

Walton, P.A., Hill, P.E., and Subramani, S. (1995). Import of stably folded proteins into peroxisomes. Molecular biology of the cell *6*, 675-683.

Wanders, R.J. (2004a). Metabolic and molecular basis of peroxisomal disorders: a review. American journal of medical genetics Part A *126A*, 355-375.

Wanders, R.J. (2004b). Peroxisomes, lipid metabolism, and peroxisomal disorders. Mol Genet Metab *83*, 16-27.

Wanders, R.J., Ferdinandusse, S., Brites, P., and Kemp, S. (2010). Peroxisomes, lipid metabolism and lipotoxicity. Biochimica et biophysica acta *1801*, 272-280.

Wang, R.H., Sengupta, K., Li, C., Kim, H.S., Cao, L., Xiao, C., Kim, S., Xu, X., Zheng, Y., Chilton, B*., et al.* (2008). Impaired DNA damage response, genome instability, and tumorigenesis in SIRT1 mutant mice. Cancer Cell *14*, 312-323.

Wilson, G.N., Holmes, R.G., Custer, J., Lipkowitz, J.L., Stover, J., Datta, N., and Hajra, A. (1986). Zellweger syndrome: diagnostic assays, syndrome delineation, and potential therapy. American journal of medical genetics *24*, 69-82.

Yamamoto, K., and Fahimi, H.D. (1987). Biogenesis of peroxisomes in regenerating rat liver. I. Sequential changes of catalase and urate oxidase detected by ultrastructural cytochemistry. European journal of cell biology *43*, 293-300.

Yamashita, A., Takada, T., Nemoto, K., Yamamoto, G., and Torii, R. (2006). Transient suppression of PPARgamma directed ES cells into an osteoblastic lineage. FEBS letters *580*, 4121-4125.

Zaar, K., Volkl, A., and Fahimi, H.D. (1986). Isolation and characterization of peroxisomes from the renal cortex of beef, sheep, and cat. European journal of cell biology *40*, 16-24.

Ziros, P.G., Basdra, E.K., and Papavassiliou, A.G. (2008). Runx2: of bone and stretch. The international journal of biochemistry & cell biology *40*, 1659-1663.

9. Index of abbreviation

ALP	Alkaline phosphatase
ACOX	Acyl-CoA oxidase
BMD	Bone Mineral Density
BGLAP	Bone γ-carboxyglutamic acid-containing protein
°C	Degree Celcius
CDKS	mitotic cyclin-dependent kinases
COL1a1	collagen, type I, alpha 1
COL1a2	collagen, type I, alpha 2
CRABPII	retinoic acid binding protein II
DHCA	dihydroxycholestanoic acid
DHE	dihydroethidium
DLP1	dynamin-like protein
ER	Endoplasmic Reticulum
ES	Embryonic Stem Cell
FACS	Fluorescence-activated cell sorting
FoxO	Forkhead box O
g	gram
H$_2$-DCFDA	dichlorodihydrofluorescein diacetate
HO-1	Heme oxygenase 1
4-HNE	4-hydroxynonenal
IBSP	integrin-binding sialoprotein
IF	immunofluorescence
IRD	Infantile Refsum's Disease
KO	Knockout
LEF	lymphoid Enhancer-Binding Factor.
LRP	low density lipoprotein receptor-related protein
M-CSF	macrophage colony-stiumlating factor
min	minute
NAC	N-Acetyl-Cysteine

NALD	Neonatal Adrenoleukodystrophy
NFATc1	nuclear factor of activated T cells cytoplasmic 1
NRF2	Nuclear factor (erythroid-derived 2)-like 2
OPN	Osteopontin
OPG	osteoprotegerin
Osx	Osterix
PBD	Peroxisome Biogenesis Disorders
PBS	Phosphate buffered saline
PFA	Paraformaldehyde
Pgc-1α	Proliferator-activated receptor γ-coactivator 1α
PMP	Peroxisomal Membrane Protein
PPARγ	Peroxisome Proliferator-Activated Receptor-γ
PP2A	protein phosphatase 2A
PTS	Peroxisomal Targeting Sequences
mPTS	Membrane Peroxisomal Targeting Sequences
NF-κB	nuclear factor κB
PBD	peroxisome biogenesis disorders
PVDF	polyvinylidene fluoride
RA	retinoic acid
RARβ	retinoic acid receptors β
RCF	relative centrifugal force
RCPD	rhizomelic chondrodysplasia punctata
ROS	Reactive oxygen species
RT	Room temperature
RT-PCR	Semi-quantitative polymerase chain reaction
RXR	Retinoid X receptor
THCA	trihydroxycholestanoic acid
PUFA	Polyunsaturated Fatty Acid
RANK	receptor activator of NF-κB
RANKL	receptor activator of NF-κB ligand
ROS	Reactive Oxygen Species

Runx2	runt-related transcription factor 2
qPCR	Quantitative real time polymerase chain reaction
s	Second
SH3	C-terminal Src homology domain
SOD2	Manganese Superoxide dismutase
RT-PCR	Semi-quantitative polymerase chain reaction
TCF	T-cell factor
VLCFA	Very Long Chain Fatty Acids
WB	Western Blot
WT	Wild Type
ZS	Zellweger Syndrome

10. Acknowledgements

11. Curriculum Vitae

The curriculum vitae was removed from the electronic version of the paper.